SiPMs for CTA Cameras

F. Giordano
University and INFN Bari

Gamma-ray observations of Tycho's supernova remnant with VERITAS and Fermi

S. Archambault[1], A. Archer[2], W. Benbow[3], R. Bird[4], E. Bourbeau[1], M. Buchovecky[4], J. H. Buckley[2], V. Bugaev[2], M. Cerruti[3], M. P. Connolly[5], W. Cui[6,7], V. V. Dwarkadas[8], M. Errando[2], A. Falcone[9], Q. Feng[1], J. P. Finley[6], H. Fleischhack[10], L. Fortson[11], A. Furniss[12], S. Griffin[1], M. Hütten[10], D. Hanna[1], J. Holder[13], C. A. Johnson[14], P. Kaaret[15], P. Kar[16], N. Kelley-Hoskins[10], M. Kertzman[17], D. Kieda[16], M. Krause[10], S. Kumar[13], M. J. Lang[5], G. Maier[10], S. McArthur[6], A. McCann[1], P. Moriarty[5], R. Mukherjee[18], D. Nieto[19], S. O'Brien[16], R. A. Ong[4], A. N. Otte[21], N. Park[22*], M. Pohl[23,10], A. Popkow[4], E. Pueschel[20], J. Quinn[20], K. Ragan[1], P. T. Reynolds[24], G. T. Richards[21], E. Roache[3], I. Sadeh[10], M. Santander[18], G. H. Sembroski[6], K. Shahinyan[11], P. Slane[25], D. Staszak[22], I. Telezhinsky[23,10], S. Trepanier[1], J. Tyler[1], S. P. Wakely[22], A. Weinstein[26], T. Weisgarber[27], P. Wilcox[15], A. Wilhelm[23,10], D. A. Williams[14], B. Zitzer[1]

ABSTRACT

High-energy gamma-ray emission from supernova remnants (SNRs) has provided a unique perspective for studies of Galactic cosmic-ray acceleration. Tycho's SNR is a particularly good target because it is a young, type Ia SNR that is well-studied over a wide range of energies and located in a relatively clean environment. Since the detection of gamma-ray emission from Tycho's SNR by VERITAS and *Fermi*-LAT, there have been several theoretical models proposed to explain its broadband emission and high-energy morphology. We report on an update to the gamma-ray measurements of Tycho's SNR with 147 hours of VERITAS and 84 months of *Fermi*-LAT observations, which represents about a factor of two increase in exposure over previously published data. About half of the VERITAS data benefited from a camera upgrade, which has made it possible to extend the TeV measurements toward lower energies. The TeV spectral index measured by VERITAS is consistent with previous results, but the expanded energy range softens a straight power-law fit. At energies higher than 400 GeV, the power-law index is $2.92 \pm 0.42_{\mathrm{stat}} \pm 0.20_{\mathrm{sys}}$. It is also softer than the spectral index in the GeV energy range, $2.14 \pm 0.09_{\mathrm{stat}} \pm 0.02_{\mathrm{sys}}$, measured by this study using *Fermi*–LAT data. The centroid position of the gamma-ray emission is coincident with the center of the remnant, as well as with the centroid

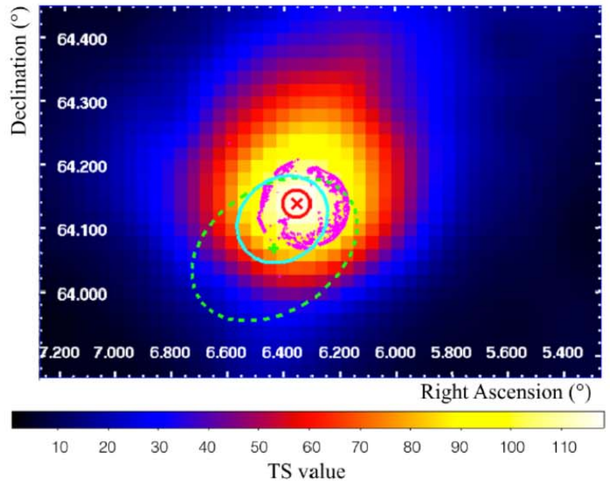

Fig. 1.— Smoothed *Fermi* TS map with the P8R2_CLEAN_V6 IRF for energies higher than 1 GeV. The map was smoothed with a Gaussian kernel with a radius of 0.06°. The magenta contours indicate the *Chandra* X-ray intensity at energies above 4.1 keV[1]. The cyan line is the previously published 95% confidence area for the *Fermi*-LAT position (Giordano et al. 2012). The centroid and error of 3FGL J0025.7+6404 are marked with a cross and dashed green line (Acero et al. 2015). The best-fit position and 68% confidence level of this study are shown with a red cross mark and a red circle.

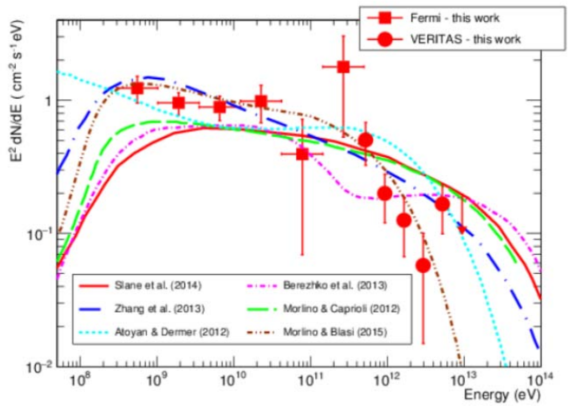

Fig. 5.— Fermi and VERITAS SEDs with theoretical models. Filled red squares show the *Fermi* results and filled red circles show the VERITAS results from this study. The models discussed in the text appear as the solid red line (prefered model A from Slane et al. (2014)), the magenta short broken dashed line (Berezhko et al. 2013), the blue large broken dashed line (Zhang et al. 2013), the green dashed line (Morlino & Caprioli 2012), the cyan dotted line (the leptonic model from Atoyan & Dermer (2012)), and the brown double-broken dashed line (Morlino & Blasi (2016) with a neutral fraction of 0.6).

Cosmic rays(1)

Composition

87% protons, 12% Helium, 1% Heavy nuclei, **0.1%** γ **rays** and neutrinos

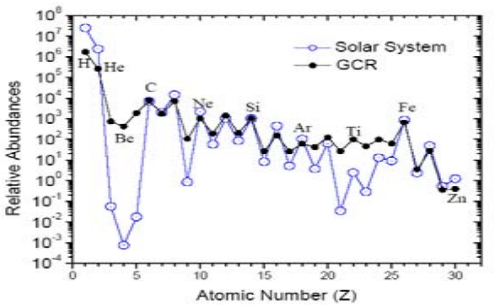

Cosmic Rays (1)

Composition

87% protons, 12% Helium, 1% Heavy nuclei, **0.1% γ rays** and neutrinos

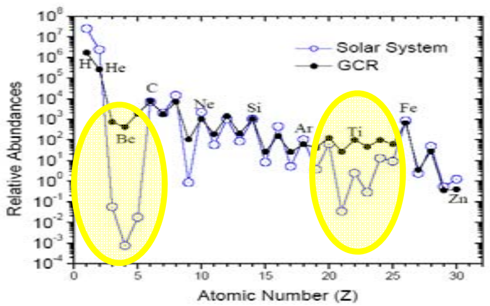

Spallation

Cosmic Rays (1)

Composition

87% protons, 12% Helium, 1% heavy nuclei, **0.1% gamma rays ad neutrinos**

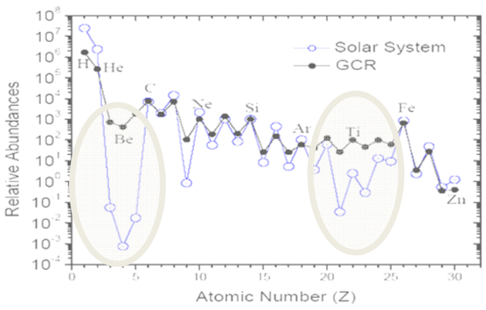

Processo di spallazione !

Spectrum

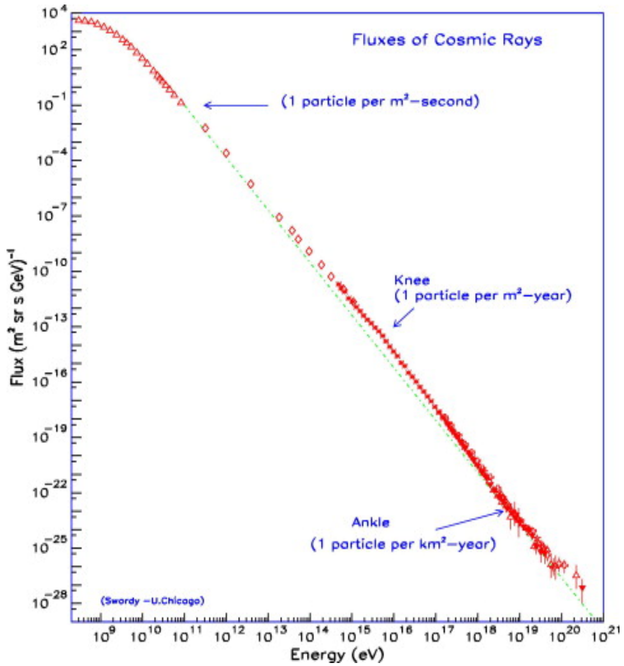

Cosmic Rays (1)

Composition

87% protoni, 12% atomi di elio, 1% nuclei pesanti, **0.1% raggi gamma** e neutrini

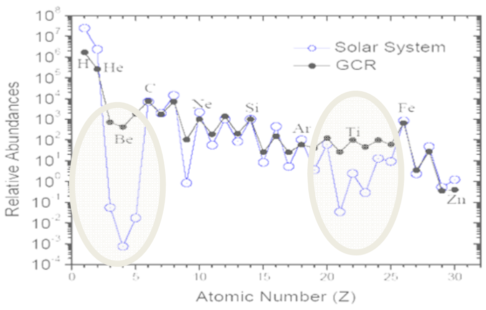

Processo di spallazione !

Spectrum

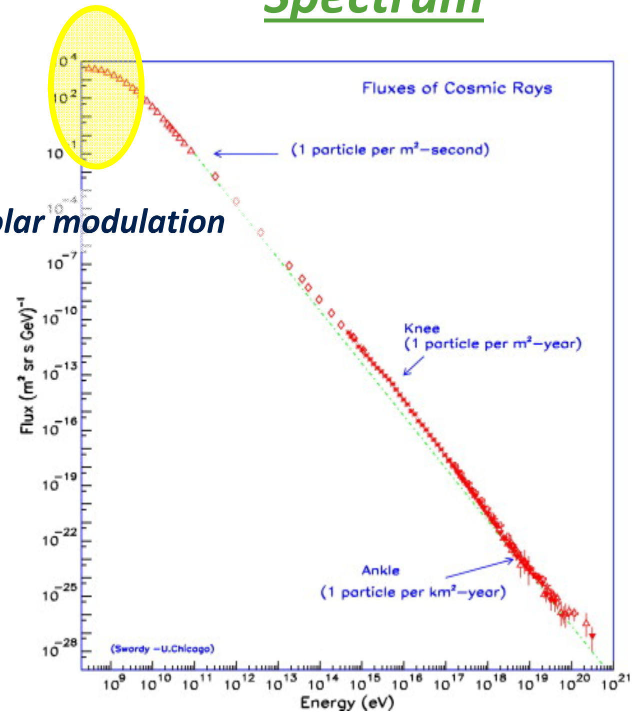

Cosmic Rays (1)

Composition

87% protoni, 12% atomi di elio, 1% nuclei pesanti, **0.1% raggi gamma** e neutrini

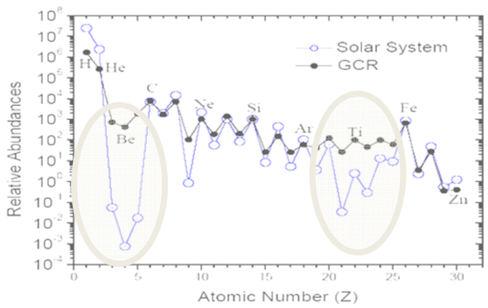

Processo di spallazione !

Spectrum

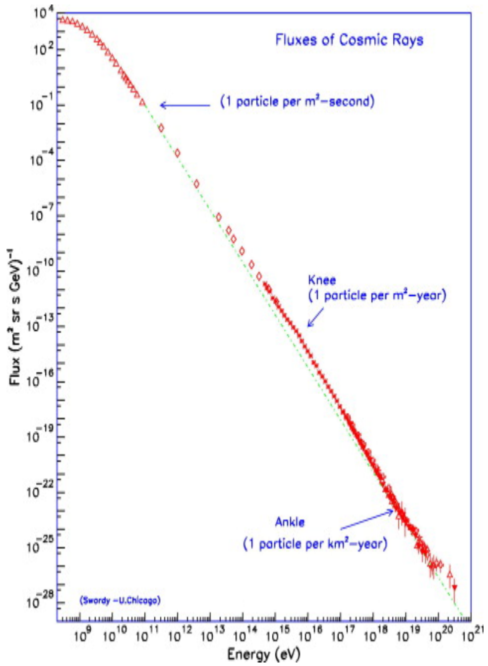

E>1 GeV

$$\frac{dN}{dE} \propto E^{-(\gamma+1)}$$

Cosmic Rays (1)

Composition

87% protoni, 12% atomi di elio, 1% nuclei pesanti, **0.1% raggi gamma** e neutrini

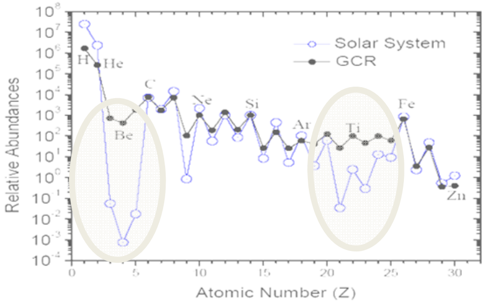

Processo di spallazione !

Spectrum

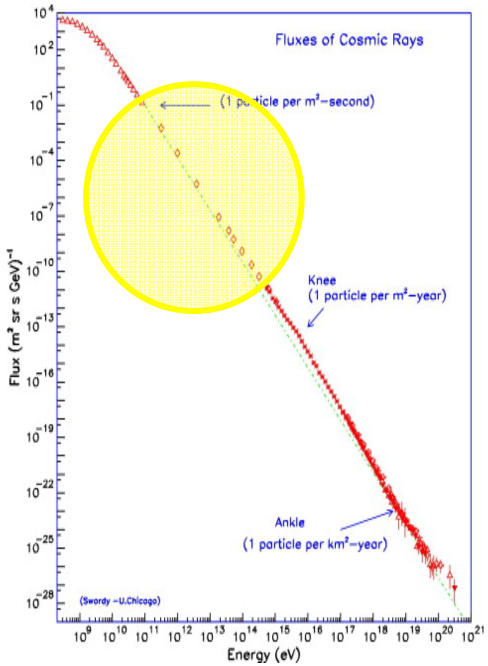

E > 1 GeV

$$\frac{dN}{dE} \propto E^{-(\gamma+1)}$$

10^9 - 10^{15} eV:

$$\gamma = 1.7$$

Cosmic Rays (1)

Composition

87% protoni, 12% atomi di elio, 1% nuclei pesanti, **0.1% raggi gamma** e neutrini

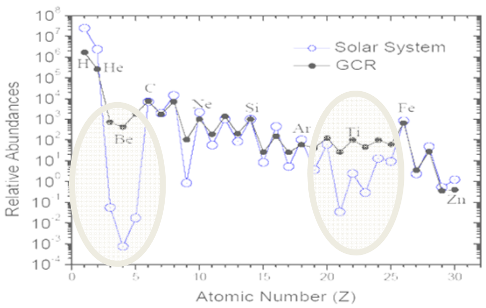

Processo di spallazione !

Spectrum

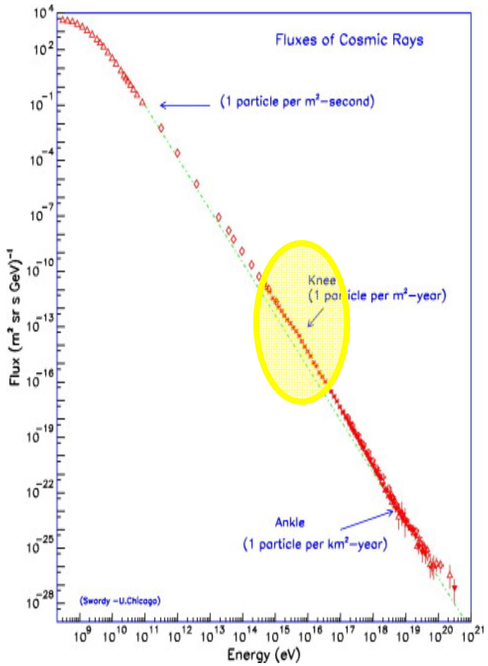

E > 1 GeV

$$\frac{dN}{dE} \propto E^{-(\gamma+1)}$$

knee:

$$\gamma = 2.1$$

Galactic origin

Cosmic Rays (1)

Composition

87% protoni, 12% atomi di elio, 1% nuclei pesanti, **0.1% raggi gamma** e neutrini

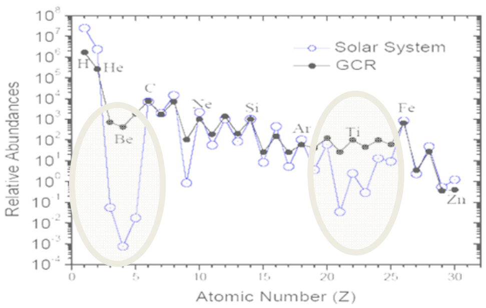

Processo di spallazione !

Spectrum

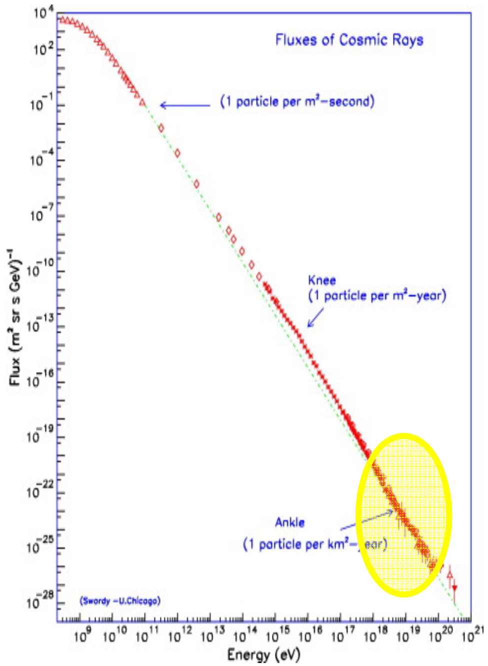

E > 1 GeV

$$\frac{dN}{dE} \propto E^{-(\gamma+1)}$$

ankle:

$$\gamma = 1.7$$

Extragal origin

Cosmic Rays (2)

Origin

What is the energy source of
galactic CRs

Cosmic Rays (2)

Origin

What is the energy source of galactic CRs

$$W_{CR} \approx 10^{49} erg$$

Cosmic Rays (2)

Origin

What is the energy source of galactic CRs

$$W_{CR} \approx 10^{49} erg$$

1 explosion /30years

$$W_{SNR} \approx 10^{51} erg$$

The shock wave may explain the energetics of the process with few % of efficiency

Cosmic Rays (2)

Origin

Qual è la fonte di energia per l'accelerazione dei raggi cosmici Galattici ?

$$W_{CR} \approx 10^{49} erg$$

$$W_{SNR} \approx 10^{51} erg$$

L'onda d'urto prodotta nell'esplosione di una Supernova può spiegare accelerazione

Propagation

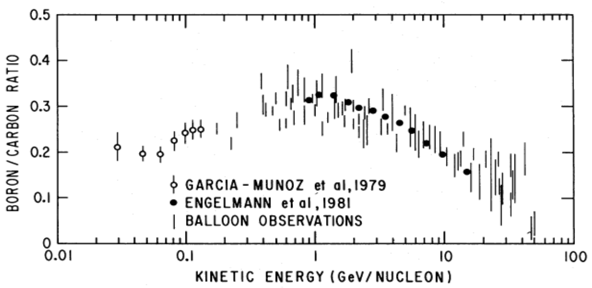

•5-10 g/cm^2 of material traversed

The material contained in the galactic disk is 10^{-3} g/cm^2

Cosmic Rays (2)

Origin

Qual è la fonte di energia per l'accelerazione dei raggi cosmici Galattici ?

$$W_{CR} \approx 10^{49}\, erg$$

$$W_{SNR} \approx 10^{51}\, erg$$

L'onda d'urto prodotta nell'esplosione di una Supernova può spiegare accelerazione

Propagation

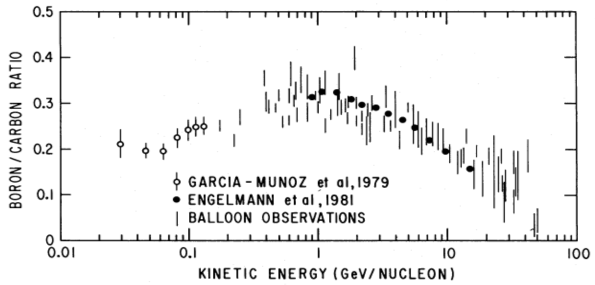

CRs traverse 100 times greater distances

Cosmic Rays (2)

Origin

Qual è la fonte di energia per l'accelerazione dei raggi cosmici Galattici ?

$$W_{CR} \approx 10^{49} erg$$

$$W_{SNR} \approx 10^{51} erg$$

L'onda d'urto prodotta nell'esplosione di una Supernova può spiegare accelerazione

Propagation

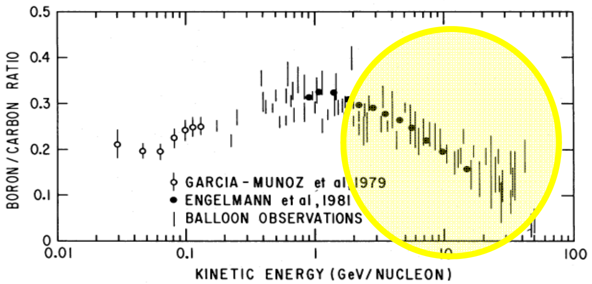

•The traversed material decrese wth energy

Cosmic Rays (2)

Origin

Qual è la fonte di energia per l'accelerazione dei raggi cosmici Galattici ?

$$W_{CR} \approx 10^{49} erg$$

$$W_{SNR} \approx 10^{51} erg$$

L'onda d'urto prodotta nell'esplosione di una Supernova può spiegare accelerazione

Propagation

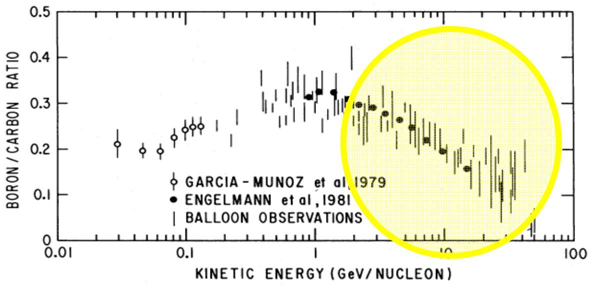

HE CRs stay less in the galaxy than lower energy CRs

Cosmic Rays (2)

Origin

Qual è la fonte di energia per l'accelerazione dei raggi cosmici Galattici ?

$$W_{CR} \approx 10^{49} erg$$

$$W_{SNR} \approx 10^{51} erg$$

L'onda d'urto prodotta nell'esplosione di una Supernova può spiegare accelerazione

Propagation

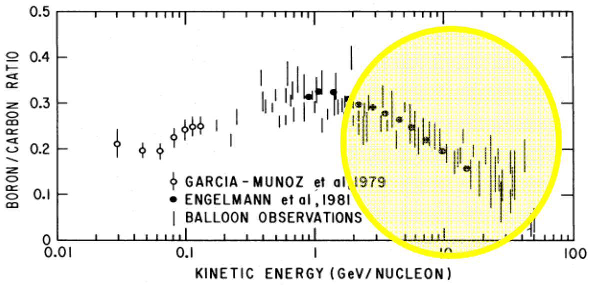

CRs are accelerated well before the propagation

Cosmic Rays (2)

Origin

Qual è la fonte di energia per l'accelerazione dei raggi cosmici Galattici ?

$$W_{CR} \approx 10^{49} erg$$

$$W_{SNR} \approx 10^{51} erg$$

L'onda d'urto prodotta nell'esplosione di una Supernova può spiegare accelerazione

Propagation

The Time needed for 20 kpc (galactic disk) is **$\tau_d \approx 6 \cdot 10^6$ anni**, much shorter than the time spent by CRs in the galaxy

Cosmic Rays (2)

Origin

Qual è la fonte di energia per l'accelerazione dei raggi cosmici Galattici ?

$$W_{CR} \approx 10^{49} erg$$

$$W_{SNR} \approx 10^{51} erg$$

L'onda d'urto prodotta nell'esplosione di una Supernova può spiegare accelerazione

Propagation

The Time needed for 20 kpc (galactic disk) is **$\tau_d \approx 6 \cdot 10^6$ anni**, much shorter than the time spent by CRs in the galaxy

Magnetic confinament

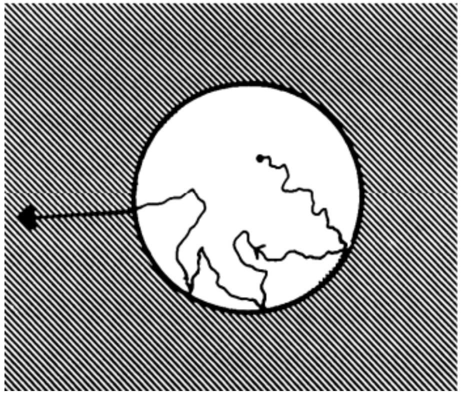

Cosmic Rays (2)

Origin

Qual è la fonte di energia per l'accelerazione dei raggi cosmici Galattici ?

$$W_{CR} \approx 10^{49} erg$$

$$W_{SNR} \approx 10^{51} erg$$

L'onda d'urto prodotta nell'esplosione di una Supernova può spiegare accelerazione

Propagation

"Cosmic ray clocks"

^{10}Be ^{26}Al

Cosmic Rays (2)

Origin

Qual è la fonte di energia per l'accelerazione dei raggi cosmici Galattici ?

$$W_{CR} \approx 10^{49}\, erg$$

$$W_{SNR} \approx 10^{51}\, erg$$

L'onda d'urto prodotta nell'esplosione di una Supernova può spiegare accelerazione

Propagation

"Cosmic ray clocks"

^{10}Be $\quad$ ^{26}Al

$$\tau_{^{10}Be} \approx 3.9 \cdot 10^{6}\, anni$$

Cosmic Rays (2)

Origin

Qual è la fonte di energia per l'accelerazione dei raggi cosmici Galattici ?

$$W_{CR} \approx 10^{49} erg$$

$$W_{SNR} \approx 10^{51} erg$$

L'onda d'urto prodotta nell'esplosione di una Supernova può spiegare accelerazione

Propagation

"Cosmic ray clocks"

^{10}Be ^{26}Al

$$\tau_{^{10}Be} \approx 3.9 \cdot 10^{6}\, anni$$

$$\tau_{esc} < \tau_{^{10}Be}$$

Cosmic Rays (2)

Origin

Qual è la fonte di energia per l'accelerazione dei raggi cosmici Galattici ?

$$W_{CR} \approx 10^{49} erg$$

$$W_{SNR} \approx 10^{51} erg$$

L'onda d'urto prodotta nell'esplosione di una Supernova può spiegare accelerazione

Propagation

"Cosmic ray clocks"

^{10}Be ^{26}Al

$$\tau_{^{10}Be} \approx 3.9 \cdot 10^{6}\, anni$$

$$\tau_{esc} < \tau_{^{10}Be} \qquad \tau_{esc} > \tau_{^{10}Be}$$

Cosmic Rays (2)

Origin

Qual è la fonte di energia per l'accelerazione dei raggi cosmici Galattici ?

$$W_{CR} \approx 10^{49} erg$$

$$W_{SNR} \approx 10^{51} erg$$

L'onda d'urto prodotta nell'esplosione di una Supernova può spiegare accelerazione

Propagation

"Cosmic ray clocks"

^{10}Be $\quad$ ^{26}Al

$$\tau_{^{10}Be} \approx 3.9 \cdot 10^{6} anni$$

~~$\tau_{esc} < \tau_{^{10}Be}$~~ $\quad$ $\tau_{esc} > \tau_{^{10}Be}$

$$\tau_{esc} \approx 2 \cdot 10^{7} yrs \Rightarrow \lambda_{esc} \approx 0.3 g / cm^{2}$$

The right volume contains also the Galactic Halo

COSMIC RAYS (3)

Acceleration processes

Second order Fermi mechanism

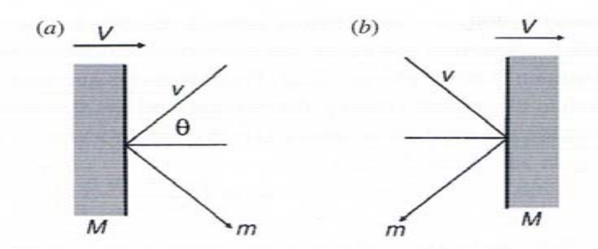

COSMIC RAYS (3)

Acceleration processes

Second order fermi mechanism

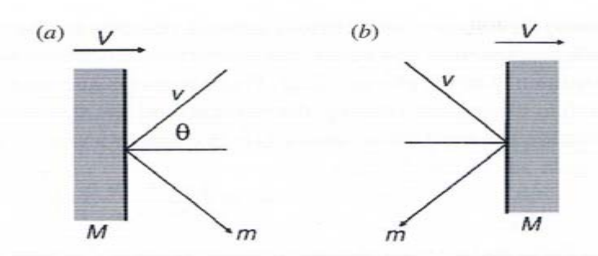

$$\left\langle \frac{\Delta E}{E} \right\rangle = \frac{8}{3}\left(\frac{V}{c}\right)^2$$

COSMIC RAYS (3)

Acceleration processes

Second order fermi Mechanism

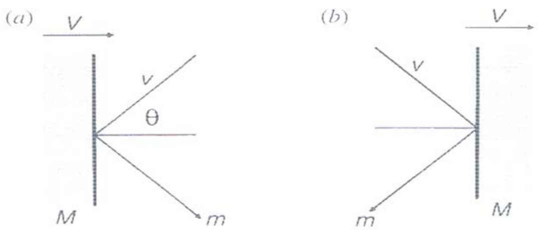

$$\left\langle \frac{\Delta E}{E} \right\rangle = \frac{8}{3}\left(\frac{V}{c}\right)^2$$

First Order Fermi Mechanism

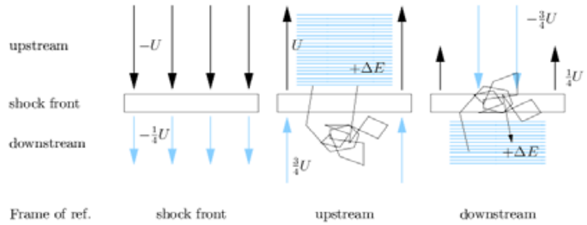

Acceleration processes

Second order fermi Mechanism

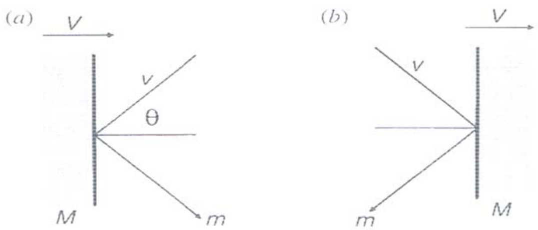

$$\left\langle \frac{\Delta E}{E} \right\rangle = \frac{8}{3}\left(\frac{V}{c}\right)^2$$

First Order Fermi Mechanism

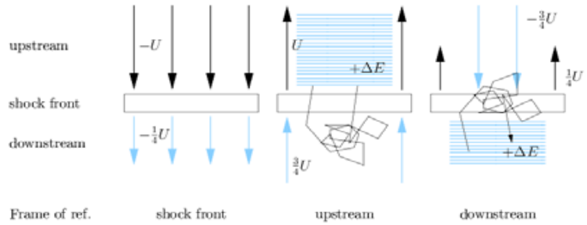

$$\left\langle \frac{\Delta E}{E} \right\rangle = \frac{4}{3}\frac{V}{c}$$

SUPERNOVAE

The expulsion of the outer layer of the star
generates the pre-Supernova

SUPERNOVA REMNANTS

Shell type

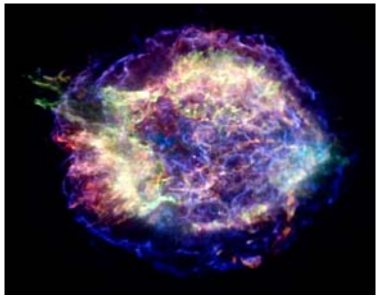

Cas A SNR

Mixed morphology remnant

W 28 SNR

Composite

G327.1-1.1 SNR

CRs interactions in the Galaxy

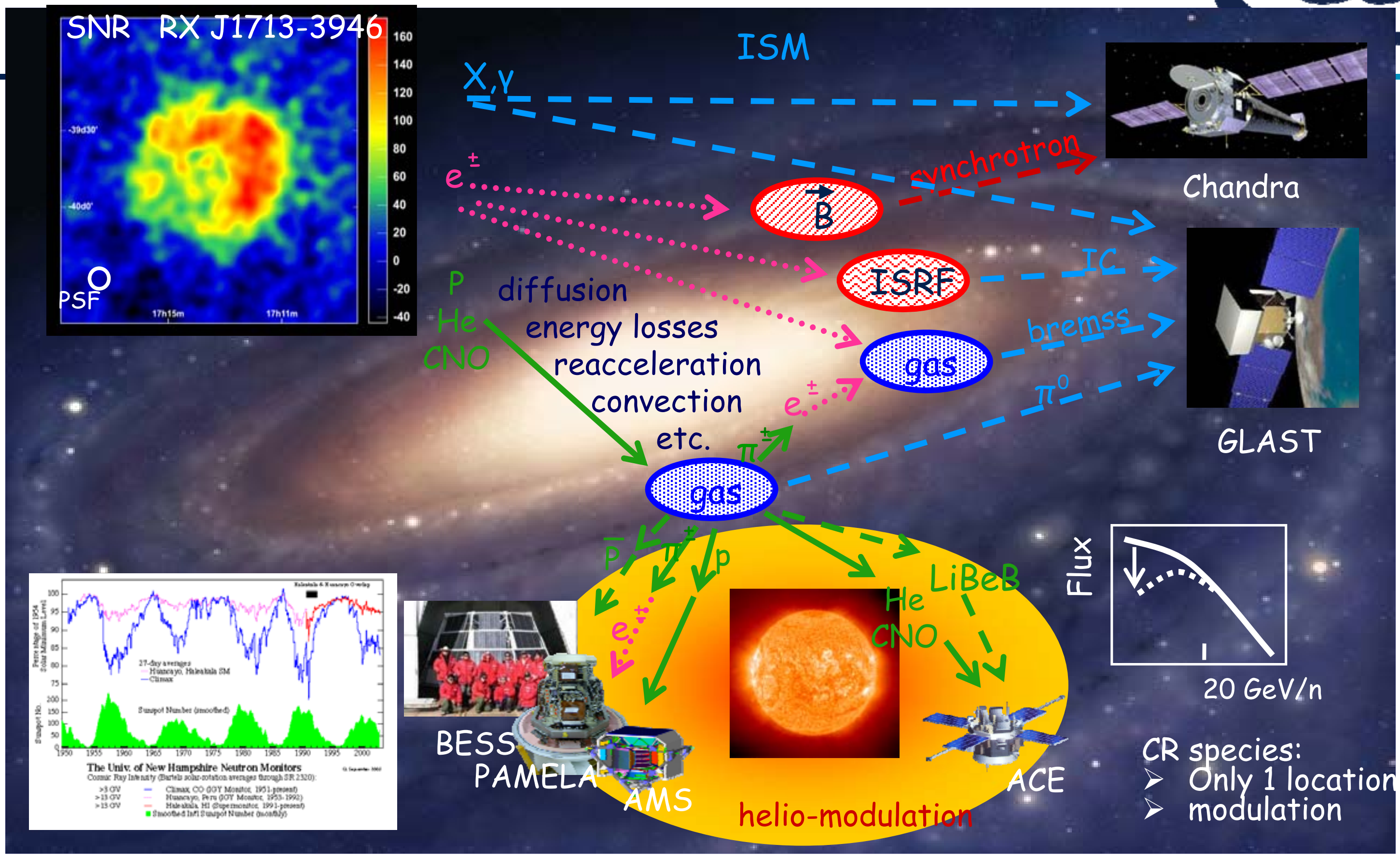

SED OF SNRs (2)

Synchrotron Radiation

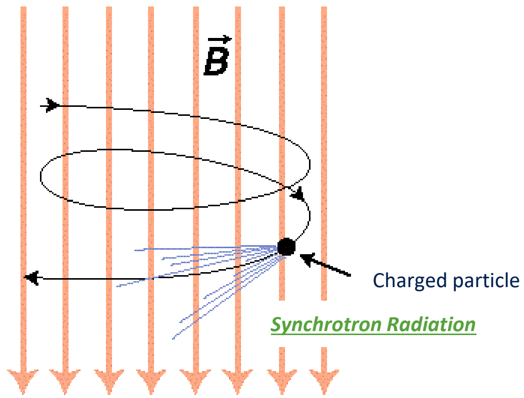

Emissivity of synchrotron radiation

$$Q_\gamma(\omega) = \frac{\sqrt{3}Be^3}{2\pi m_e c^2}\frac{4\pi}{\beta c}\int \frac{dN_e}{dE_e} R\left(\frac{\omega}{\omega_c}\right) dE_e$$

SED OF SNRs (2)

Synchrotron Radiation

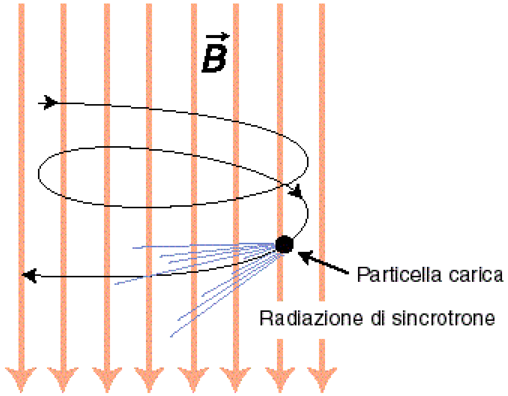

Emissivity of synchrotron radiation

$$Q_\gamma(\omega) = \frac{\sqrt{3}\,Be^3}{2\pi m_e c^2}\,\frac{4\pi}{\beta c}\int \frac{dN_e}{dE_e} R\left(\frac{\omega}{\omega_c}\right) dE_e$$

Magnetic field of Supernova Remnant

SED OF SNRs (2)

Synchrotron Radiation

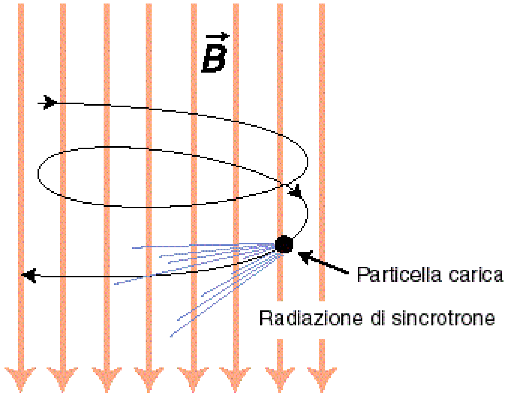

Emissivity of synchrotron radiation

$$Q_\gamma(\omega) = \frac{\sqrt{3}Be^3}{2\pi m_e c^2}\frac{4\pi}{\beta c}\int \frac{dN_e}{dE_e} R\left(\frac{\omega}{\omega_c}\right) dE_e$$

Injection of electrons

SED OF SNRs (2)

Synchrotron Radiation

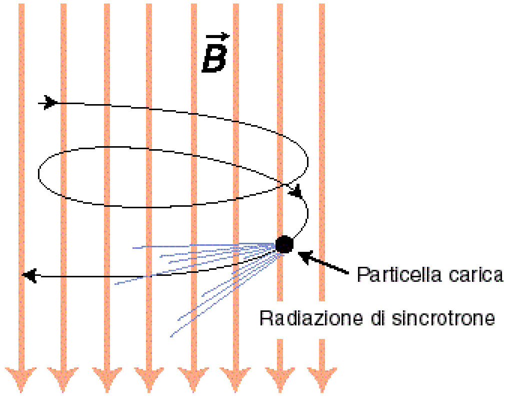

Emissivity of synchrotron radiation

$$Q_\gamma(\omega) = \frac{\sqrt{3}Be^3}{2\pi m_e c^2}\frac{4\pi}{\beta c}\int \frac{dN_e}{dE_e} R\left(\frac{\omega}{\omega_c}\right) dE_e$$

Synchrotron radiation of a single electron in magnetic field with chaotic directions

with $\omega_c = 1.5\ Bp^2/(mc)^3$ *characteristic frequency*

SED OF SNRs (3)

Inverse Compton radiation

Emissivity of inverse Compton radiation

$$Q_\gamma(E_\gamma) = \int \frac{dN_e}{dE_e} dE_e \int n(E_s)\sigma_{K-N}(E_s, E_e, E_\gamma) dE_s$$

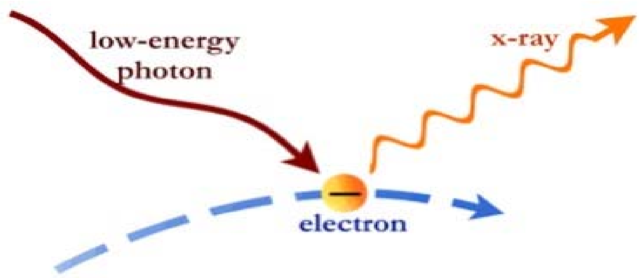

SED OF SNRs (3)

Inverse Compton radiation

Emissivity of inverse Compton radiation

$$Q_\gamma(E_\gamma) = \int \frac{dN_e}{dE_e} dE_e \int n(E_s)\sigma_{K-N}(E_s, E_e, E_\gamma) dE_s$$

Distribution of seed photons (CMB)

$$n(E_s) = \frac{15U}{(\pi kT)^4} \frac{E_s^2}{\exp\left(\frac{E_s}{kT}\right) - 1}$$

- U = 0.26 eV/cm^3
- T = 2.73 K

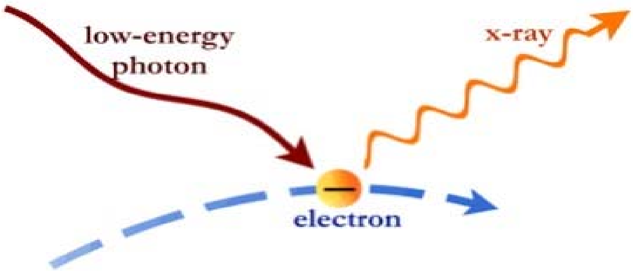

SED OF SNRs (3)

Inverse Compton radiation

Emissivity of inverse Compton radiation

$$Q_\gamma(E_\gamma) = \int \frac{dN_e}{dE_e} dE_e \int n(E_s)\sigma_{K-N}(E_s, E_e, E_\gamma) dE_s$$

Klein-Nishina cross section

$$\sigma_{K-N}(E_s, E_e, E_\gamma) = \frac{2\pi r_0^2}{E_s E_e^2}\left[2q\log_e q + 1 + q - 2q^2 + \frac{\Gamma^2 q^2 (1-q)}{2(1+\Gamma q)}\right]$$

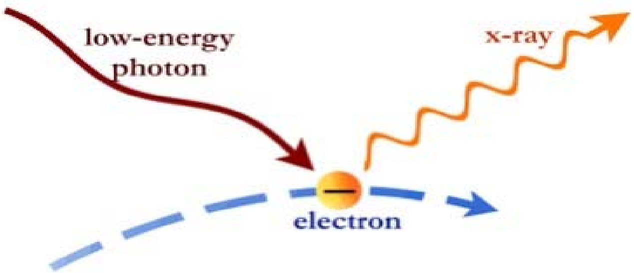

SED OF SNRs (4)

Bremsstrahlung

Emissivity of bremsstrahlung radiation

$$Q_\gamma(\varepsilon) = 4\pi n_H \int \frac{dN_e}{dE_e} \frac{d\sigma_{B-H}}{d\varepsilon} dE_e$$

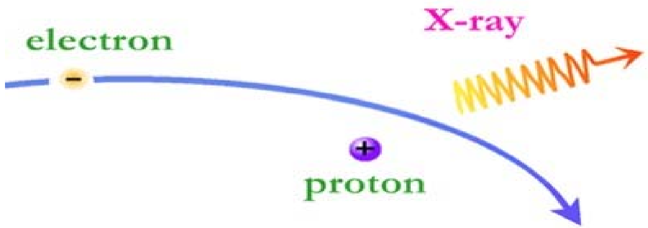

SED OF SNRs (4)

Bremsstrahlung

Emissivity of bremsstrahlung radiation

$$Q_{\gamma}(\varepsilon) = 4\pi n_H \int \frac{dN_e}{dE_e} \frac{d\sigma_{B-H}}{d\varepsilon} dE_e$$

Density of environment (protons)

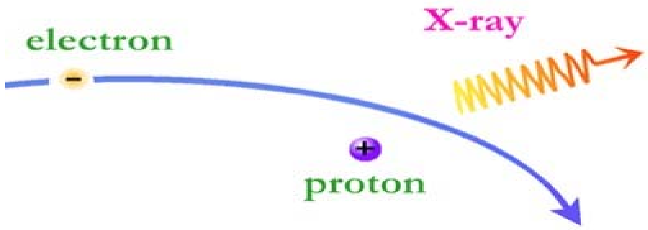

SED OF SNRs (4)

Bremsstrahlung

Emissivity of bremsstrahlung radiation

$$Q_\gamma(\varepsilon) = 4\pi n_H \int \frac{dN_e}{dE_e} \frac{d\sigma_{B-H}}{d\varepsilon} dE_e$$

Bethe-Heitler ultra-relativistic cross section

$$\frac{d\sigma}{d\varepsilon} = 4\frac{\alpha_f r_0^2}{\varepsilon}\left[1+\left(\frac{\gamma-\varepsilon}{\gamma}\right)^2 - \frac{2}{3}\frac{\gamma-\varepsilon}{\gamma}\right]\left[\log\frac{2\gamma(\gamma-\varepsilon)}{\varepsilon} - \frac{1}{2}\right]$$

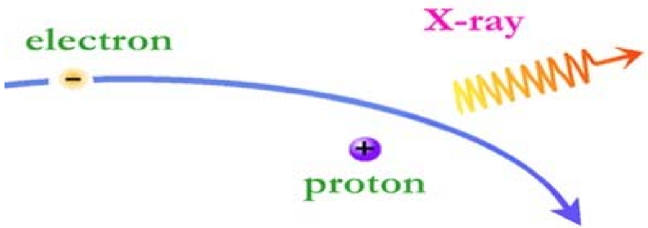

SED OF SNRs (5)

π^0 decay

$$p + p \rightarrow \pi^0 + X$$

$$\hookrightarrow \gamma + \gamma$$

Emissivity of photons produced in p-p interaction

$$Q_\gamma(E_\gamma) = \frac{4\pi}{\beta c} n_H \int \frac{dN_p}{dE_p} \frac{d\sigma(E_p / E_\gamma)}{dE_\gamma} dE_p$$

SED OF SNRs (5)

π^0 decay

$$p + p \rightarrow \pi^0 + X$$
$$\hookrightarrow \gamma + \gamma$$

Emissivity of photons produced in p-p interaction

$$Q_\gamma(E_\gamma) = \frac{4\pi}{\beta c} n_H \int \frac{dN_p}{dE_p} \frac{d\sigma(E_p / E_\gamma)}{dE_\gamma} dE_p$$

Injection of protons

SED OF SNRs (5)

π^0 decay

$$p + p \rightarrow \pi^0 + X$$
$$\quad \rightarrow \gamma + \gamma$$

Emissivity of photons produced in p-p interaction

$$Q_\gamma(E_\gamma) = \frac{4\pi}{\beta c} n_H \int \frac{dN_p}{dE_p} \frac{d\sigma(E_p / E_\gamma)}{dE_\gamma} dE_p$$

Kamae et al. (2006)
cross section

- Non-diffrattive interaction ;
- Diffractive interaction;
- Eccitation of resonance Δ(1232);
- Eccitation of resonance res (1600).

$$\frac{d\sigma(E_\gamma \mid E_p)}{d\left(\log E_\gamma\right)} = F(x) F_{kl}(x)$$

Flusso dei raggi γ a Terra

$$F_{\gamma,SNR} = Q_{\gamma} \frac{V_{SNR}}{4\pi d^2}$$

Flusso dei raggi γ a Terra

$$F_{\gamma,SNR} = Q_{\gamma}\frac{V_{SNR}}{4\pi d^2}$$

Volume of the SNR

Flusso dei raggi γ a Terra

$$F_{\gamma,SNR} = Q_{\gamma} \frac{V_{SNR}}{4\pi d^2}$$

Distance from the Earth

Range energetico:
20 MeV – 300 GeV

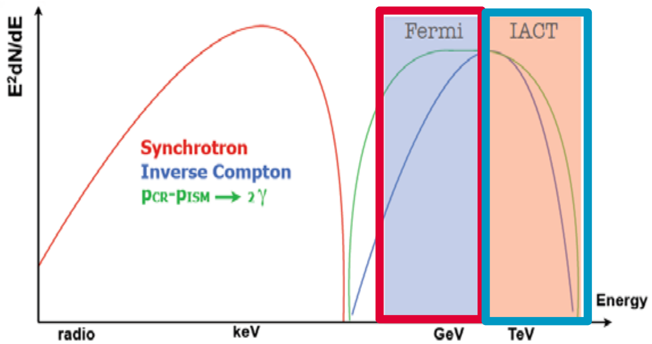

Satellite are able to discriminate hadronic vs leptonic emission

IACT determine maximum enrgy, roll off of teh spectrum, test accelration processes at theri extreeme phase

γ ray SPECTRA (1)

Injection

$$\frac{dN_{e,p}}{dE_{e,p}} = A_{e,p}\left(\frac{E_{e,p}}{E_0}\right)^{-\gamma_{1;e,p}}\left[1+\left(\frac{E_{e,p}}{E_{br;e,p}}\right)^{\frac{(\gamma_{2;e,p}-\gamma_{1;e,p})}{\gamma_{3;e,p}}}\right]^{-\gamma_{3;e,p}}$$

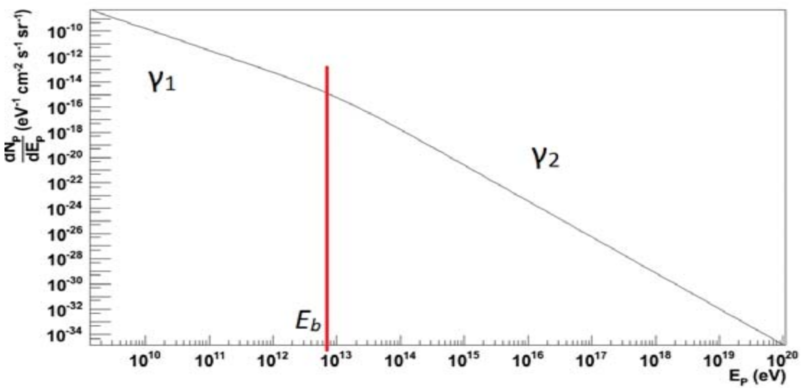

γ ray SPECTRA (1)

$$\frac{dN_{e,p}}{dE_{e,p}} = A_{e,p}\left(\frac{E_{e,p}}{E_0}\right)^{-\gamma_{1;e,p}}\left[1+\left(\frac{E_{e,p}}{E_{br;e,p}}\right)^{\frac{(\gamma_{2;e,p}-\gamma_{1;e,p})}{\gamma_{3;e,p}}}\right]^{-\gamma_{3;e,p}}$$

Normalization:
Linked to the efficiency
of the process

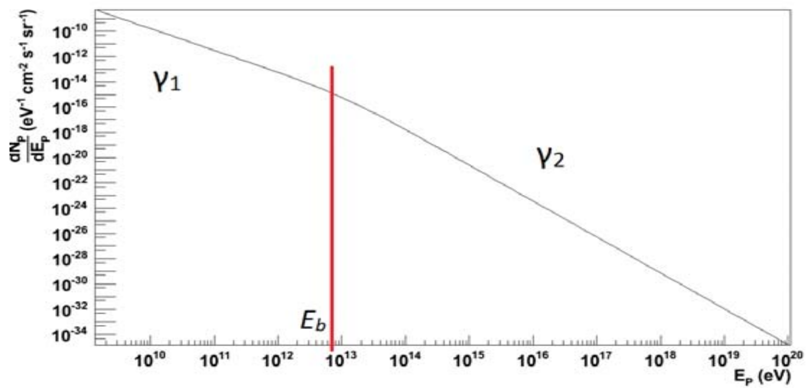

γ ray SPECTRA (1)

$$\frac{dN_{e,p}}{dE_{e,p}} = A_{e,p}\left(\frac{E_{e,p}}{E_0}\right)^{-\gamma_{1;e,p}}\left[1+\left(\frac{E_{e,p}}{E_{br;e,p}}\right)^{\frac{(\gamma_{2;e,p}-\gamma_{1;e,p})}{\gamma_{3;e,p}}}\right]^{-\gamma_{3;e,p}}$$

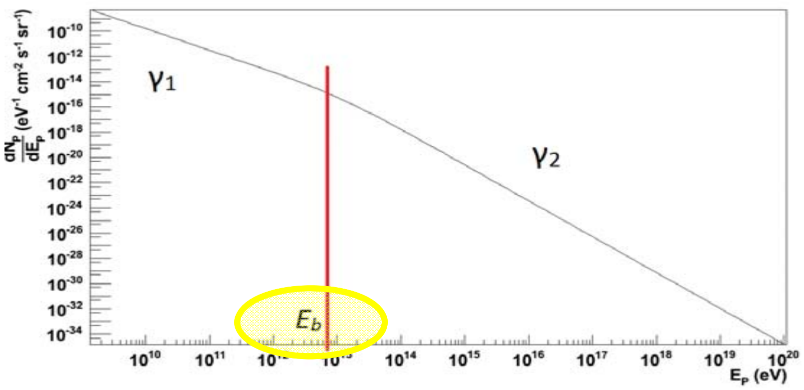

Maximum energy allowed

SPETTRI γ DEGLI SNR (1)

Energy distribution

$$\frac{dN_{e,p}}{dE_{e,p}} = A_{e,p}\left(\frac{E_{e,p}}{E_0}\right)^{-\gamma_{1;e,p}}\left[1+\left(\frac{E_{e,p}}{E_{br;e,p}}\right)^{\frac{(\gamma_{2;e,p}-\gamma_{1;e,p})}{\gamma_{3;e,p}}}\right]^{-\gamma_{3;e,p}}$$

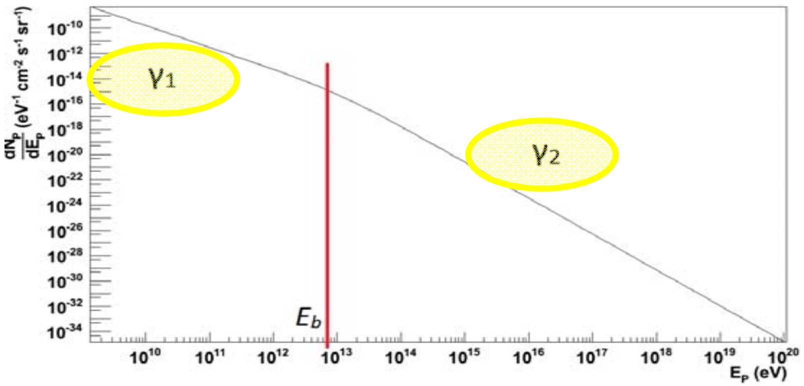

Spectral indexes:
$\gamma_2 > \gamma_1$, $\gamma_3 = 1$

SPETTRI γ DEGLI SNR (1)

Energy Distribution

$$\frac{dN_{e,p}}{dE_{e,p}} = A_{e,p}\left(\frac{E_{e,p}}{E_0}\right)^{-\gamma_{1;e,p}}\left[1+\left(\frac{E_{e,p}}{E_{br;e,p}}\right)^{\frac{(\gamma_{2;e,p}-\gamma_{1;e,p})}{\gamma_{3;e,p}}}\right]^{-\gamma_{3;e,p}}$$

- $E_0 = 10$ GeV
- $\gamma_{3;\,e,p} = 1$

Main parameters

- $A_{e,p}$
- $E_{br;e,p}$
- $\gamma_{1;e,p}$; $\gamma_{2;e,p}$

SPETTRI γ DEGLI SNR (2)

Tycho SNR

- ***SN 1572***
- ***SN type:*** Ia
- ***Age:*** 349 anni
- ***Distance:*** ~ 3.5 kpc
- ***Radius:*** ~ 3.7 pc
- n_H = 0.24 cm^{-3}

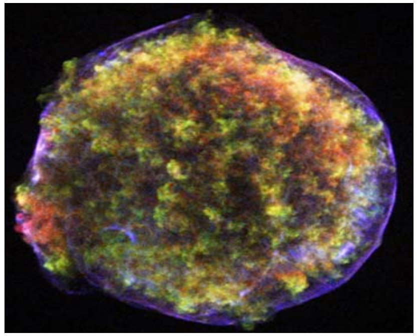

Immagine raggi-X (Chandra)

SPETTRI γ DEGLI SNR (2)

Tycho SNR

- ***SN 1572***
- ***SN type:*** Ia
- ***Age:*** 349 anni
- ***Distance:*** ~ 3.5 kpc
- ***Radius:*** ~ 3.7 pc
- n_H = 0.24 cm^{-3}

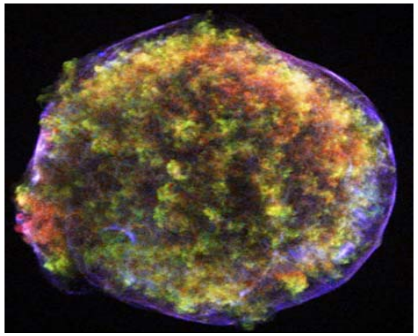

Immagine raggi-X (Chandra)

Elettroni

- A_e = (1.40±0.12)·10^{-11} eV^{-1} cm^{-2} s^{-1} sr^{-1}
- $E_{br,e}$ = (1.24±0.13) TeV
- $\gamma_{1,e}$ = 2.16±0.05
- $\gamma_{2,e}$ = 4.57±0.39
- W_e = (7.29±0.63)·10^{46} erg

Protoni

- A_p = (1.32±o.26)·10^{-8} eV^{-1} cm^{-2} s^{-1} sr^{-1}
- $E_{br,p}$ = 5.64 TeV
- $\gamma_{1,p}$ = 2.24±0.07
- $\gamma_{2,p}$ = 2.24±0.13
- W_p = (5.47±0.81)·10^{49} erg

SPETTRI γ DEGLI SNR (2)

Tycho SNR

- ***SN 1572***
- ***SN type:*** Ia
- ***Età:*** 349 anni
- ***Distanza:*** ~ 3.5 kpc
- ***Raggio:*** ~ 3.7 pc
- n_H = 0.24 cm^{-3}

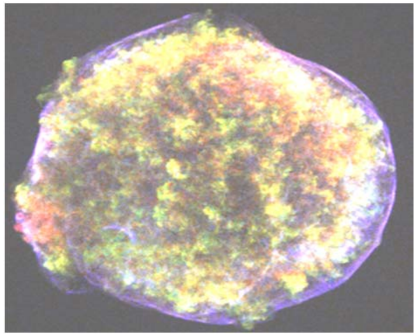

Immagine raggi-X (Chandra)

Elettroni

- A_e = (1.40±0.12)·10^{-11} eV^{-1} cm^{-2} s^{-1} sr^{-1}
- $E_{br,e}$ = (1.24±0.13) TeV
- $\gamma_{1,e}$ = 2.16±0.05
- $\gamma_{2,e}$ = 4.57±0.39
- W_e = (7.29±0.63)·10^{46} e

Pro

- A_p = (1.32±o.26)·10^{-8} eV^{-1} cm^{-2} s^{-1} sr^{-1}
- $E_{br,p}$ = 5.64 TeV
- $\gamma_{1,p}$ = 2.24±0.07
- $\gamma_{2,p}$ = 2.24±0.13
- W_p = (5.47±0.81)·10^{49} erg

Efficiency

$$W_{e,p} = \rho_{e,p} V_{SNR}$$

SPETTRI γ DEGLI SNR (2)

Tycho SNR

- ***SN 1572***
- ***SN type:*** Ia
- ***Età:*** 349 anni
- ***Distanza:*** ~ 3.5 kpc
- ***Raggio:*** ~ 3.7 pc
- n_H = 0.24 cm^{-3}

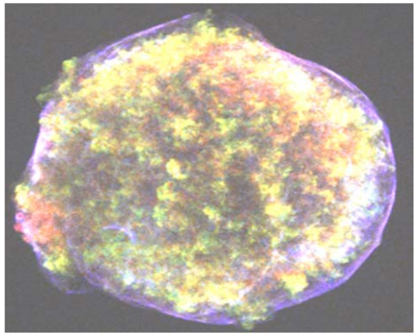

Immagine raggi-X (Chandra)

Elettroni

- $A_e = (1.40 \pm 0.12) \cdot 10^{-11}\ eV^{-1}\ cm^{-2}\ s^{-1}\ sr^{-1}$
- $E_{br,e} = (1.24 \pm 0.13)$ TeV
- $\gamma_{1,e} = 2.16 \pm 0.05$
- $\gamma_{2,e} = 4.57 \pm 0.39$
- $W_e = (7.29 \pm 0.63) \cdot 10^{46}$ e

Pro

- $A_p = (1.32 \pm 0.26) \cdot 10^{-8}$ eV
- $E_{br,p} = 5.64$ TeV
- $\gamma_{1,p} = 2.24 \pm 0.07$
- $\gamma_{2,p} = 2.24 \pm 0.13$
- $W_p = (5.47 \pm 0.81) \cdot 10^{49}$ erg

Efficienza

$$W_{e,p} = \rho_{e,p} V_{SNR}$$

$$\rho_{e,p} = \frac{4\pi}{\beta c} \int E_{e,p} \frac{dN_{e,p}}{dE_{e,p}} dE_{e,p}$$

SPETTRI γ DEGLI SNR (2)

Tycho SNR

- ***SN 1572***
- ***SN type:*** Ia
- ***Age:*** 349 anni
- ***Distance:*** ~ 3.5 kpc
- ***Radius:*** ~ 3.7 pc
- $\boldsymbol{n_H}$ = 0.24 cm^{-3}

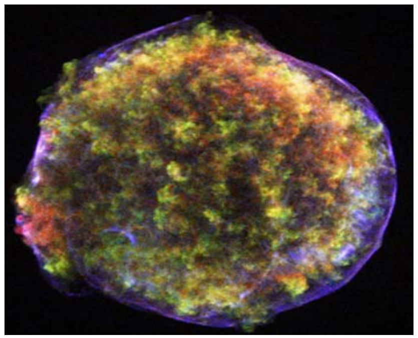

Immagine raggi-X (Chandra)

Elettroni

- A_e = (1.40±0.12)·10^{-11} $eV^{-1}\,cm^{-2}\,s^{-1}\,sr^{-1}$
- $E_{br,e}$ = (1.24±0.13) TeV
- $\gamma_{1,e}$ = 2.16±0.05
- $\gamma_{2,e}$ = 4.57±0.39
- W_e = (7.29±0.63)·10^{46} erg

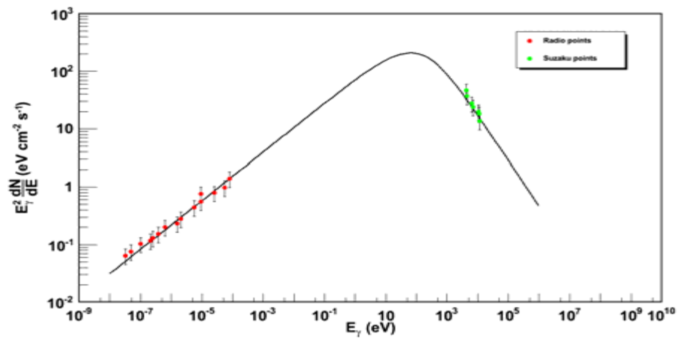

SPETTRI γ DEGLI SNR (2)

Tycho SNR

- ***SN 1572***
- ***SN type:*** Ia
- ***Age:*** 349 anni
- ***Distance:*** ~ 3.5 kpc
- ***Radius:*** ~ 3.7 pc
- $n_H = 0.24\ cm^{-3}$

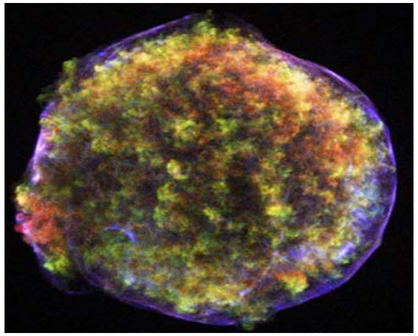

Immagine raggi-X (Chandra)

Protoni

- $A_p = (1.32 \pm 0.26) \cdot 10^{-8}\ eV^{-1}\ cm^{-2}\ s^{-1}\ sr^{-1}$
- $E_{br,p} = 5.64$ TeV
- $\gamma_{1,p} = 2.24 \pm 0.07$
- $\gamma_{2,p} = 2.24 \pm 0.13$
- $W_p = (5.47 \pm 0.81) \cdot 10^{49}$ erg

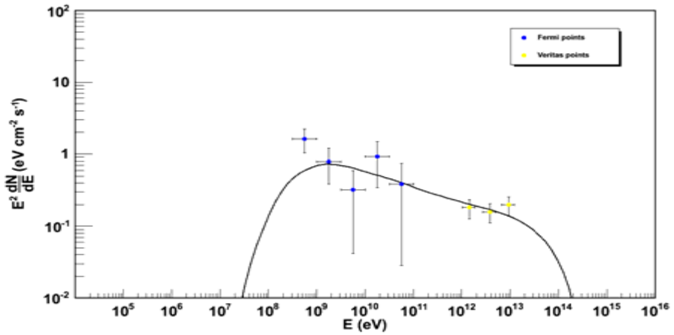

SPETTRI γ DEGLI SNR (2)

Tycho SNR

SED

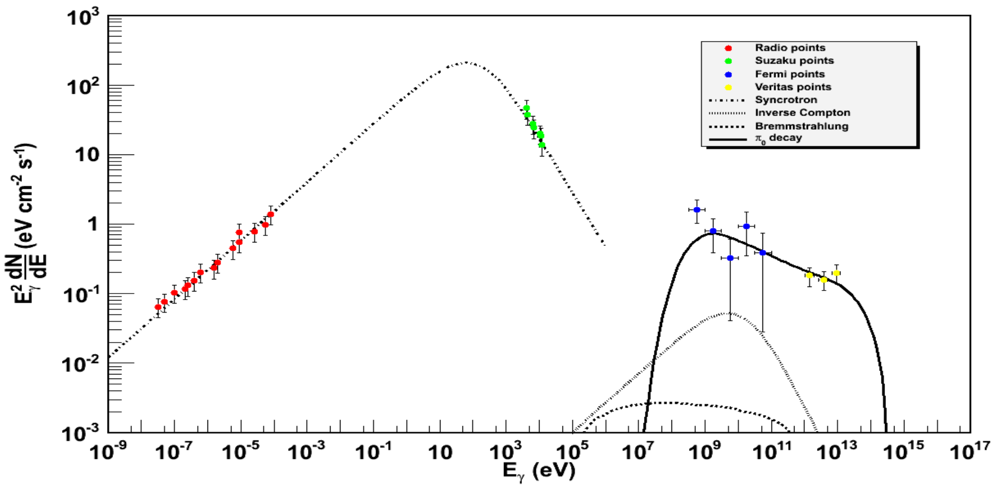

SED OF SNRs (1)

Spectrum Energy Distribution (SED)

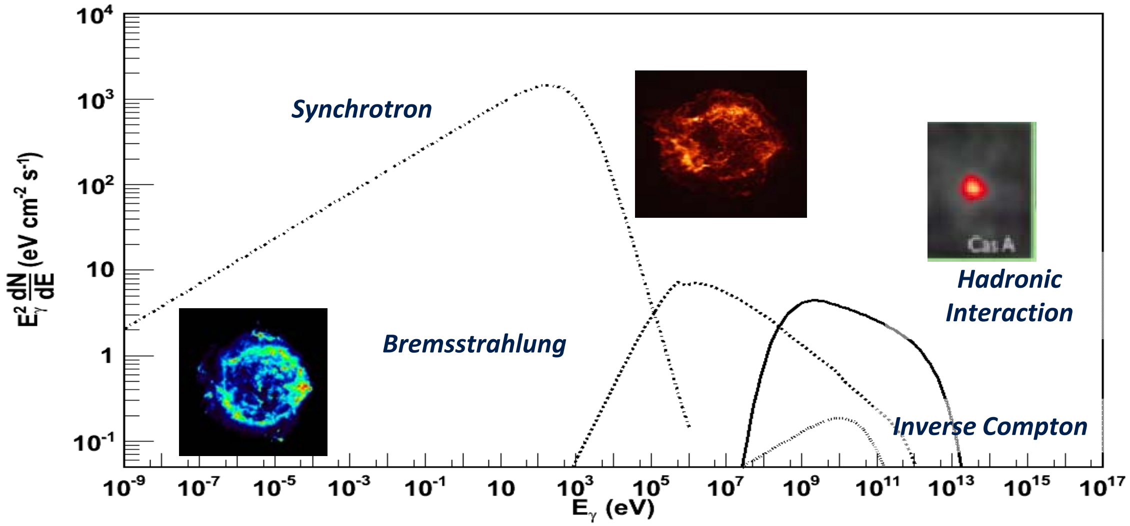

Transparency of the atmosphere

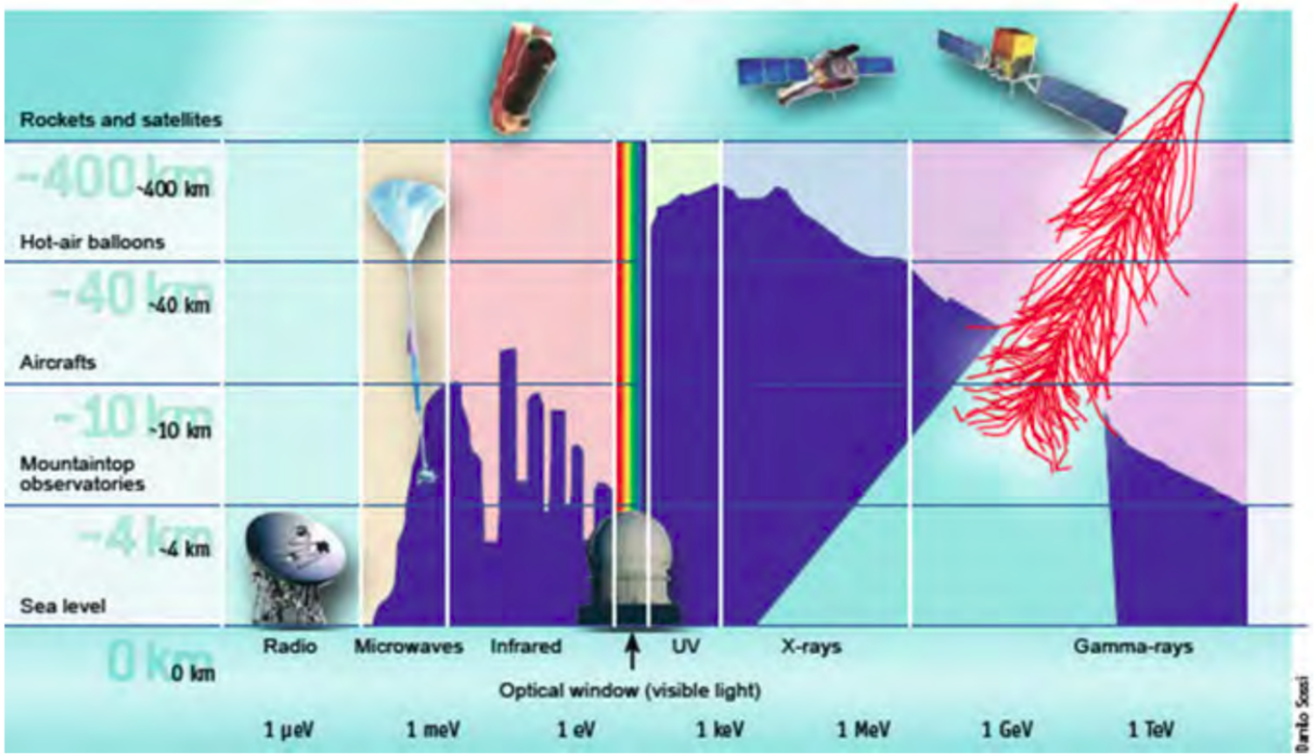

LAT overview

Si-strip Tracker (TKR)
18 planes XY ~ 1.7 x 1.7 m^2 w/ converter
Single-sided Si strips 228 μm pitch, ~10^6 channels
Measurement of the gamma direction

AntiCoincidence Detector (ACD)
89 scintillator tiles around the TKR
Reduction of the background from charged particles

Astroparticle groups INFN/University Bari, Padova, Perugia, Pisa, Roma2, Udine/Trieste

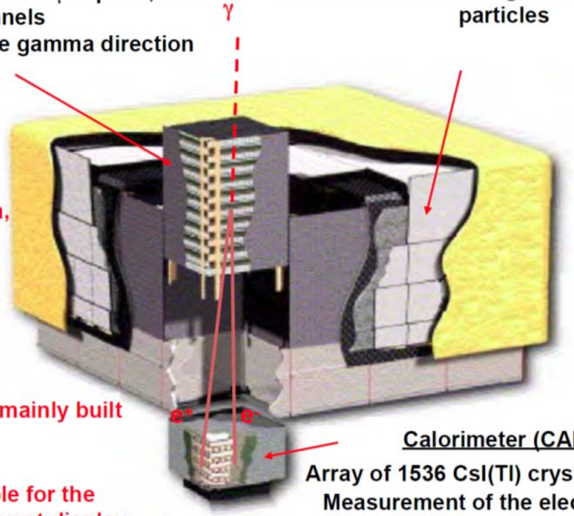

The Silicon tracker is mainly built in Italy

Italy is also responsible for the detector simulation, event display and GRB physics

Calorimeter (CAL)
Array of 1536 CsI(Tl) crystals in 8 layers
Measurement of the electron energy

Launch!

- Launch from Cape Canaveral Air Station 11 June 2008 at 12:05PM EDT
- Circular orbit, 565 km altitude (96 min period), 25.6 deg inclination.

Detection of a gamma-ray

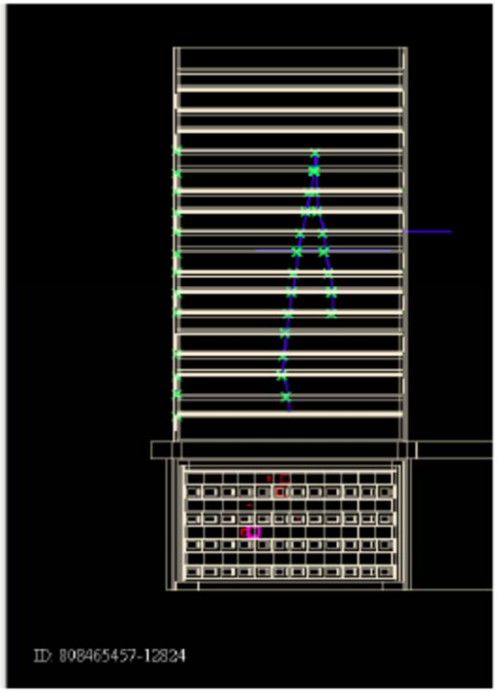

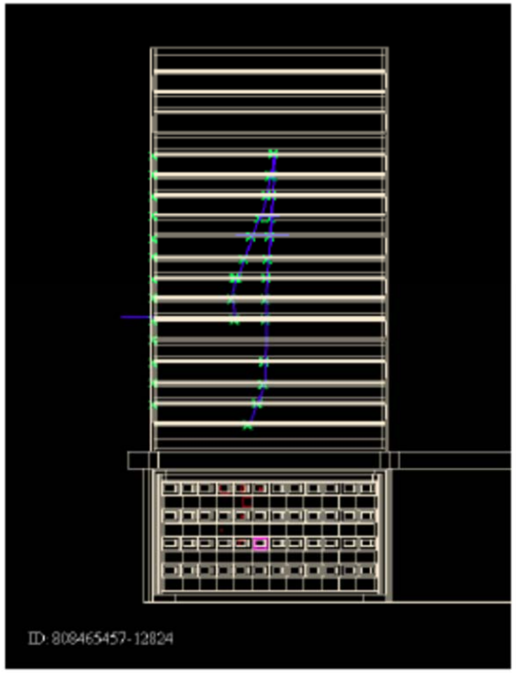

LAT 4-year Point Source Catalog (3FGL)

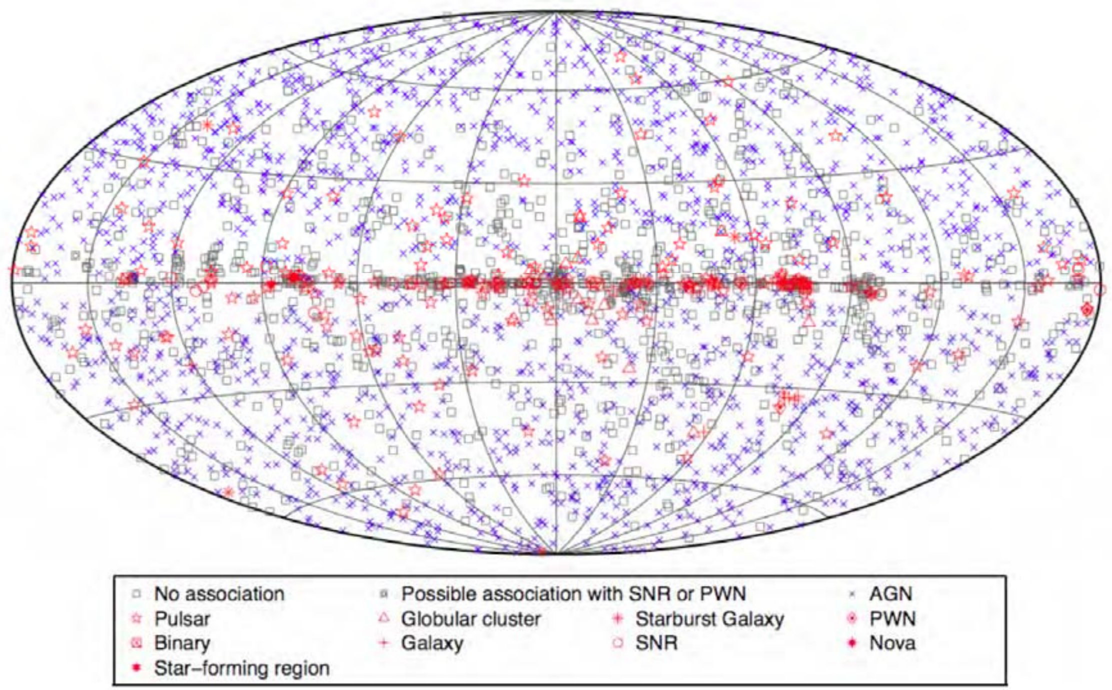

Performance of Fermi (Pass 8)

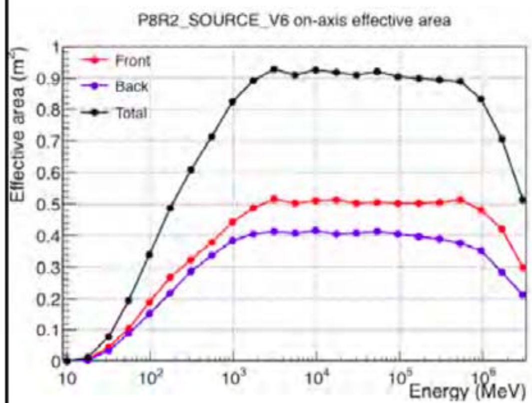

Effective area (Area x efficiency)

~ $1m^2$

Grows as k lnE from 2 MeV to 2 GeV
Then ~0.9 m^2 from 2 GeV to 700 GeV
Then decreases as k' lnE

Acceptance: 2.5 sr

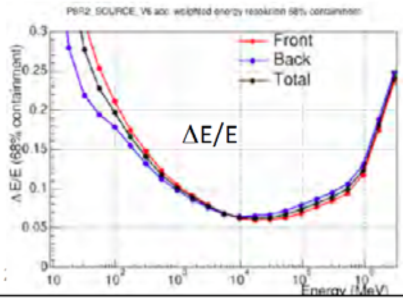

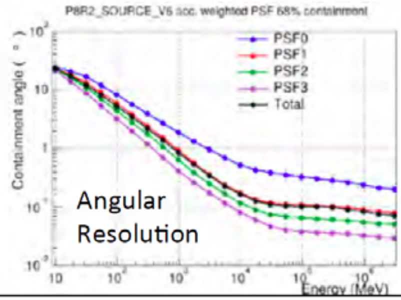

Padova :

First clear hadronic signature

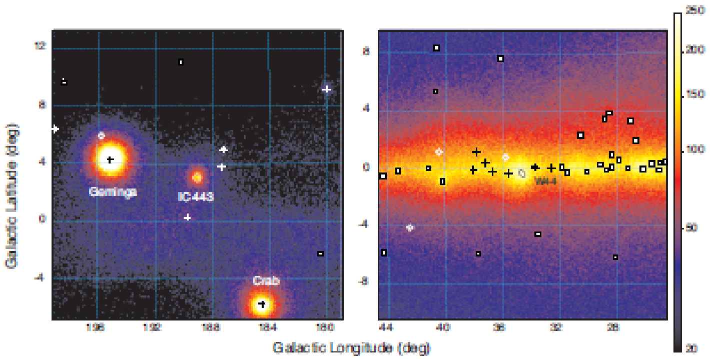

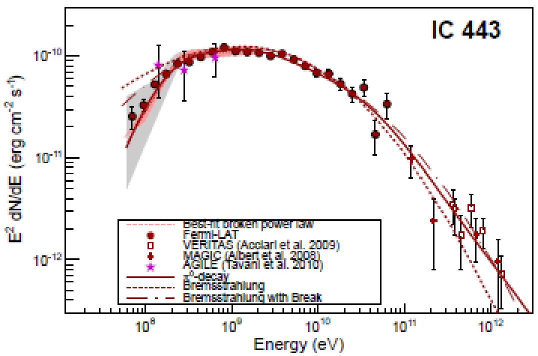

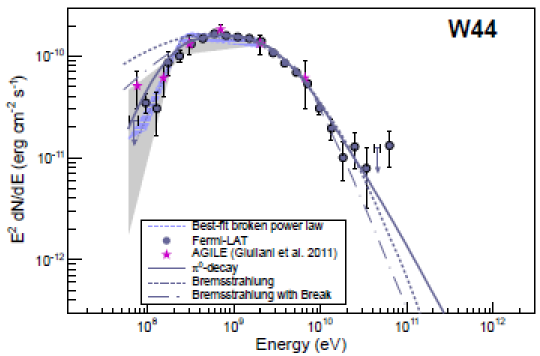

Morphology and spectra

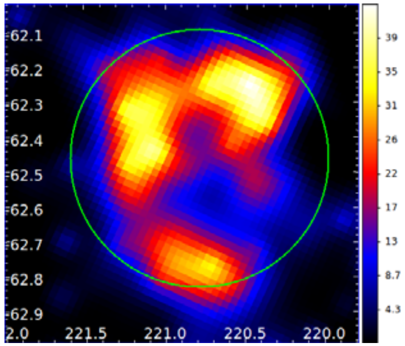

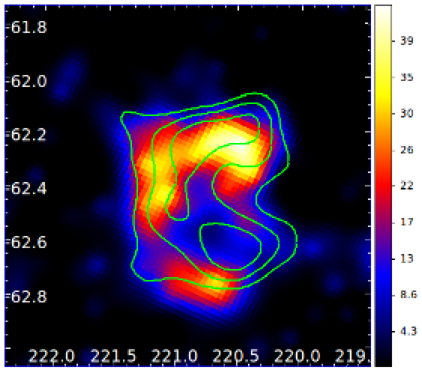

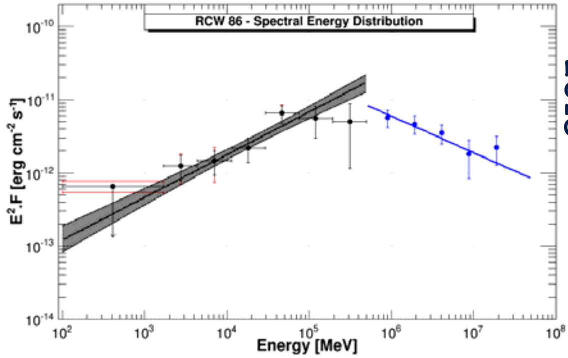

ICRC 2015

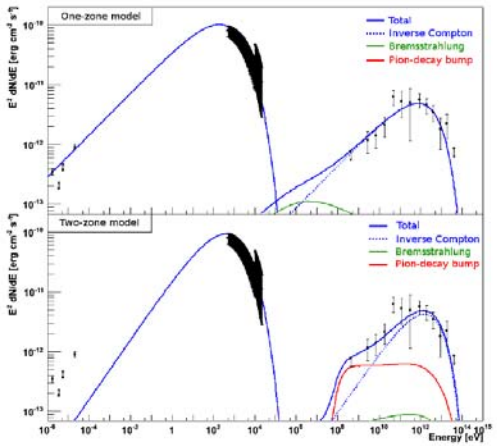

GeV γ-rays sky by Fermi

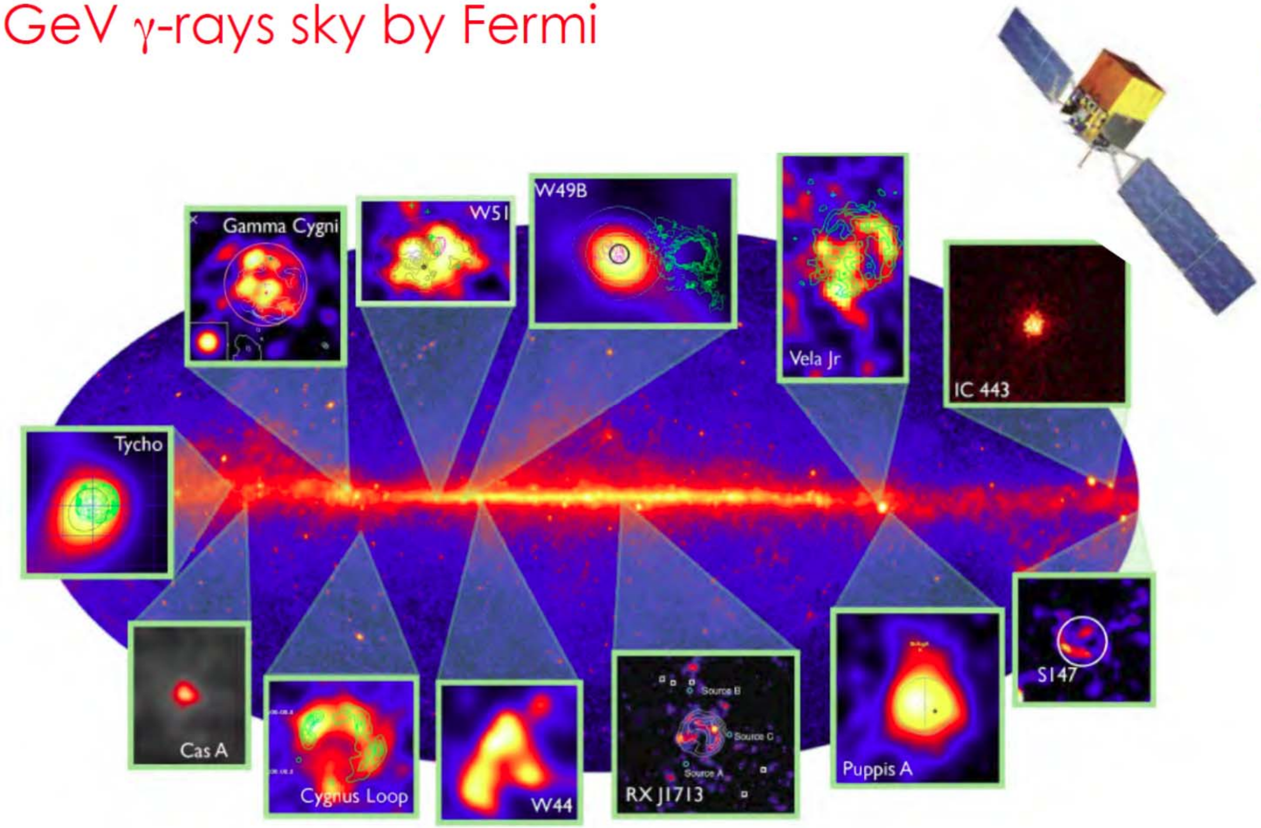

The sky >50GeV

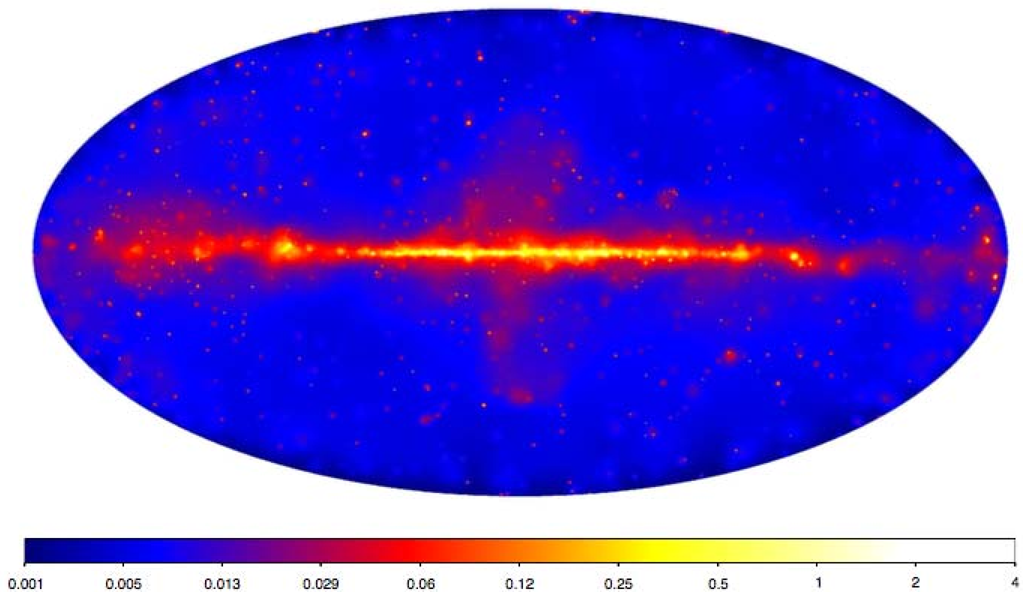

And sources above 50GeV

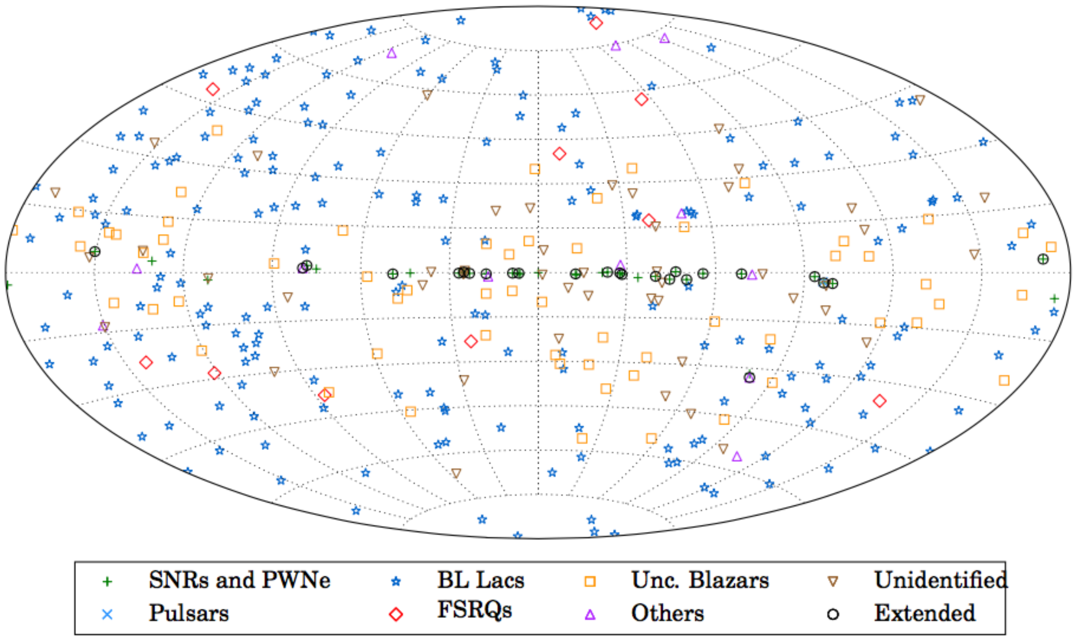

The VHE Galaxy

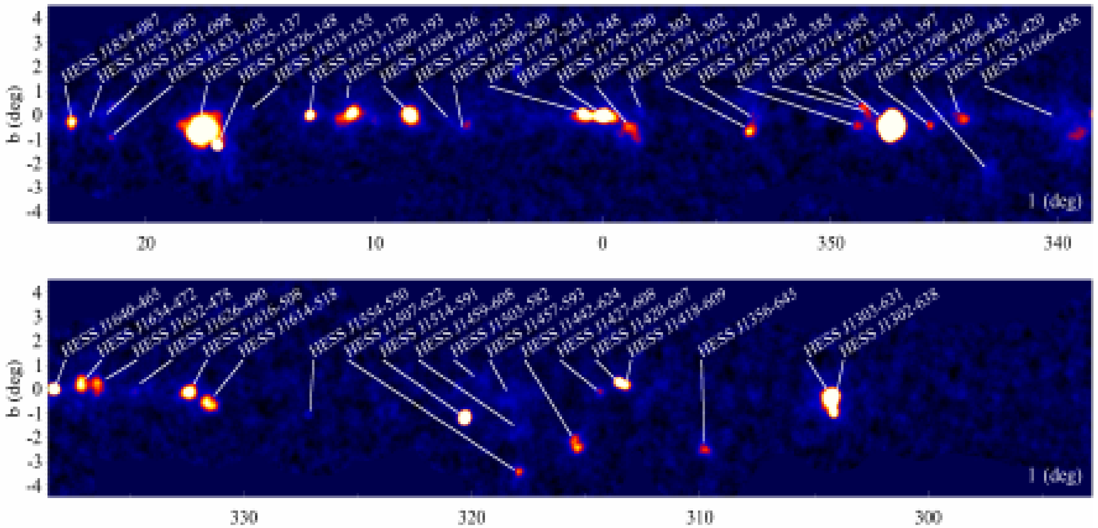

Source count evolution

1989: 1 source (Whipple)
2000: 10 sources (Whipple/HEGRA/Durham)
2010: 100 sources (HESS, MAGIC, VERITAS)
2020: 1000 sources (CTA)?

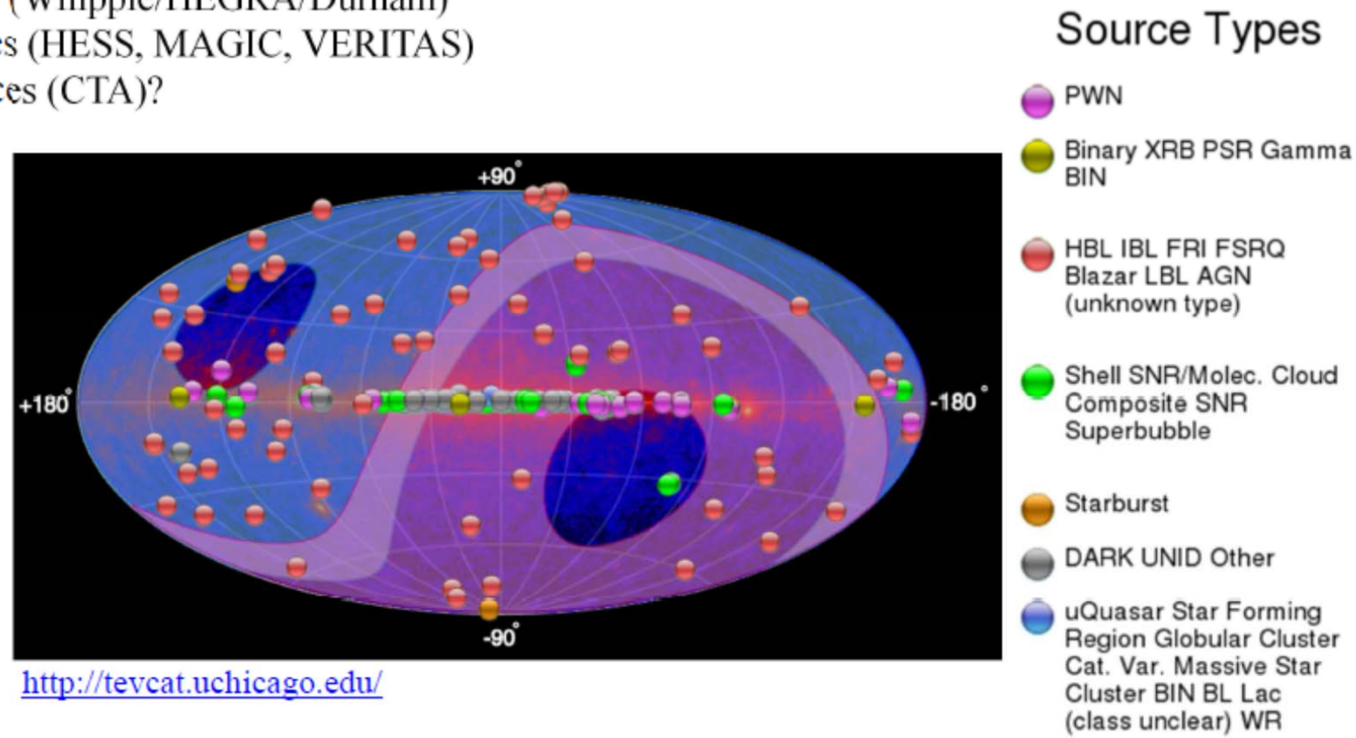

http://tevcat.uchicago.edu/

The IACT Precision

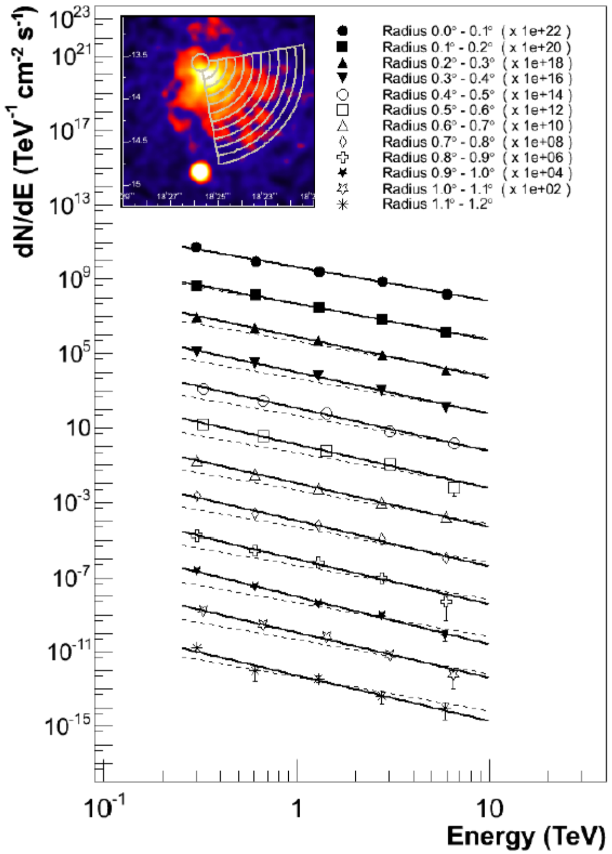

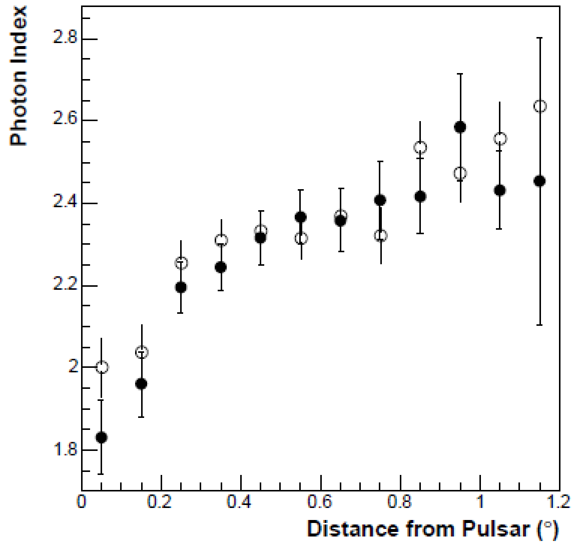

The CTA Predictions - I

order of magnitude improvement in sensitivity over HESS and VERITAS

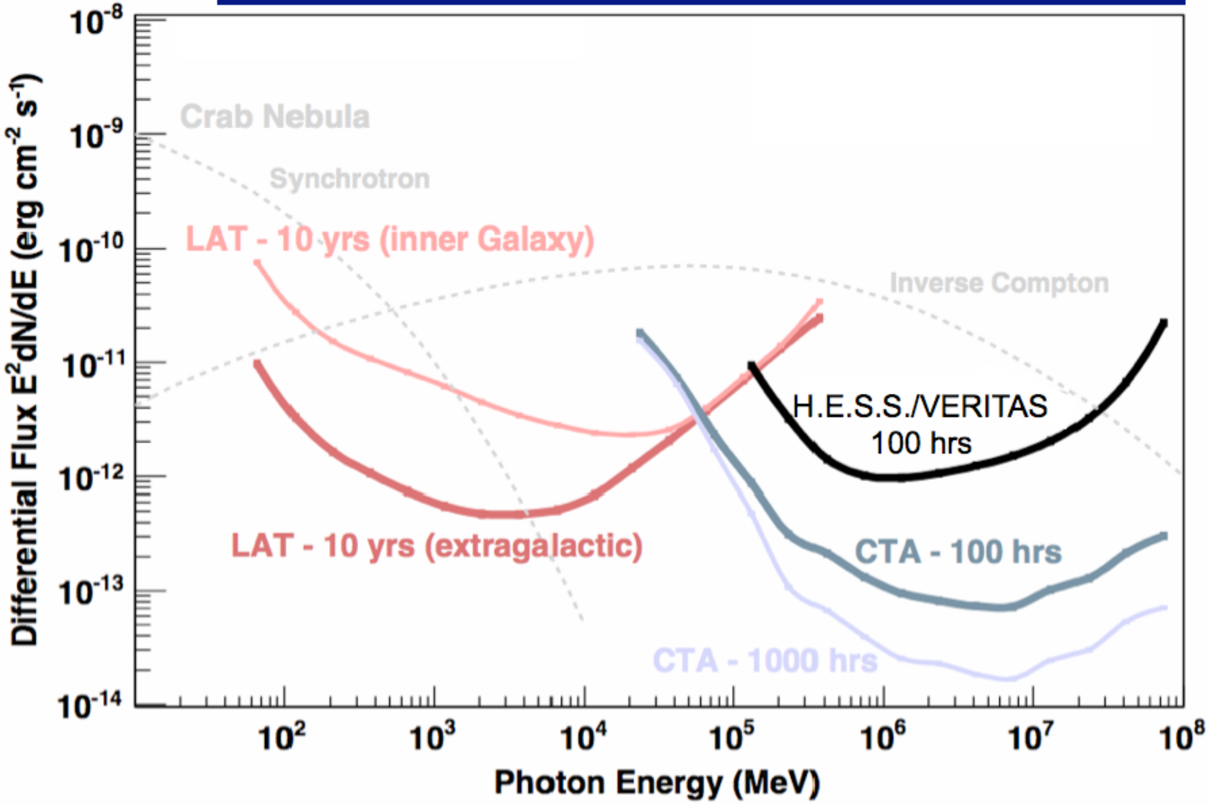

The CTA Predictions - II

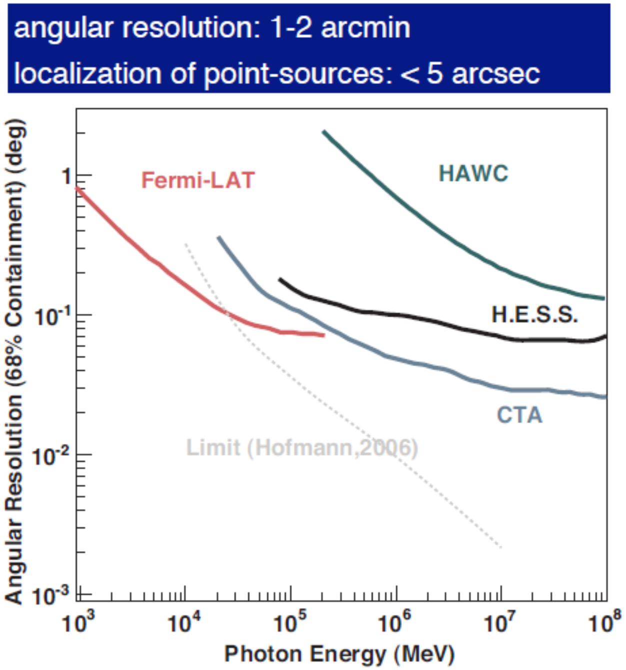

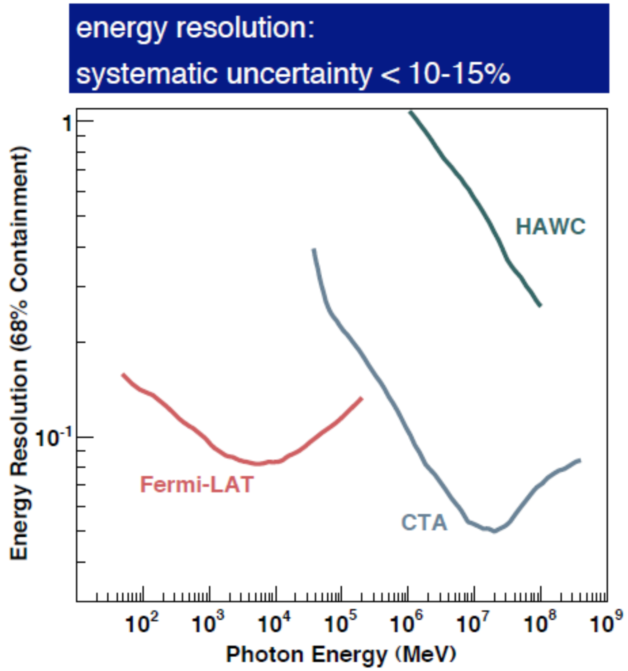

plane surveyed to < 3.8 mCrab - several 100's of sources

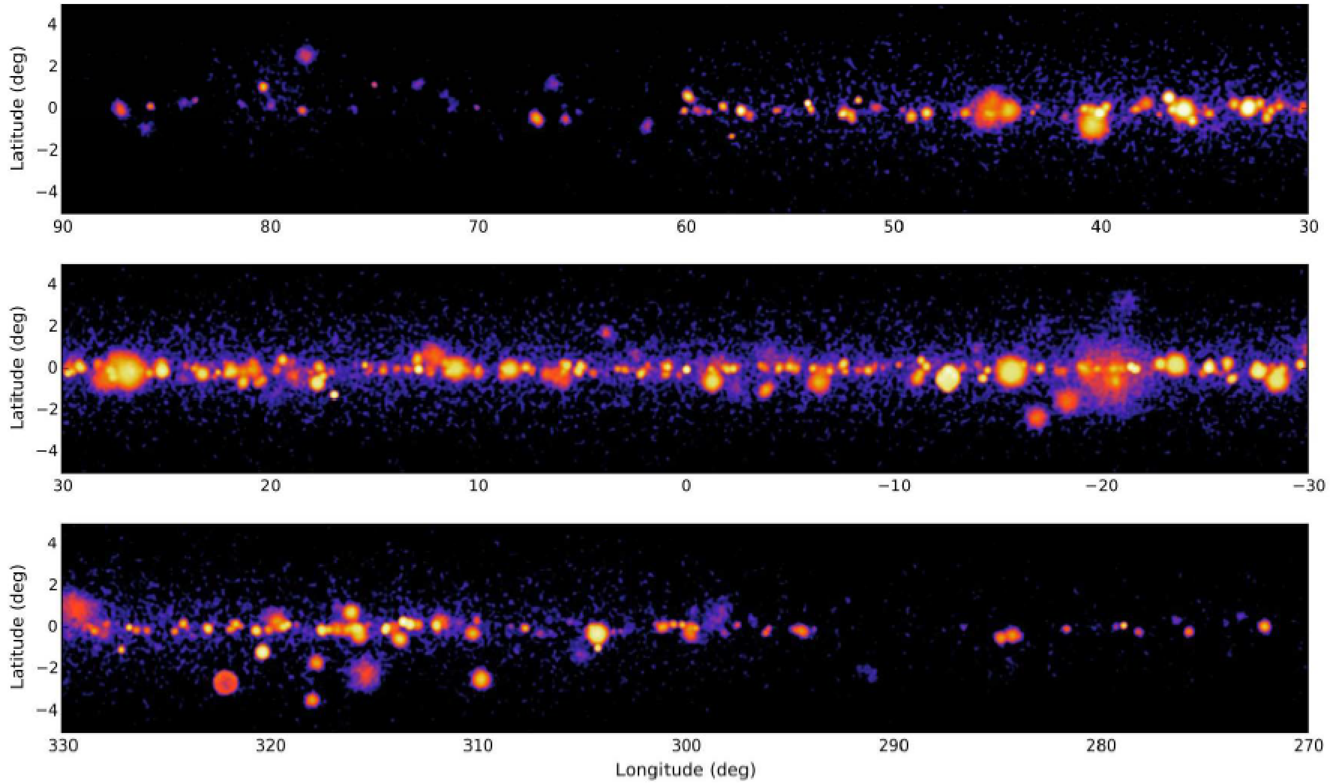

One important guy: the RXJ1713

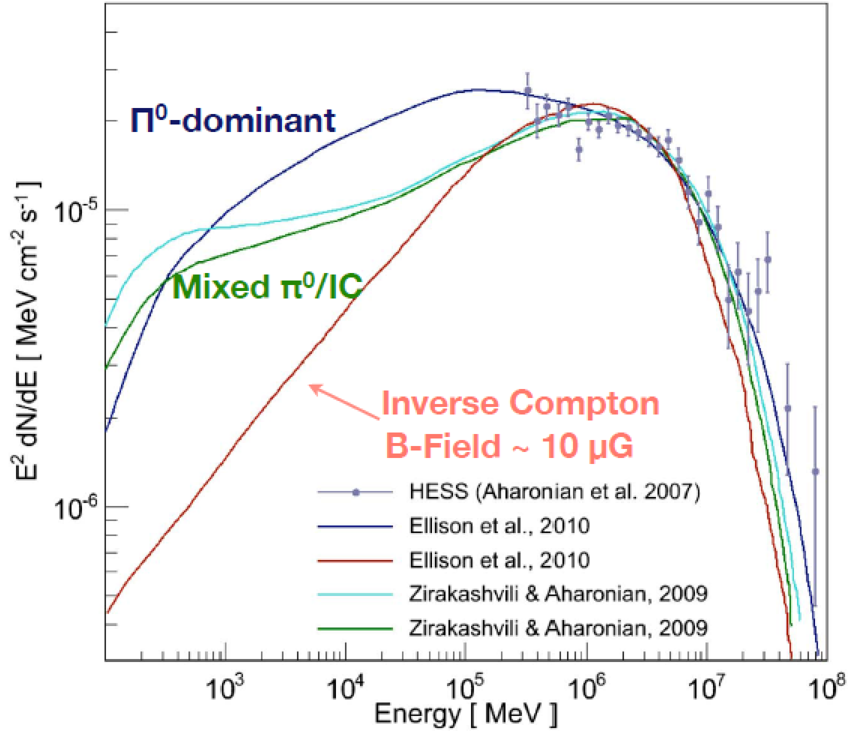

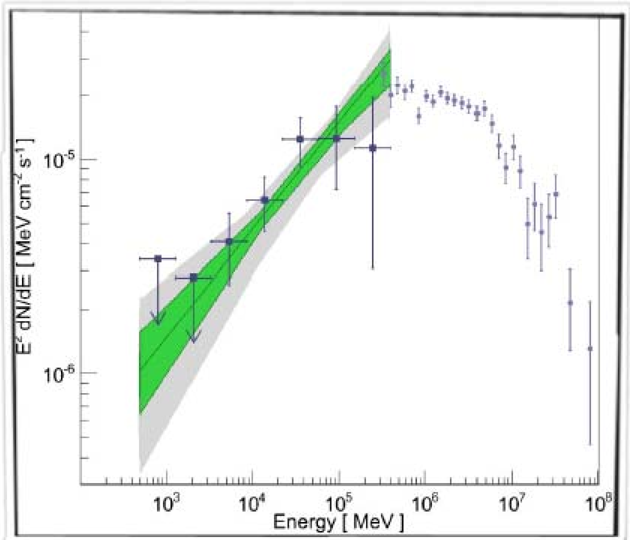

E^2 dN/dE [MeV cm^{-2} s^{-1}]
10^{-5}
10^{-6}
10^3
10^4
10^5
10^6
10^7
10^8
Energy [MeV]

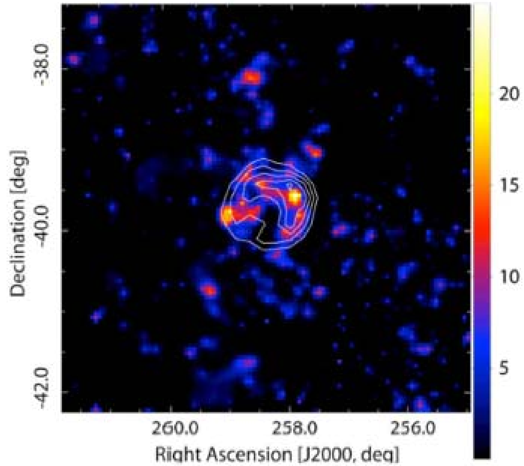

Declination [deg]
-38.0
-40.0
-42.0
260.0
258.0
256.0
Right Ascension [J2000, deg]
20
15
10
5

Hadronic or leptonic

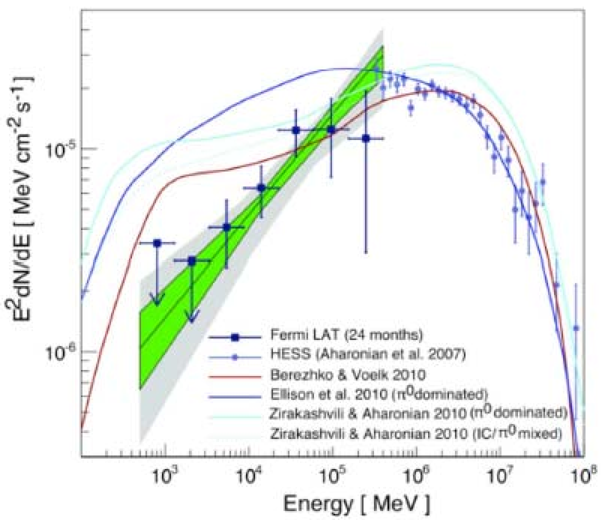

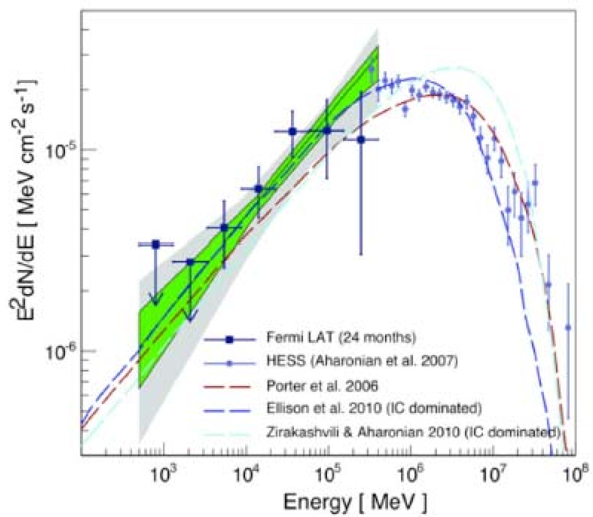

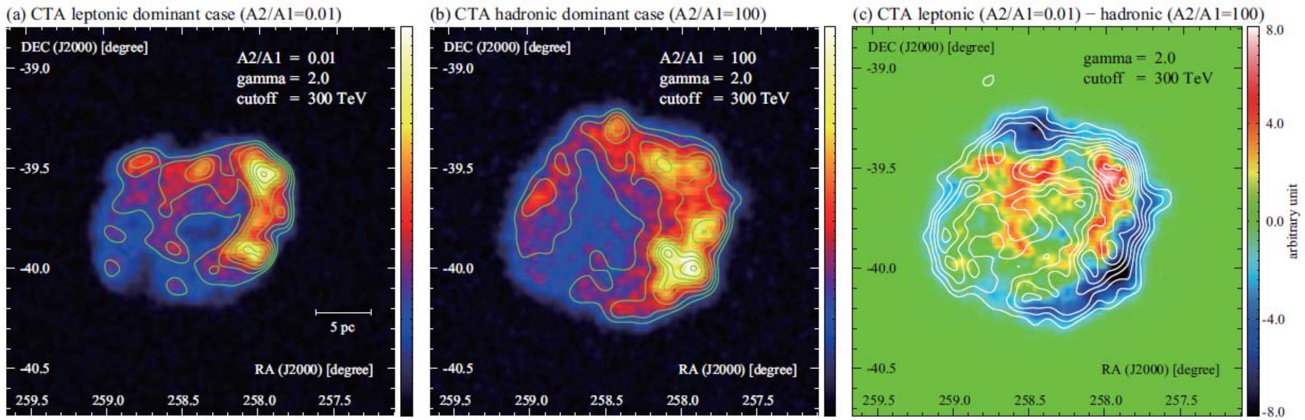

Xmm
contours

CO and HI

Difference + Hess

50 hrs, 1-100 TeV

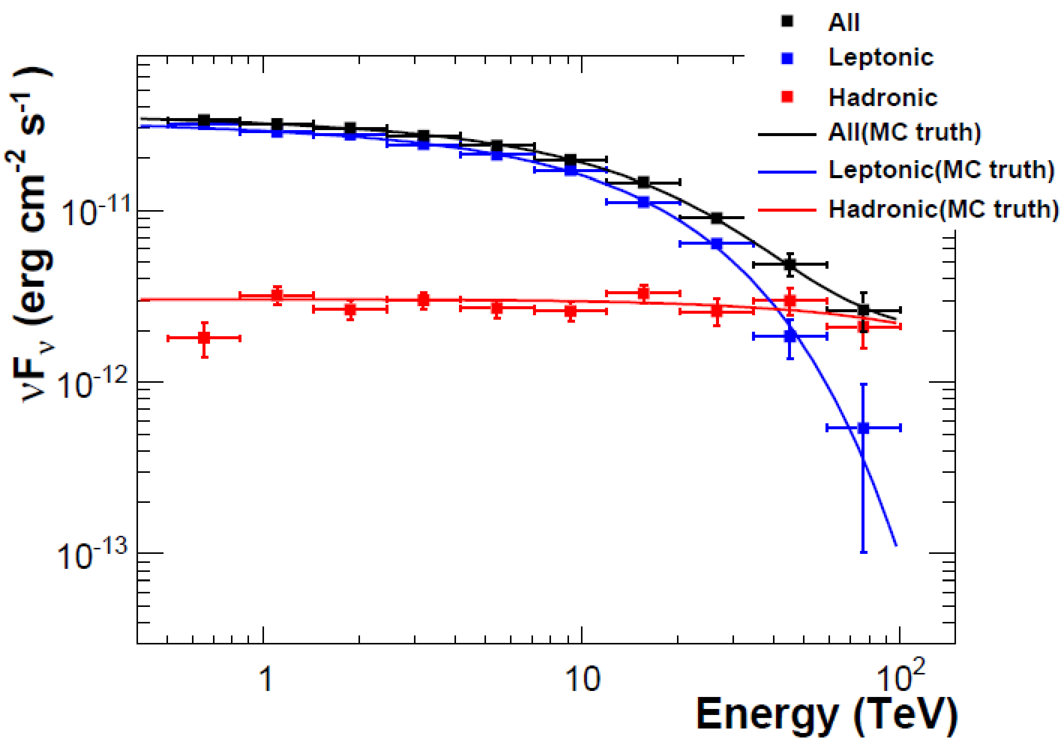

All
Leptonic
Hadronic
All(MC truth)
Leptonic(MC truth)
Hadronic(MC truth)
νF_ν (erg cm^{-2} s^{-1})
10^{-11}
10^{-12}
10^{-13}
1
10
10^2
Energy (TeV)

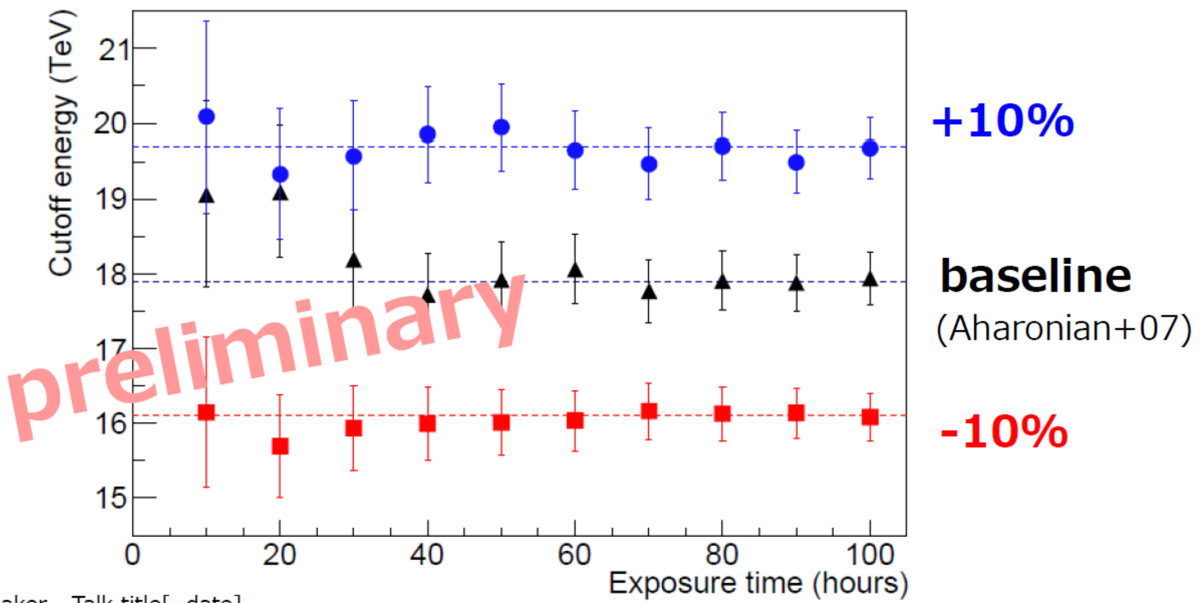

Speaker - Talk title[, date]

1st year and 10th year of operations

The events: shower hits Earth surface

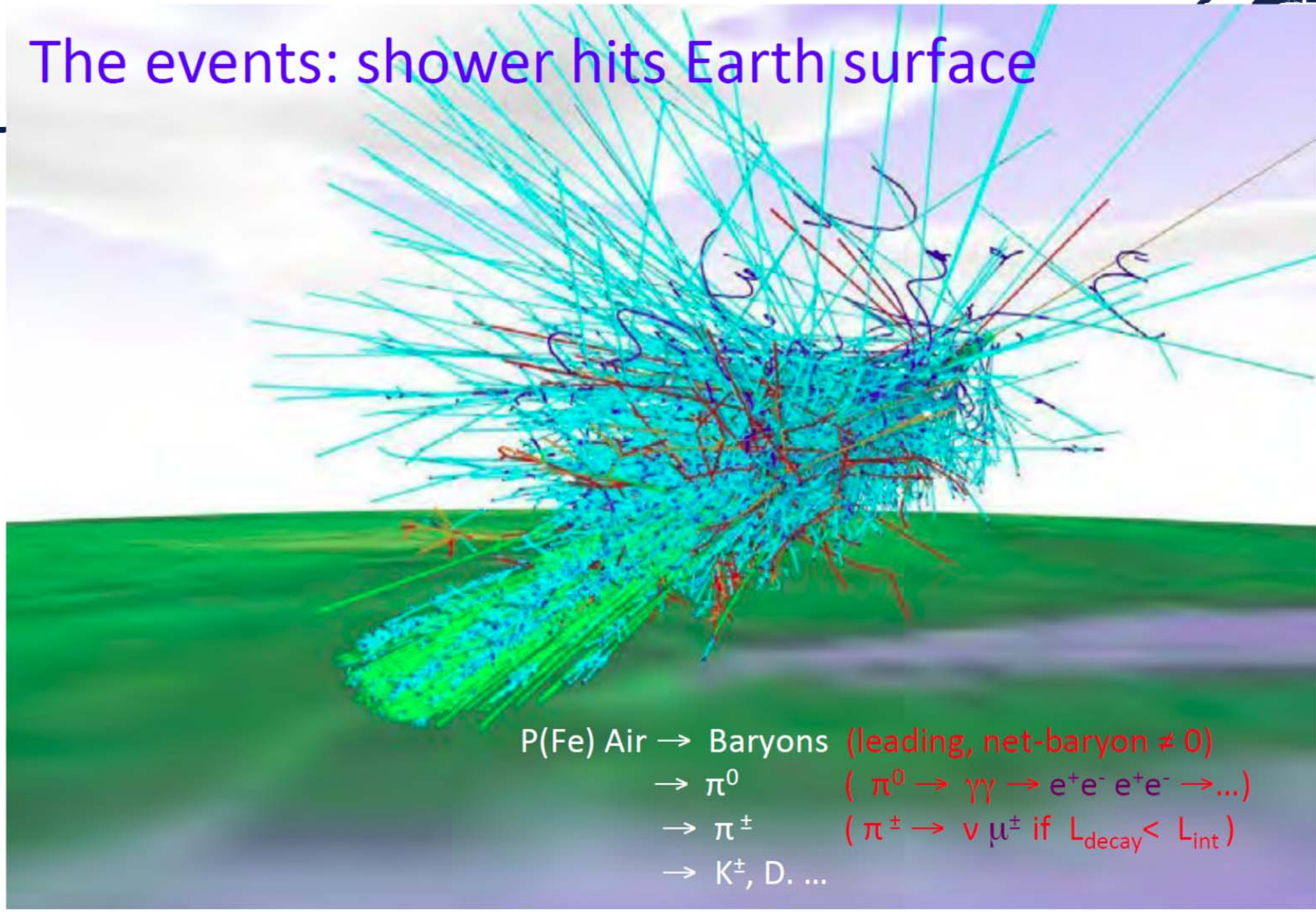

P(Fe) Air $\rightarrow$ Baryons (leading, net-baryon $\neq$ 0)

$\rightarrow \pi^0$ ($\pi^0 \rightarrow \gamma\gamma \rightarrow e^+e^- e^+e^- \rightarrow$...)

$\rightarrow \pi^\pm$ ($\pi^\pm \rightarrow \nu\, \mu^\pm$ if $L_{decay} < L_{int}$)

$\rightarrow K^\pm$, D. ...

Extensive air showers (EAS)

- Showers due to the interaction of HE particles with the atmosphere.
- High-energy hadrons, photons, and electrons interact in the high atmosphere. The process i conceptually similar.
- For photons and electrons above a few hundred MeV, the cascade process is dominated by the pair production and the bremsstrahlung mechanisms.
- The maximum shower size occurs approximately ln(E/Eo) radiation lengths, the radiation length for air being about 37 g/cm^2 (approximately 300m at sea level and NTP). The critical energy is about 80 MeV in air.
- The hadronic interaction length in air is about 61 g/cm^2 for protons (500 meters for air at NTP), being shorter for heavier nuclei—the dependence of the cross section on the mass number A is approximately $A^{2/3}$.
- The transverse profile of hadronic showers is in general wider than for electromagnetic showers, and fluctuations are larger.
- Particles release energy in the atmosphere, which acts like a calorimeter, through different mechanisms—which give rise to a measurable signal.

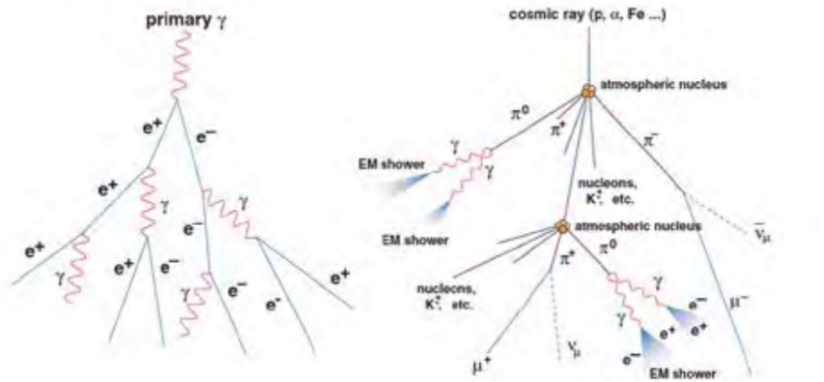

A frequent experimental problem: γ/hadron separation

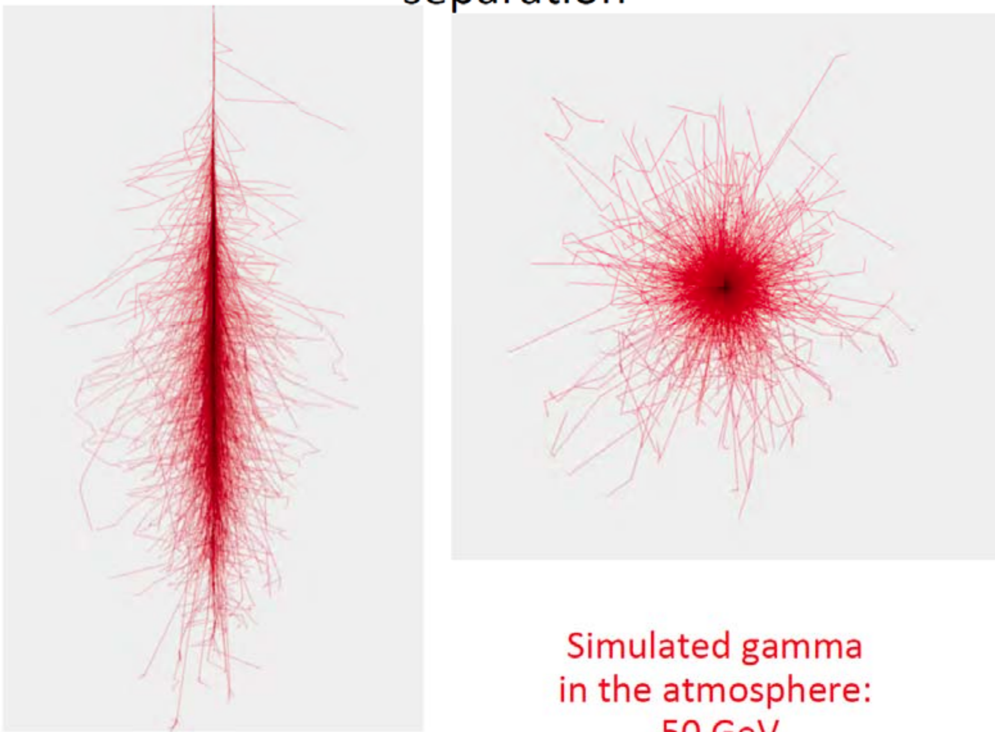

Simulated gamma
in the atmosphere:
50 GeV

Simulated gamma
1 TeV

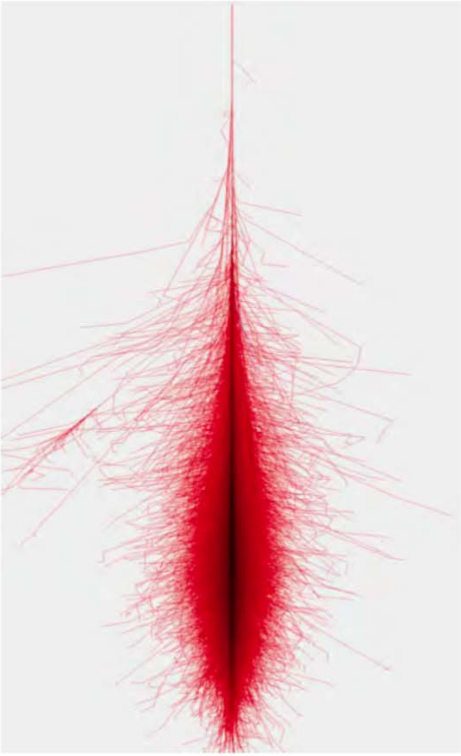

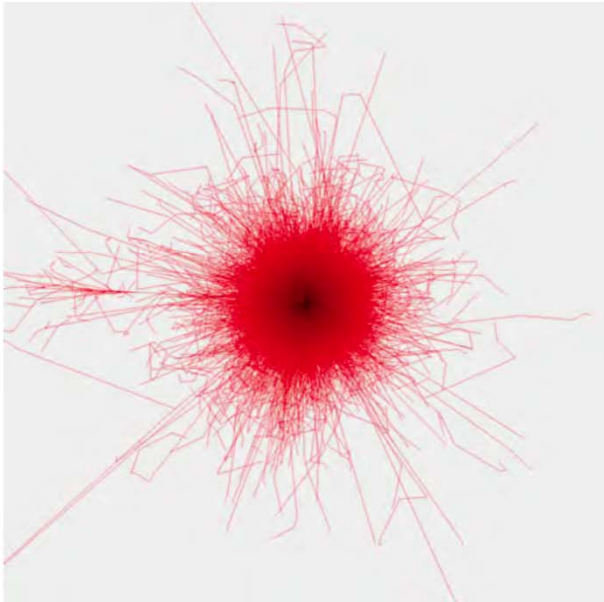

Simulated proton
100 GeV (the ennemy)

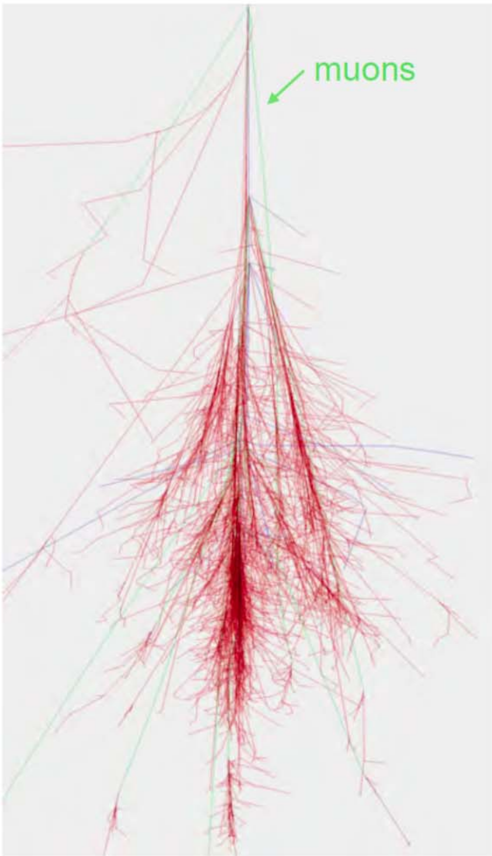

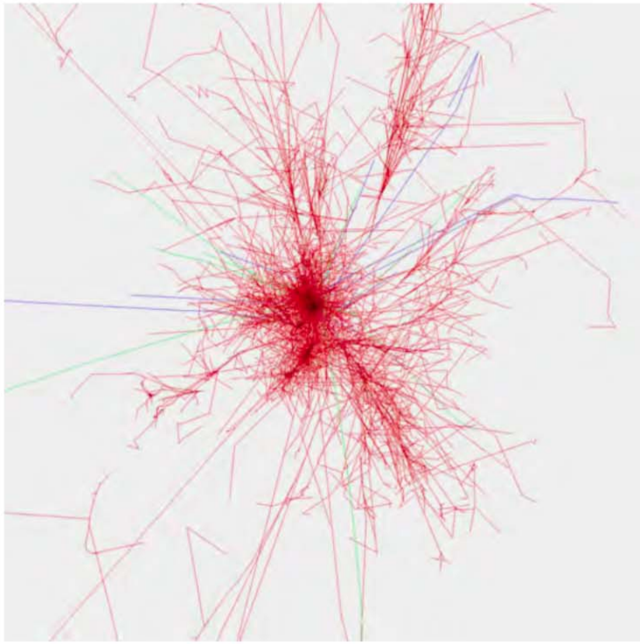

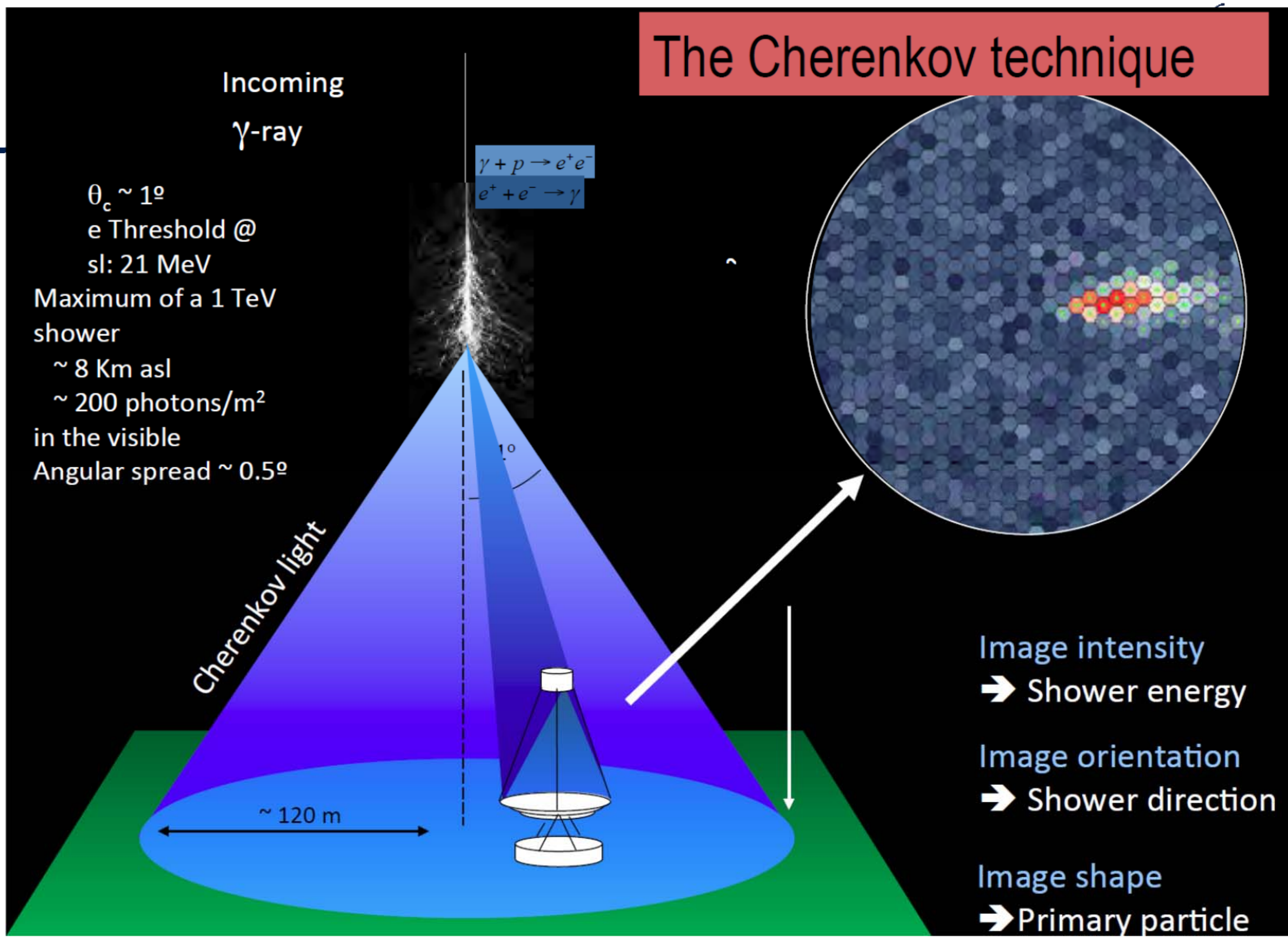
The Cherenkov technique
Incoming
γ-ray
θc ~ 1º
e Threshold @
sl: 21 MeV
Maximum of a 1 TeV
shower
~ 8 Km asl
~ 200 photons/m²
in the visible
Angular spread ~ 0.5º
$\gamma + p \rightarrow e^+e^-$
$e^+ + e^- \rightarrow \gamma$
1º
Cherenkov light
~ 120 m
Image intensity
➔ Shower energy
Image orientation
➔ Shower direction
Image shape
➔ Primary particle

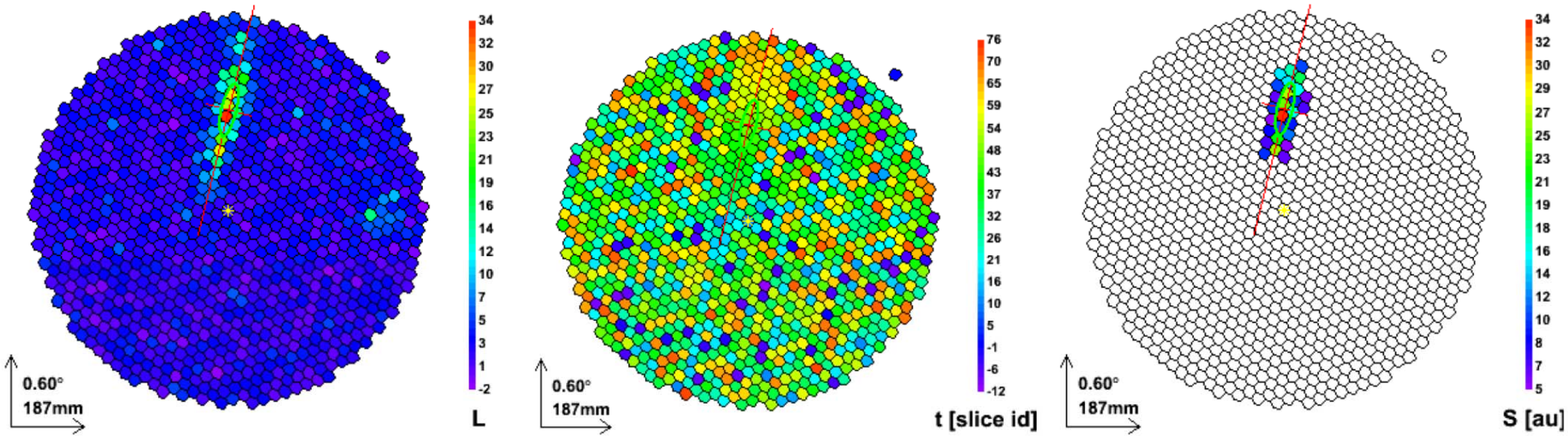

(a) Reconstructed charges (phe) (b) Arrival times (FADC slices) (c) Cleaned image

γ/h Separation

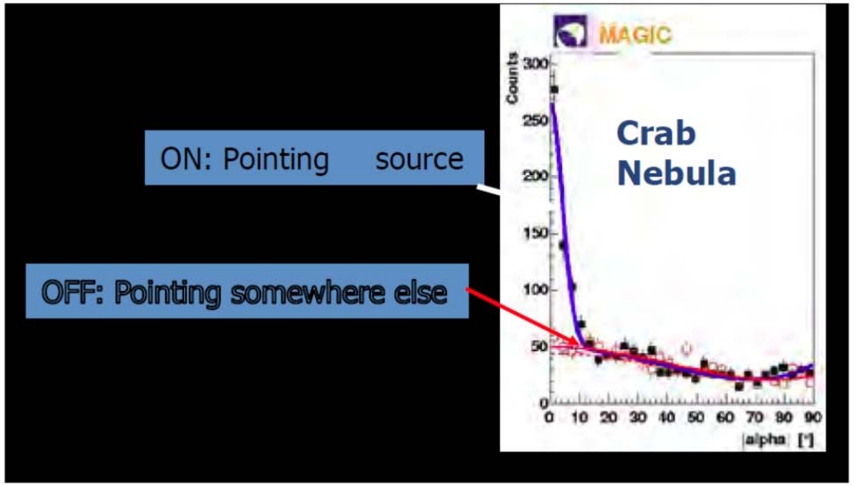

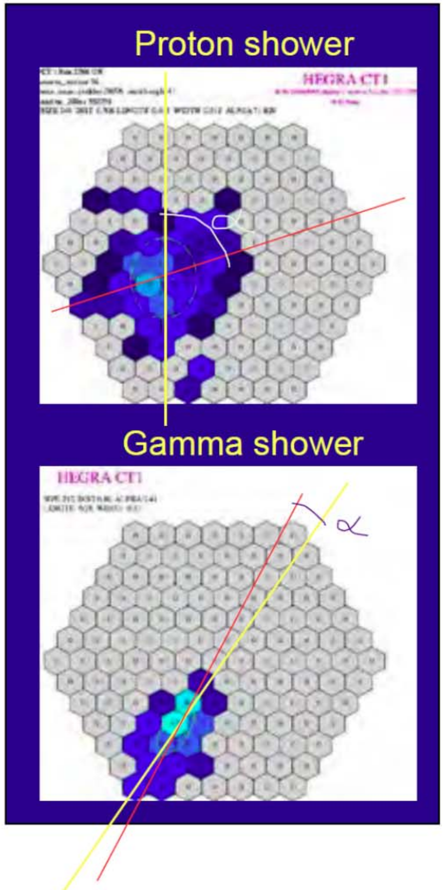

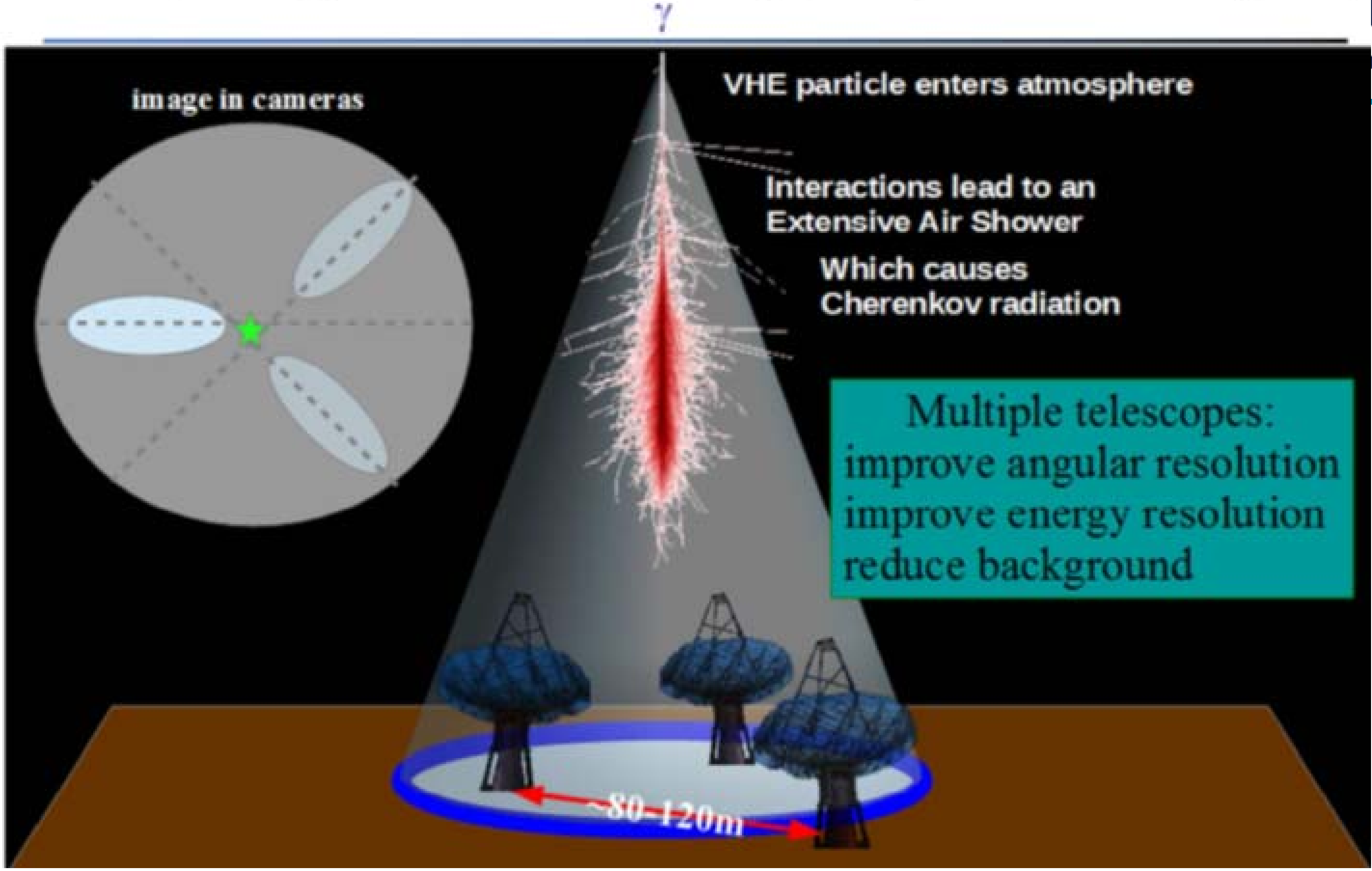
γ
VHE particle enters atmosphere
image in cameras
Interactions lead to an
Extensive Air Shower
Which causes
Cherenkov radiation
Multiple telescopes:
improve angular resolution
improve energy resolution
reduce background
~80-120m

Instr.	Tels. #	Tel. A (m^2)	FoV (°)	Tot A (m^2)	Thresh. (TeV)	PSF (°)	Sens. (%Crab)
H.E.S.S.	4	107	5	428	0.1	0.06	0.7
MAGIC	2	236	3.5	472	0.05(0.03)	0.06	0.8
VERITAS	4	106	4	424	0.1	0.07	0.7

Plus a 600 m2 telescope (CT5) operating since 2015

(0.03 for CT5)

HESS (Namibia)

4 telescopes (~12m) operational since 2003

HESS 2: 5th telescope (26-28m) commissioned in 2015

MAGIC: Two 17m Ø Imaging Atmospheric Cherenkov Telescopes
1st telescope since 2004, 2nd since 2009, upgrade in 2013

~160 physicists from 10 countries:

Bulgaria, Croatia, Finland, Germany, India, Italy, Japan, Poland, Spain, Switzerland

Canary island of La Palma

at 2400 m a.s.l.

Key elements

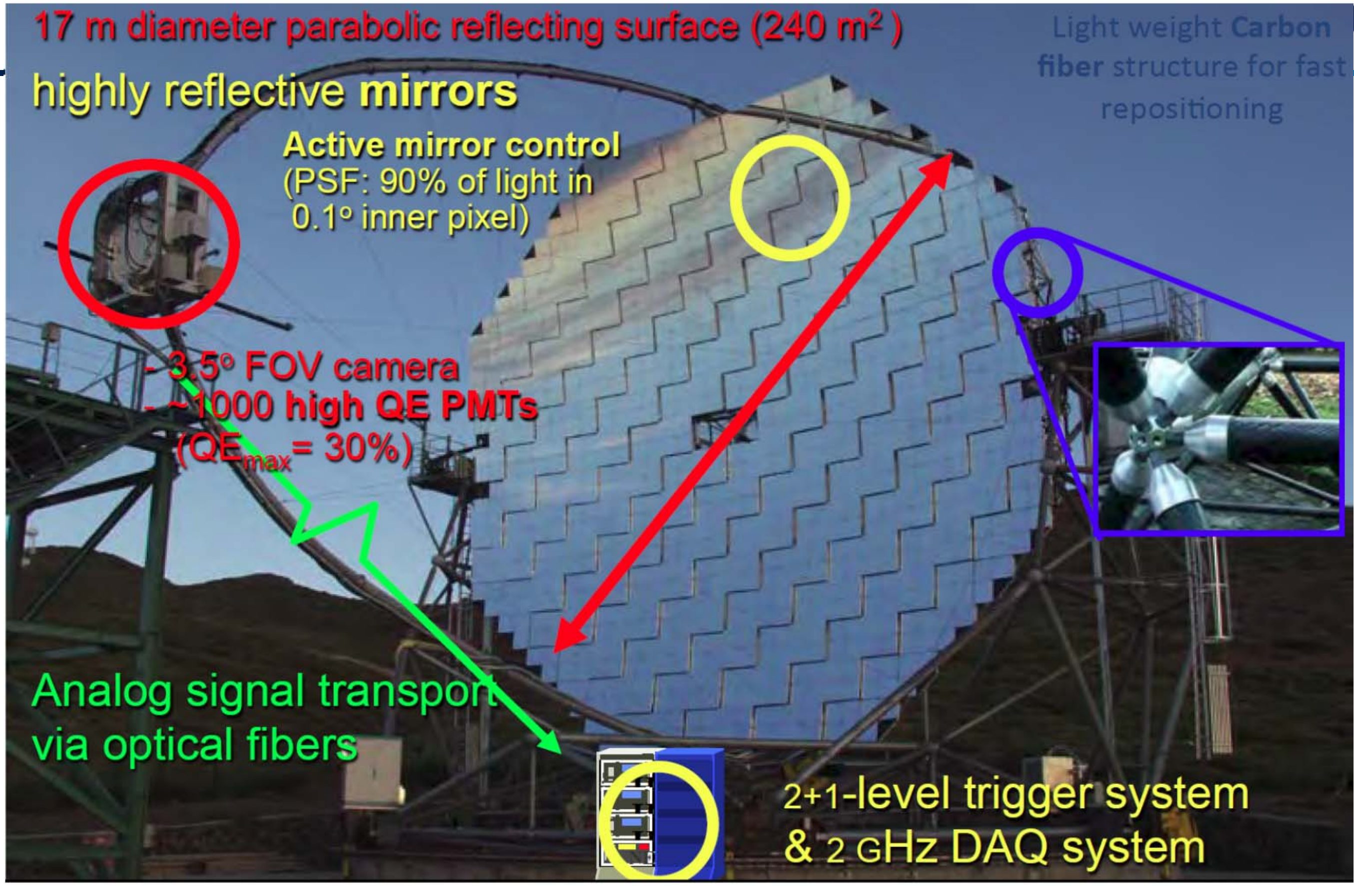

Light weight **Carbon fiber** structure for fast repositioning

How to do better with IACT arrays?

- More events
  - More photons = better spectra, images, fainter sources
    - ✓ Larger collection area for gamma-rays
- Better events
  - More precise measurements of atmospheric cascades and hence primary gammas
    - ✓ Improved angular resolution
    - ✓ Improved background rejection power

→ More telescopes!

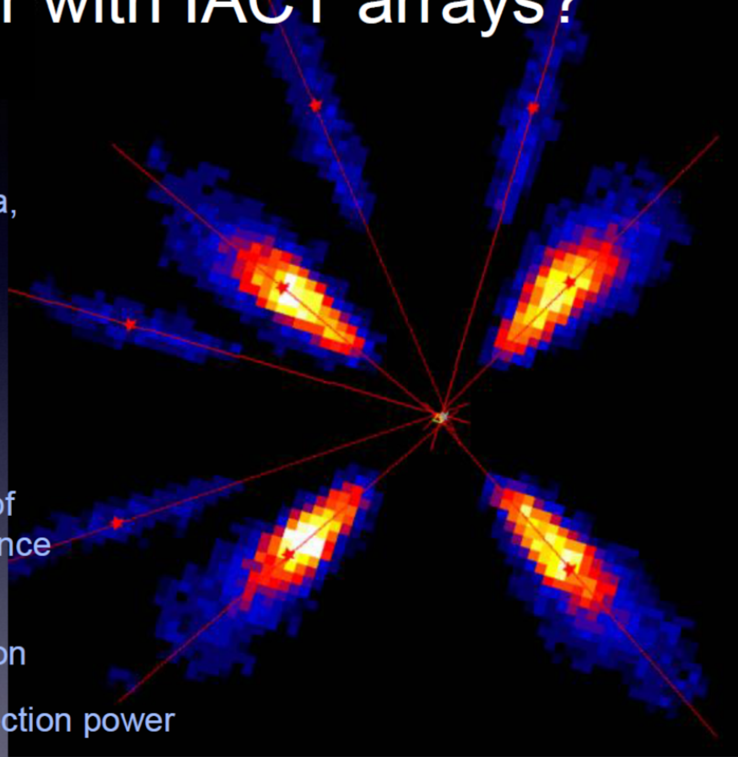

Simulation:
Superimposed images from 8 cameras

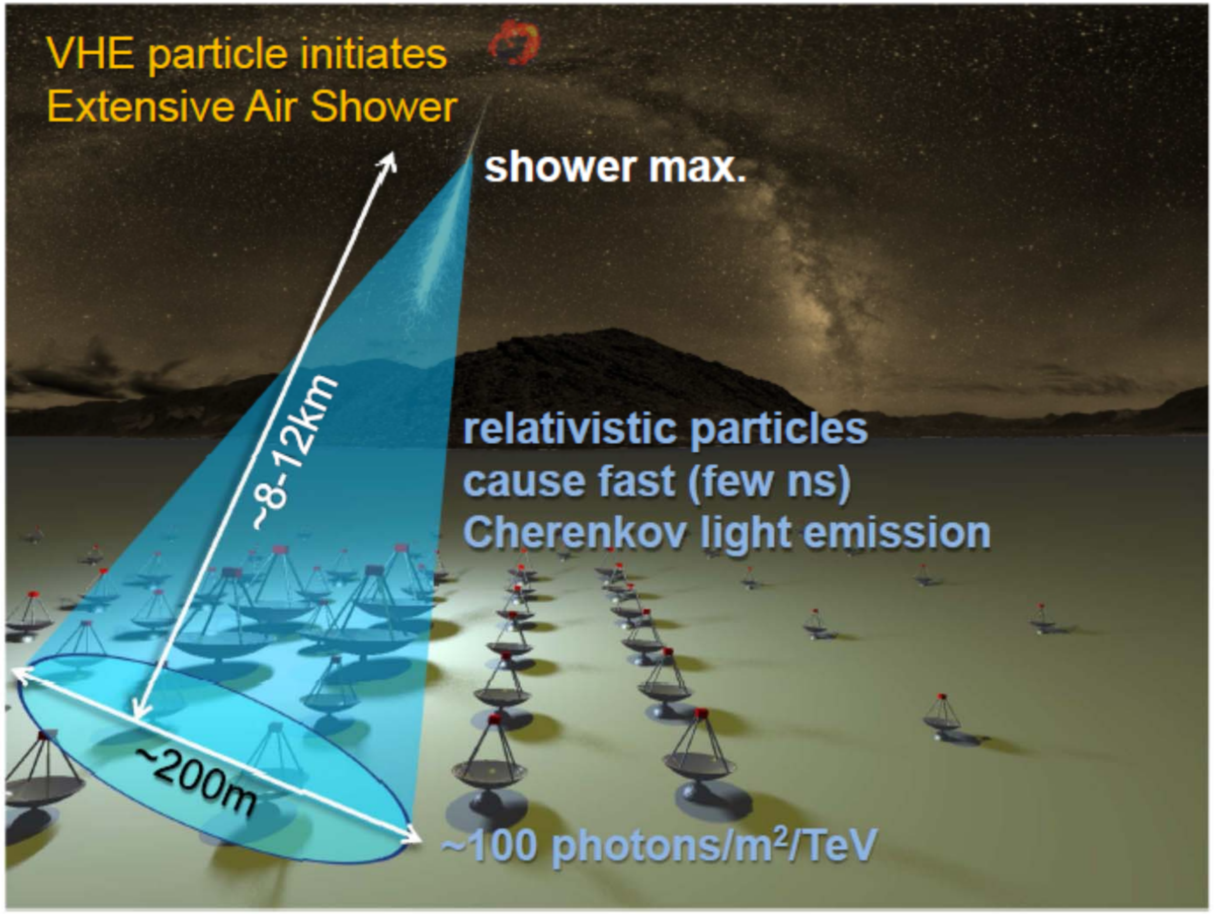
VHE particle initiates
Extensive Air Shower
shower max.
~8-12km
relativistic particles
cause fast (few ns)
Cherenkov light emission
~200m
~100 photons/m²/TeV

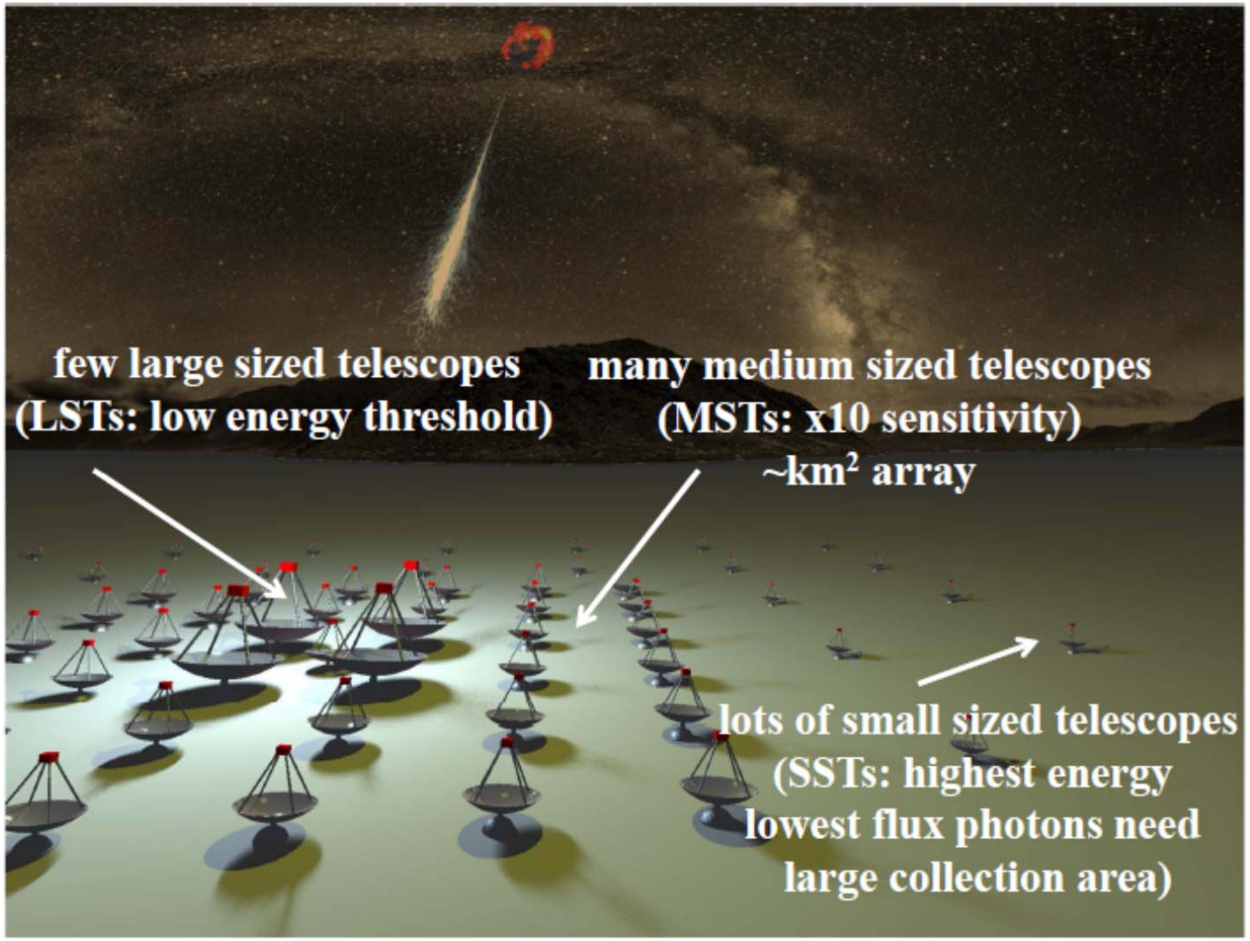
few large sized telescopes
(LSTs: low energy threshold)
many medium sized telescopes
(MSTs: x10 sensitivity)
~km² array
lots of small sized telescopes
(SSTs: highest energy
lowest flux photons need
large collection area)

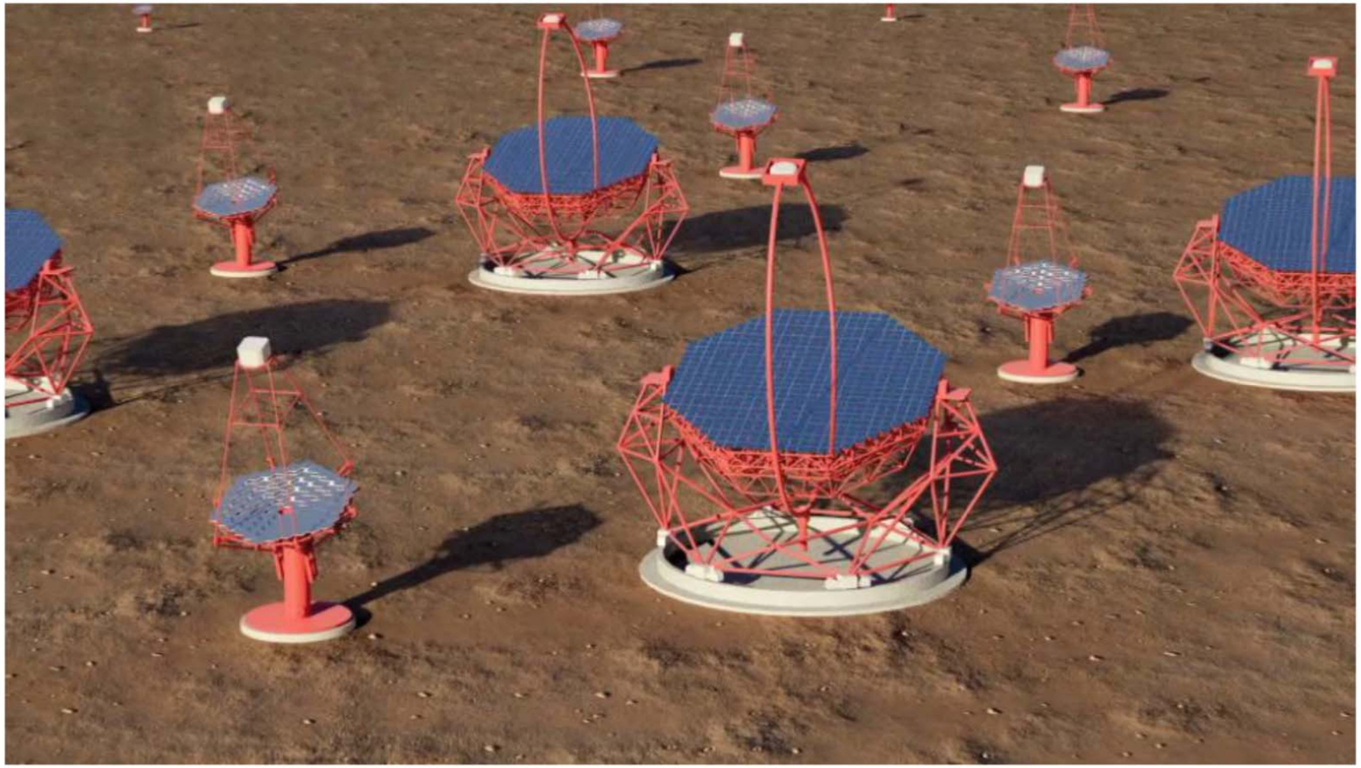

CTA consortium: a world-wide effort

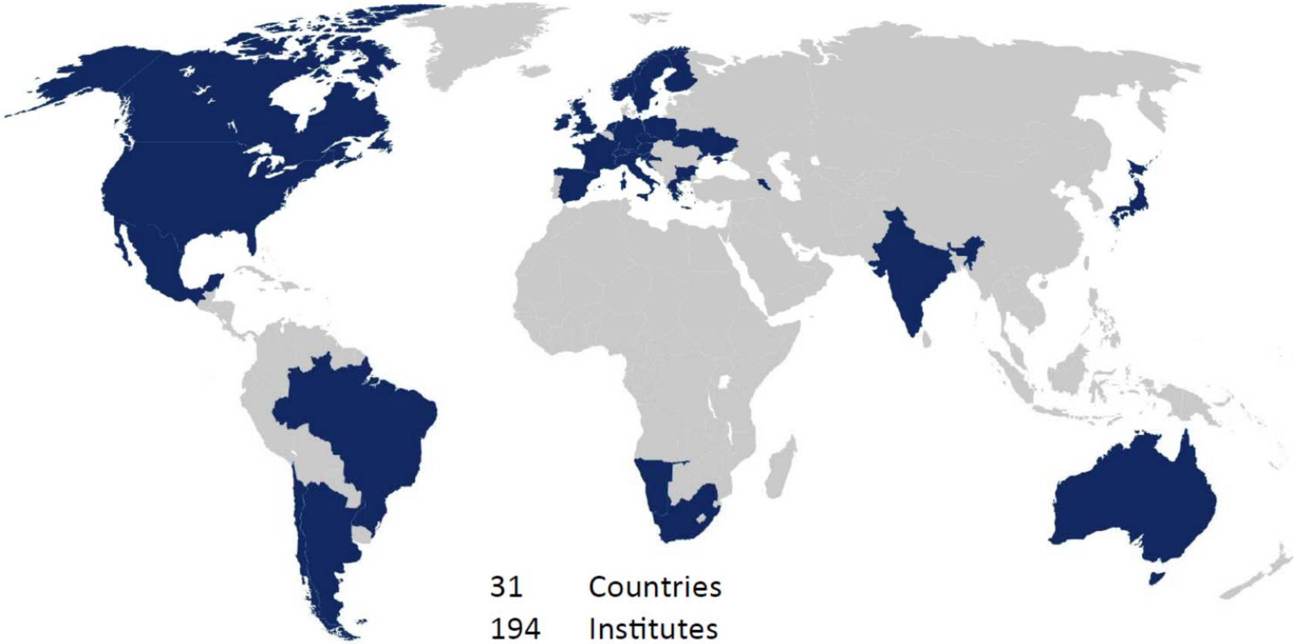

31 Countries
194 Institutes
>1200 Members

Numbers from CDR- June 2015

All-sky coverage: two observatories

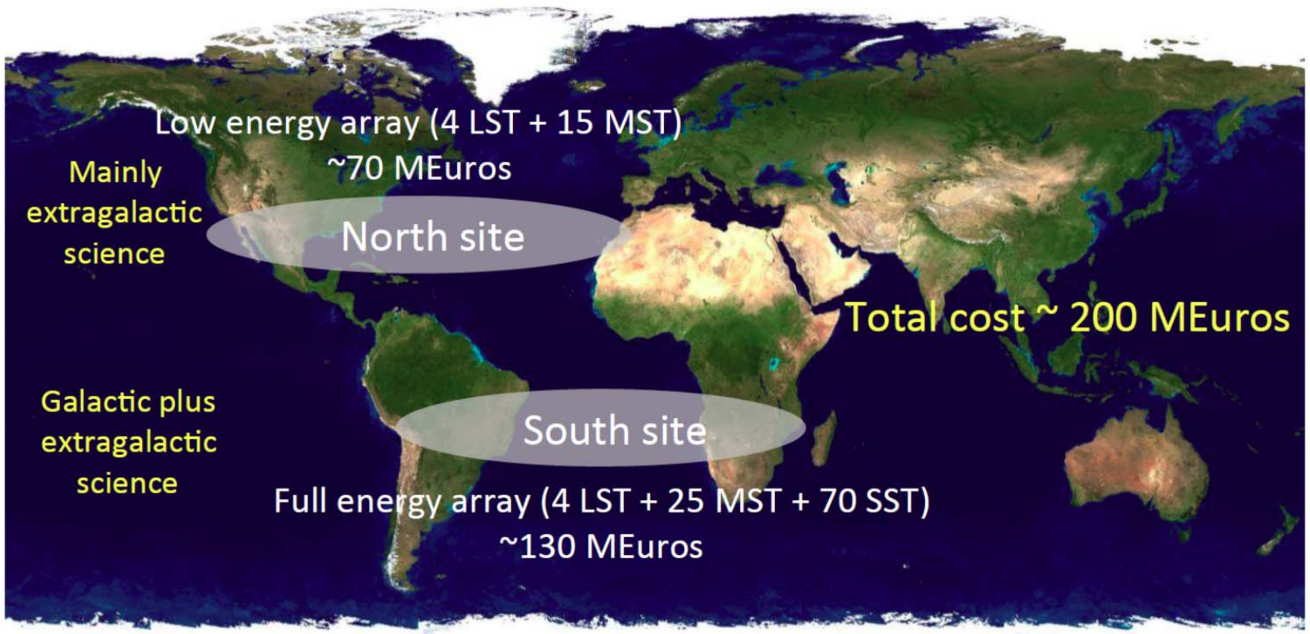

array layoutS

Reference (baseline) layouts

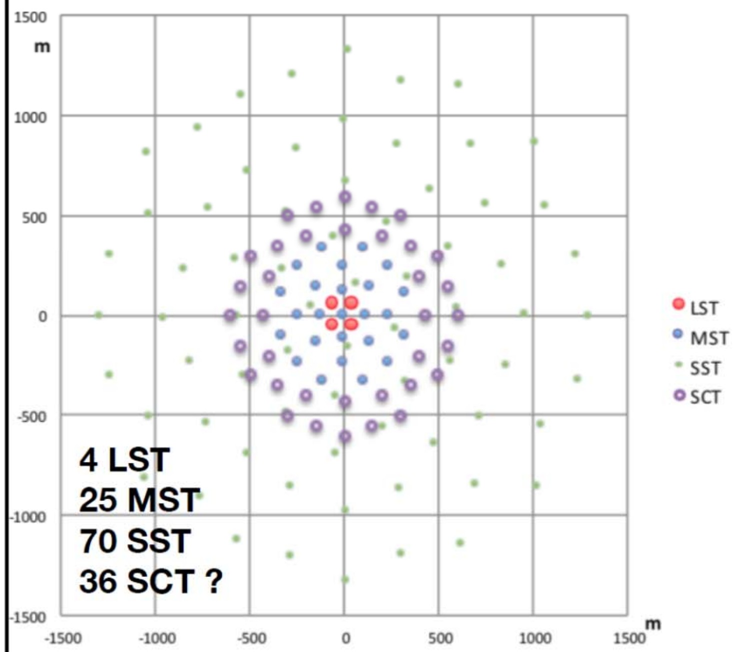

CTA-South

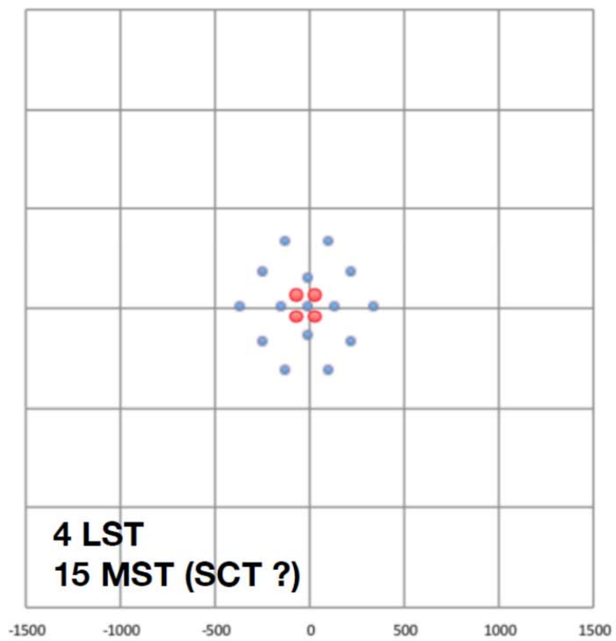

CTA-North

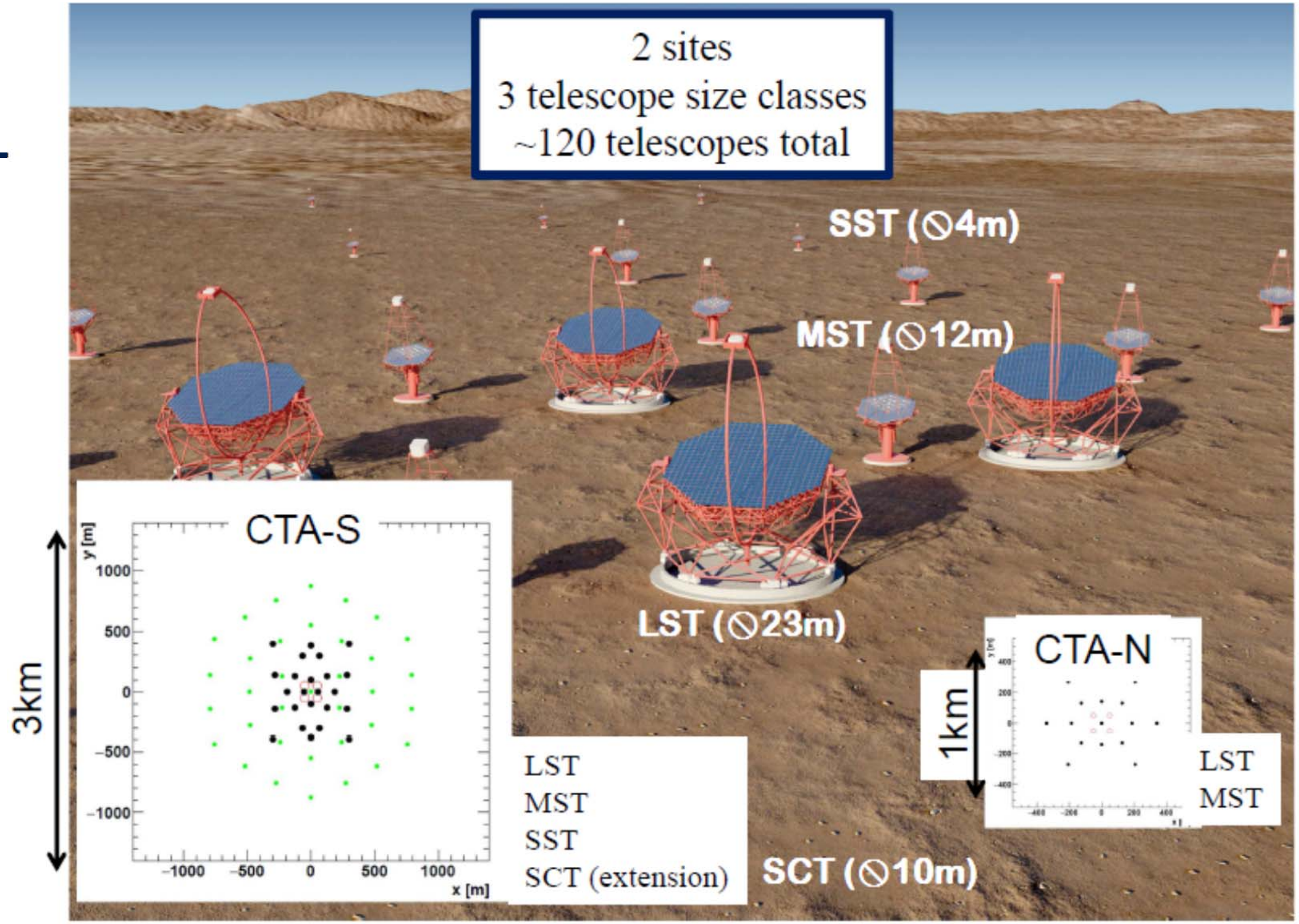
2 sites
3 telescope size classes
~120 telescopes total
SST (⦸4m)
MST (⦸12m)
LST (⦸23m)
SCT (⦸10m)
CTA-S
3km
LST
MST
SST
SCT (extension)
CTA-N
1km
LST
MST

CTA sensitivity in units of Crab flux

for 5 σ detection & $N_\gamma > 10$ in each 0.2-dex bin in E, in 50 h

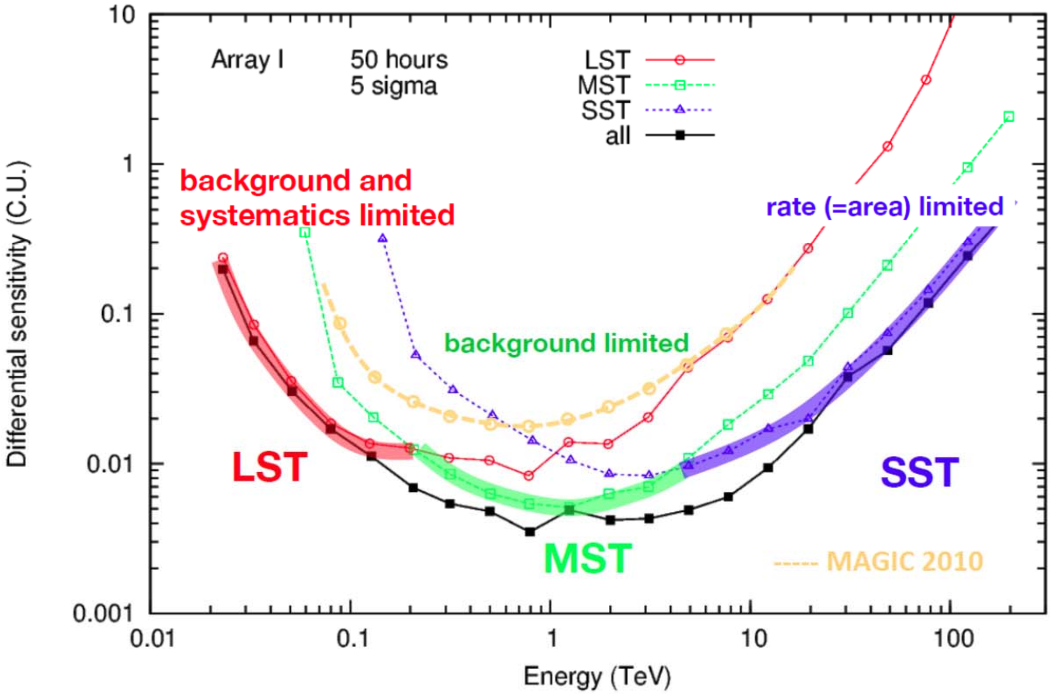

Telescope Specifications

SiPM Cameras

3 SST types

	LST "large"	MST "medium"	SCT "medium 2-M"	SST "small"
Number	**4 (S) 4 (N)**	**25 (S) 15 (N)**	**≤ 24 (S and N)**	**70 (S)**
Energy range	20 GeV to 1 TeV	200 GeV to 10 TeV	200 GeV to 10 TeV	> few TeV
Effective mirror area	> 330 m^2	> 90 m^2	> 50 m^2	> 5 m^2
Field of view	> 4.4°	> 7°	> 7°	> 8°
Pixel size ~PSF θ_{80}	< 0.12°	< 0.18°	< 0.07°	< 0.25°
Positioning time	50 s, 20 s goal	90 s, 60 s goal	90 s, 60 s goal	90 s, 60 s goal
Target capital cost	7.4 M€	1.6 M€	< 2.0 M€	500 k€


CTA-N
La Palma
CTA-S
Chile
2015: 2 sites selected for final negotiations
Imagery ©2015 NASA, TerraMetrics

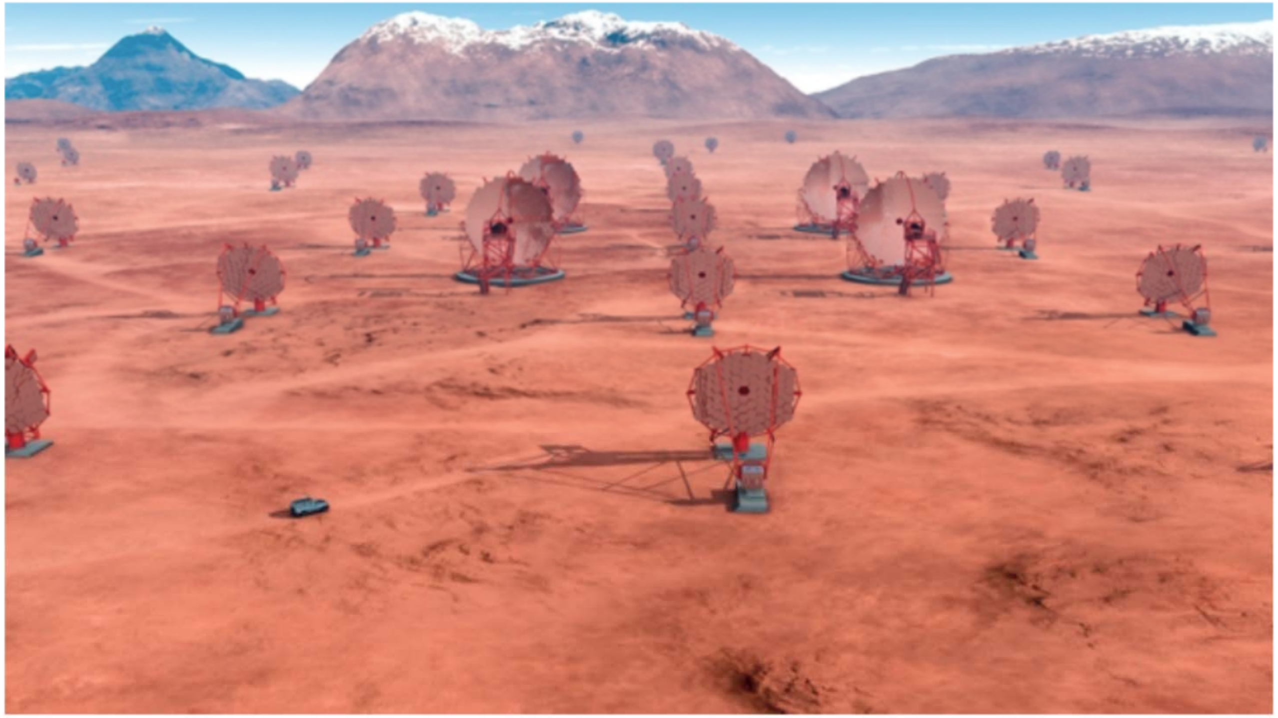

DESY/Milde Science Comm./Exozet

CTA-South in Paranal, an artist's view
Work to set up the observatory starting beginning 2017?

CTA-N: possible scheme

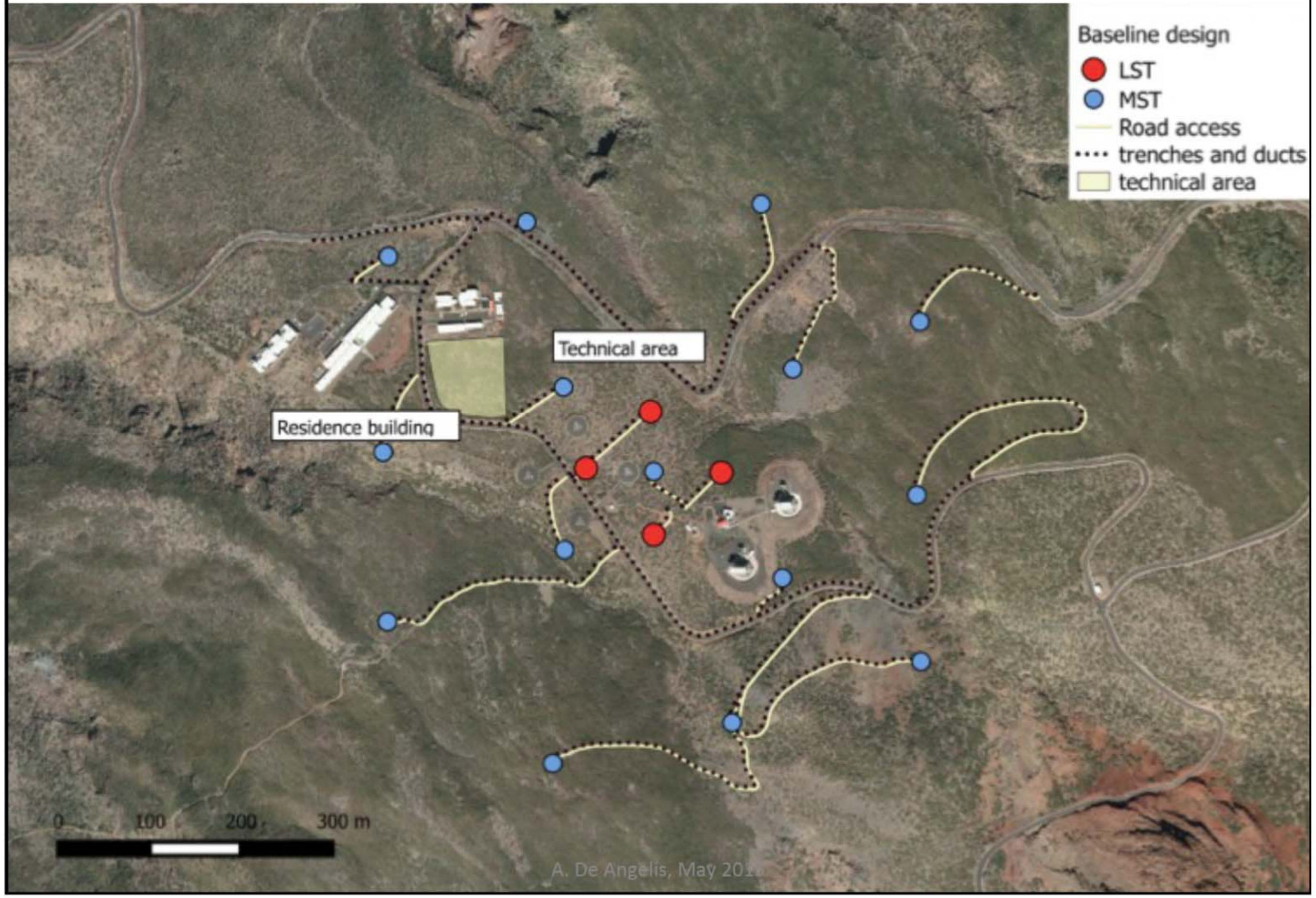

Science drivers
Lowest energies (< 200 GeV)
Transient phenomena, DM, AGN, GRB, pulsars

Characteristics
23m diameter parabolic design
370 m^2 effective mirror area
28 m focal length
1.5 m mirror facets with active mirror control
4.5° field of view composed of 0.11° PMT pixels
Carbon-fibre arch structure (fast repointing)

Array layout
South site: 4 LST
North site: 4 LST

Status
Some elements prototyped
Prototype telescope under construction in
La Palma (to become first full LST)

Science drivers
Mid energies (100 GeV – 10 TeV)
DM, AGN, SNR, PWN, binaries, starbursts, EBL, IGM

Characteristics
Modified Davies-Cotton design
12 m diameter, 90 m^2 effective mirror area
1.2 m mirror facets
16 m focal length
8° field of view with 0.18° PMT pixels

Array layout
South site: 25 MST
North site: 15 MST

Status
Telescope prototyped (Berlin-Adlershof)
Prototype cameras under construction (2 types: NectarCAM & FlashCam)

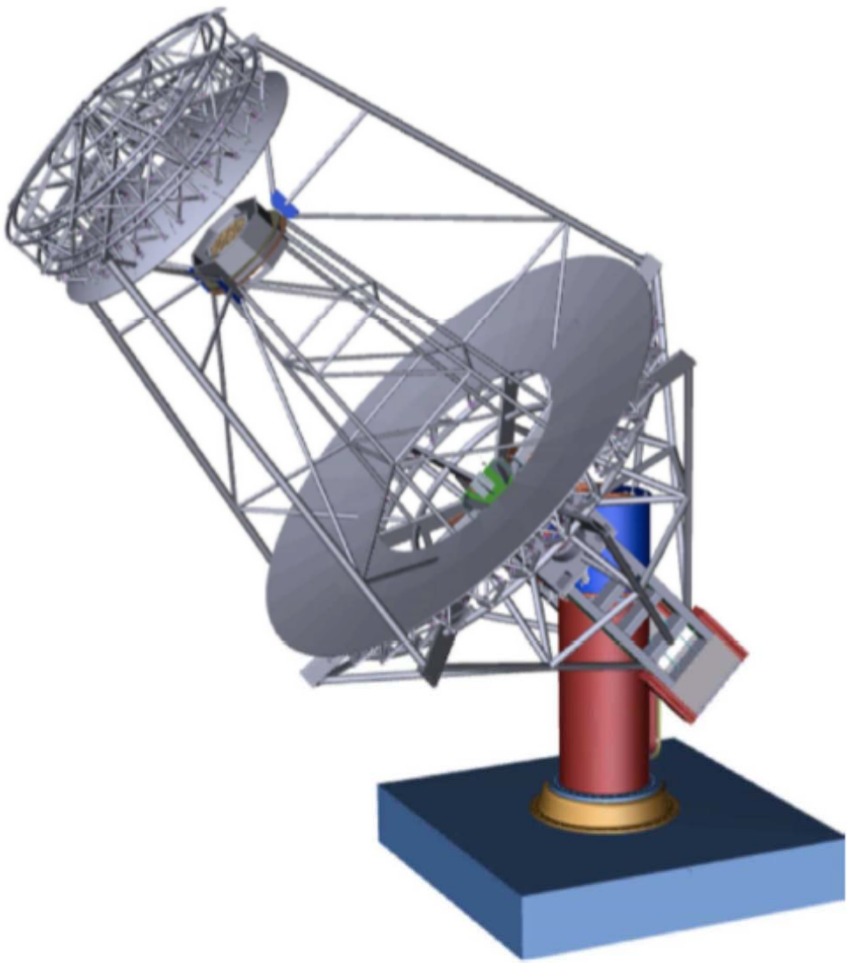

Science drivers
Mid energies (200 GeV – 10 TeV)
DM, AGN, SNR, PWN, binaries, starbursts, EBL, IGM

Characteristics
Schwarzschild-Couder design
9.7 m primary diameter
5.4 m secondary diameter
40 m^2 effective mirror area
5.6 m focal length
8° field of view
0.07° PMT pixels

Array layout
South site: 24 SCT
North site: -

Status
Prototype telescope, including camera, under construction on VERITAS site (Arizona)

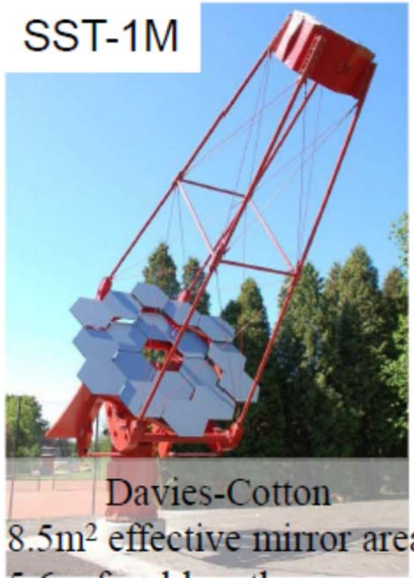

Davies-Cotton
$8.5m^2$ effective mirror area
5.6m focal length
9 °fov 0.24°SiPM pixels

Schwarzchild-Couder
$6m^2$ effective mirror area
2.2m focal length
9.6 °fov 0.17°SiPM pixels

Schwarzchild-Couder
$6m^2$ effective mirror area
2.3m focal length
8.6 °fov 0.16°SiPM pixels

Science drivers
Highest energies (> 5 TeV)
Galactic science, PeVatrons, Fundamental Physics (ALPs, LIV)

Array layout
South site: 70 SST
North site: -

Status
Prototypes in Krakow (SST-1M), Mt. Etna (ASTRI), Paris (GCT)

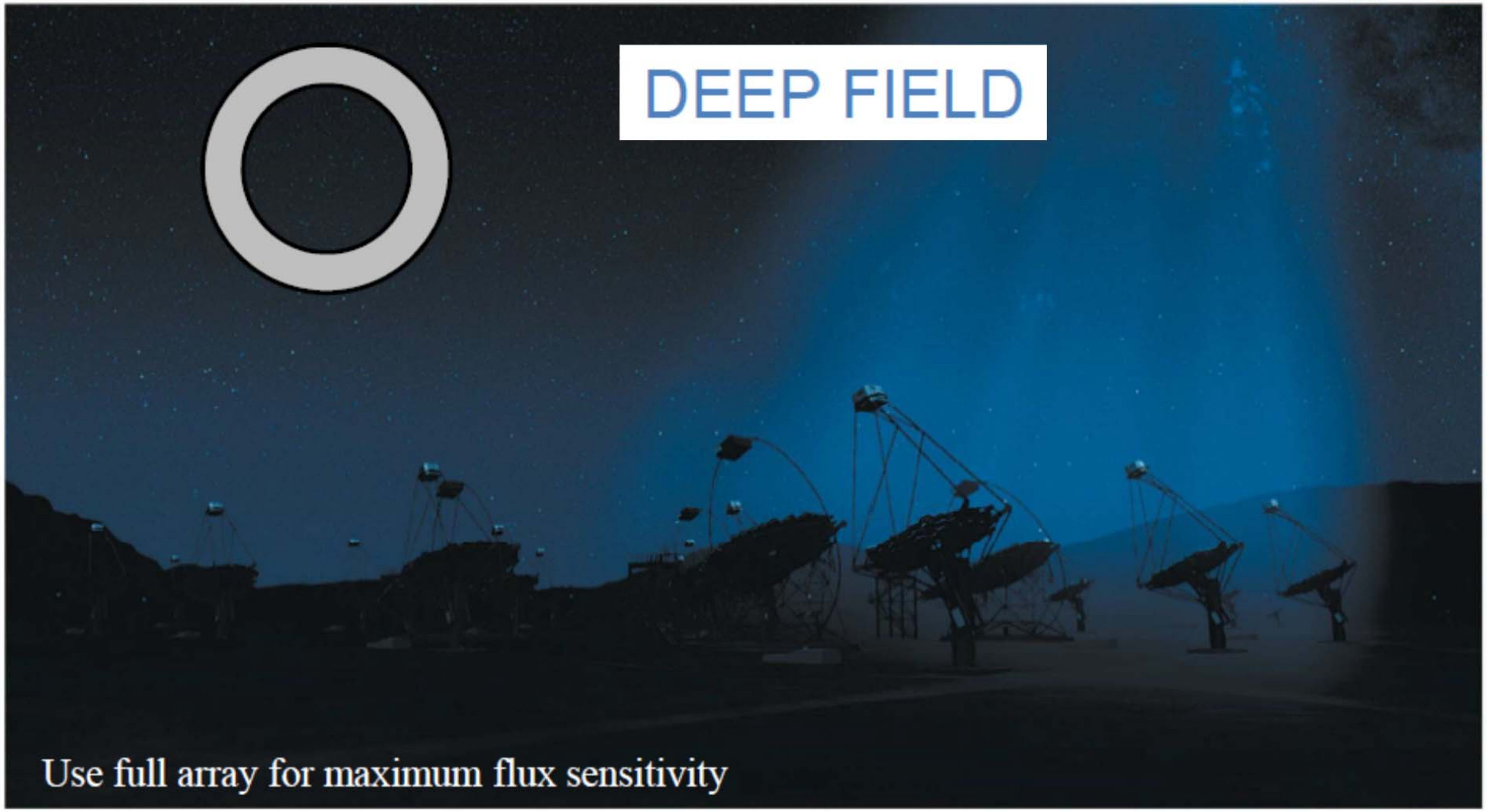
DEEP FIELD
Use full array for maximum flux sensitivity

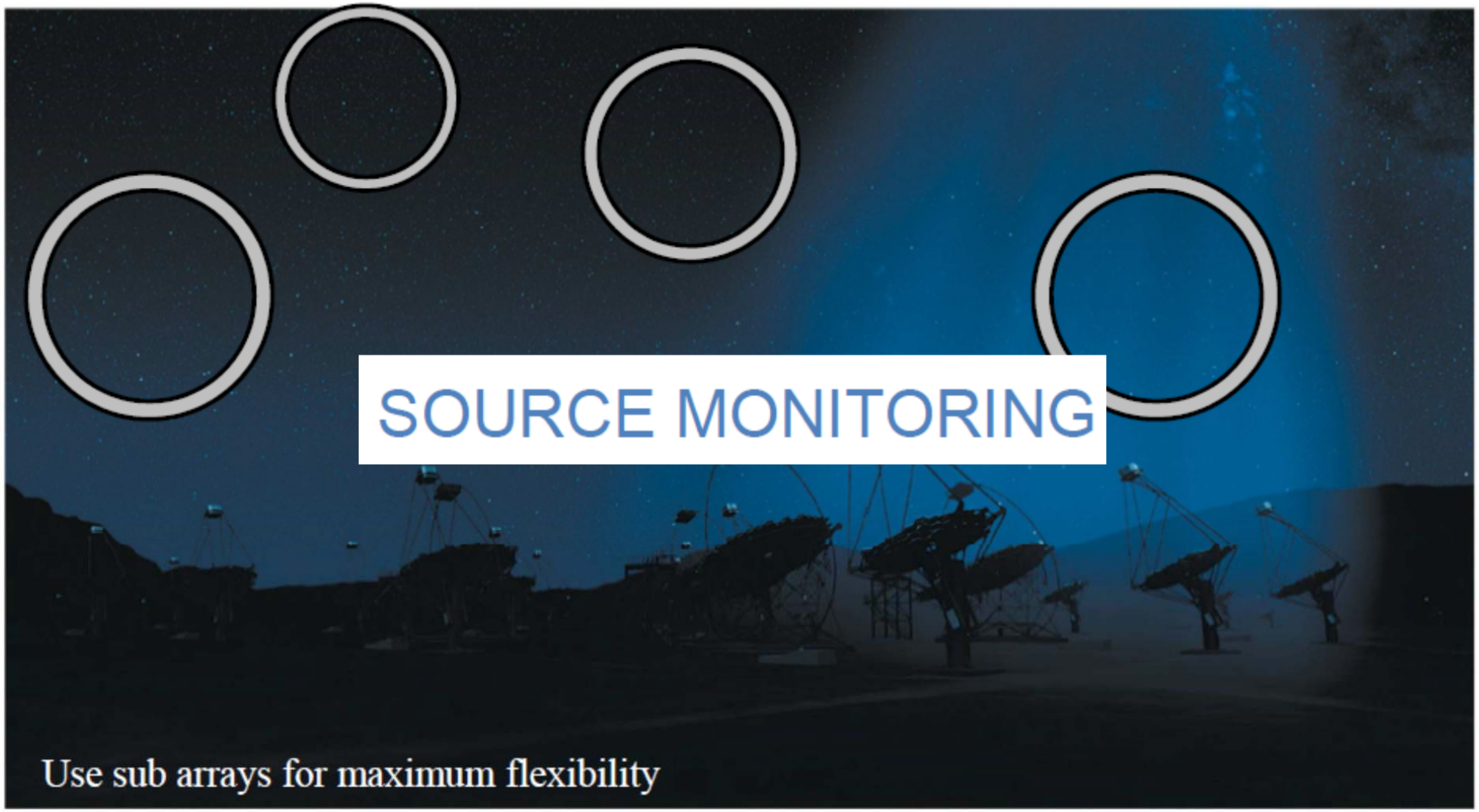
SOURCE MONITORING
Use sub arrays for maximum flexibility


SURVEY
Divergent pointing for maximum coverage

Sensitivity gain

- access VHE populations
- sample fast variability (AGN, GRB)

FoV > 8°

- measure extended sources/diffuse emissions
- efficient survey of large fields

Arcmin angular resolution

- resolve extended sources (SNR, starbursts)

Broad energy coverage

- < 100 GeV to reach higher redshifts
- >>10 TeV to search for PeVatrons
- enhanced energy resolution (eg DM lines)

Time Domain Astronomy

- Coverage from seconds to years

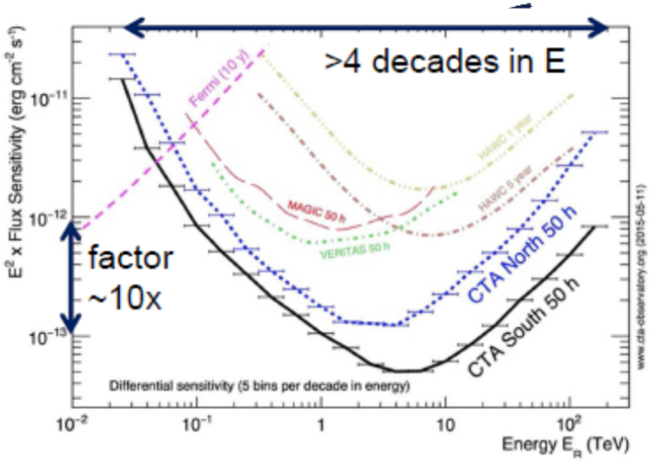

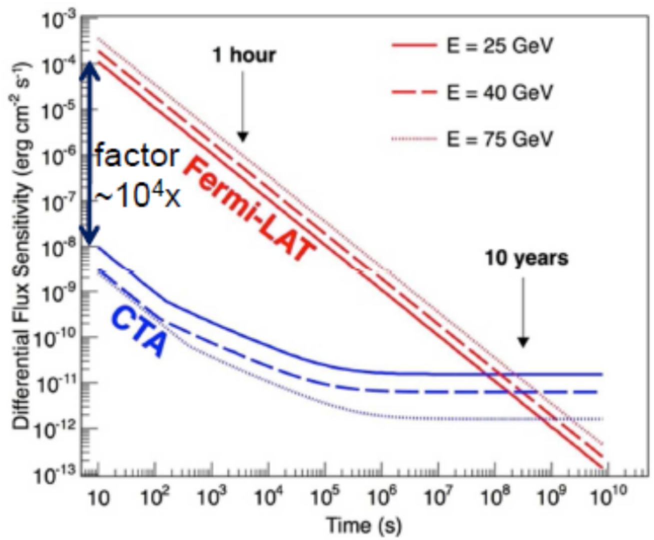

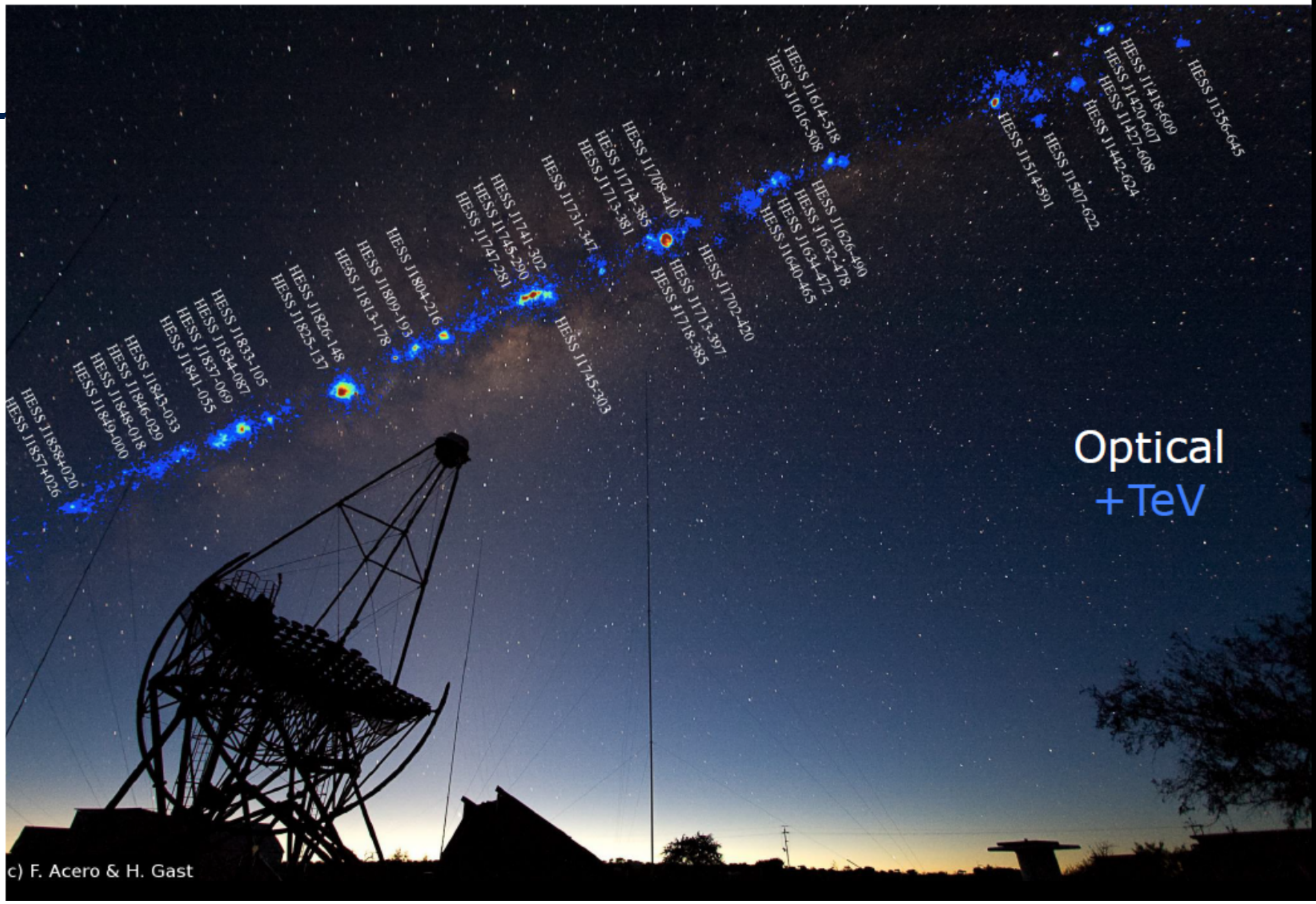
HESS J1857+026
HESS J1858+020
HESS J1849-000
HESS J1848-018
HESS J1846-029
HESS J1843-033
HESS J1841-055
HESS J1837-069
HESS J1834-087
HESS J1833-105
HESS J1825-137
HESS J1826-148
HESS J1813-178
HESS J1809-193
HESS J1804-216
HESS J1747-281
HESS J1745-290
HESS J1741-302
HESS J1745-303
HESS J1731-347
HESS J1713-381
HESS J1714-385
HESS J1708-410
HESS J1718-385
HESS J1713-397
HESS J1702-420
HESS J1640-465
HESS J1634-472
HESS J1632-478
HESS J1626-490
HESS J1616-508
HESS J1614-518
HESS J1514-591
HESS J1507-622
HESS J1442-624
HESS J1427-608
HESS J1420-607
HESS J1418-609
HESS J1356-645
Optical
+TeV
c) F. Acero & H. Gast

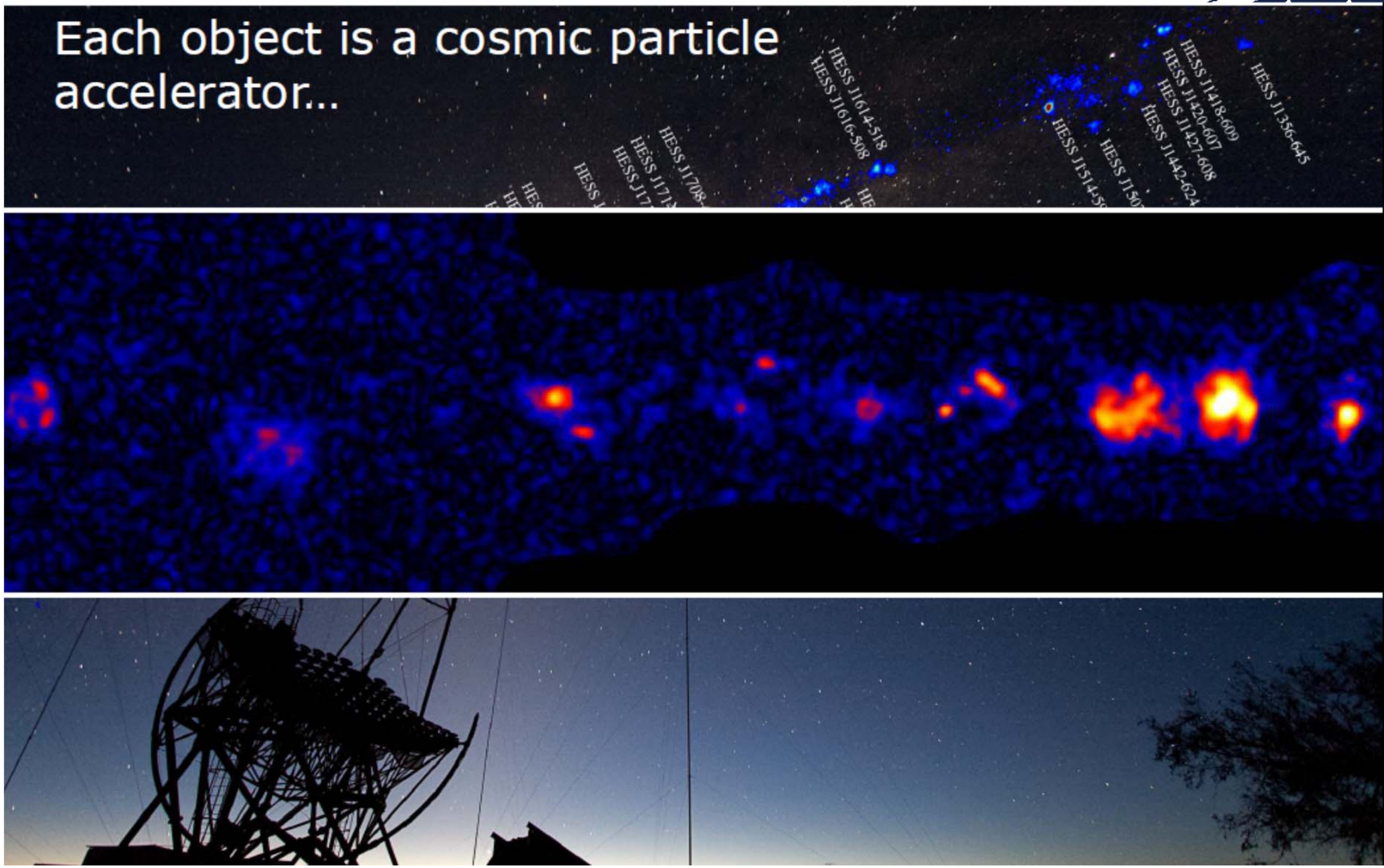
Each object is a cosmic particle accelerator…
HESS J1614-518
HESS J1616-508
HESS J1418-609
HESS J1420-607
HESS J1427-608
HESS J1442-624
HESS J1356-645

Galactic plane survey

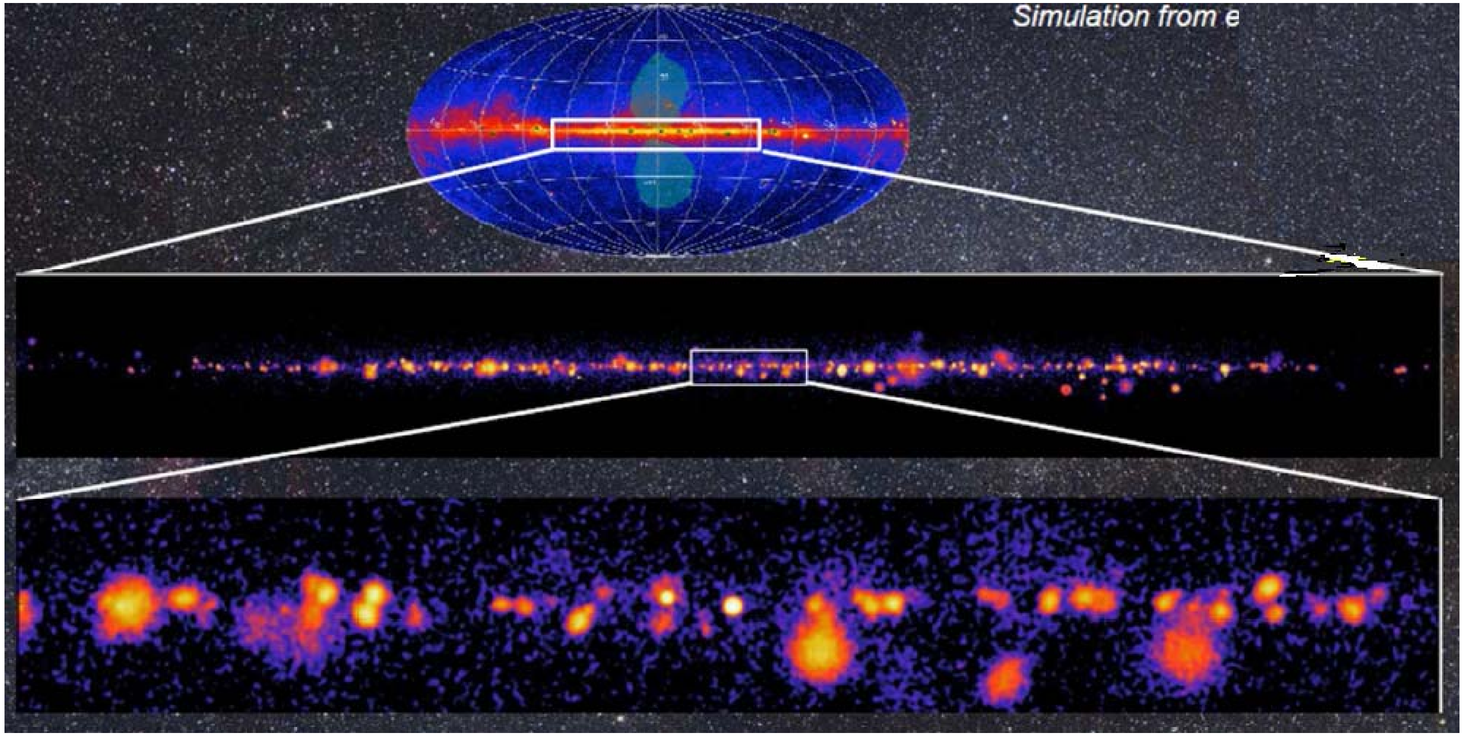

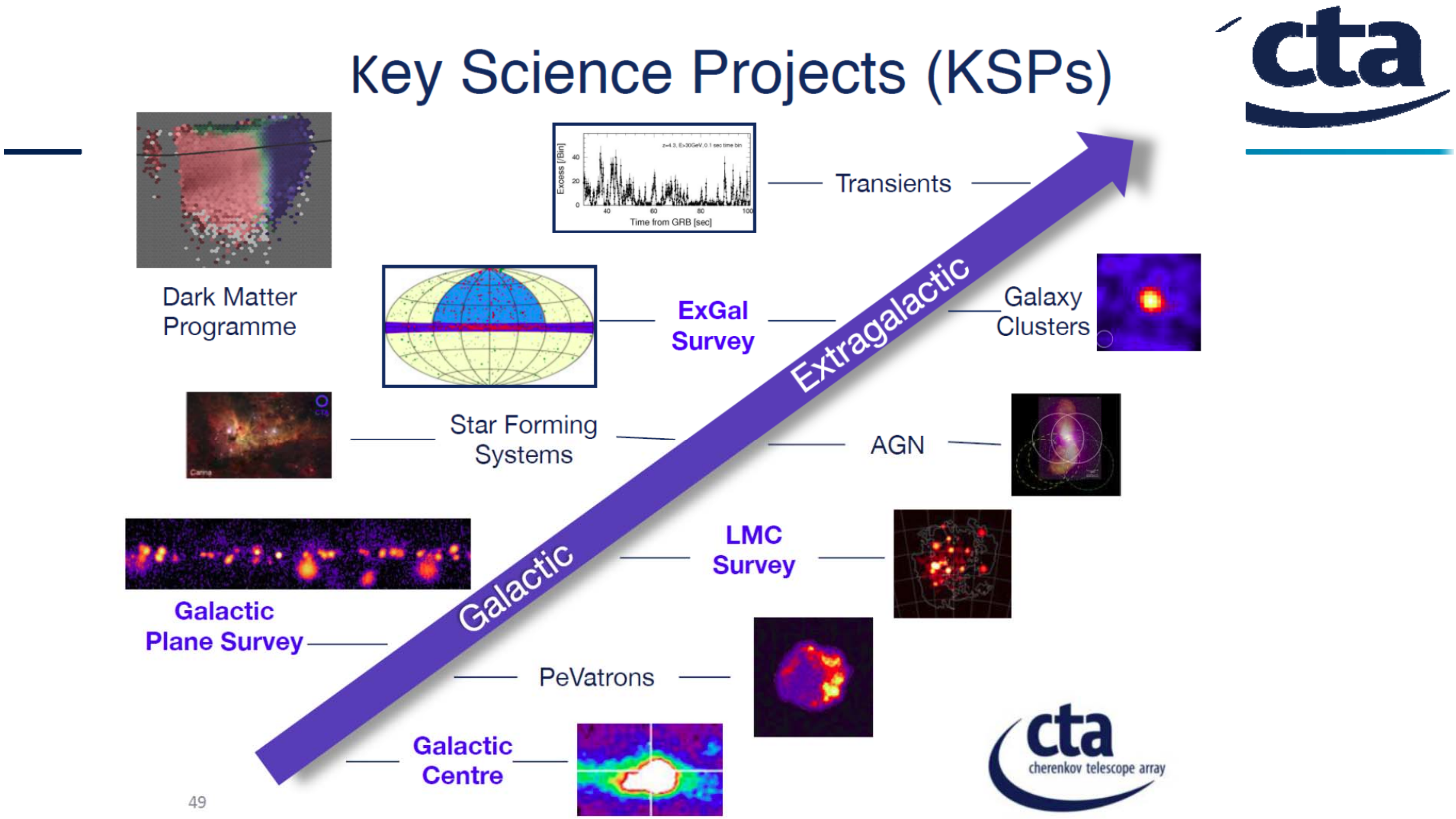
Key Science Projects (KSPs)
Excess [/Bin]
Time from GRB [sec]
Transients
Dark Matter
Programme
ExGal
Survey
Galaxy
Clusters
Extragalactic
Star Forming
Systems
AGN
LMC
Survey
Galactic
Plane Survey
Galactic
PeVatrons
Galactic
Centre
cta
cherenkov telescope array
49

Criteria:

- scale in terms of observing hours
- need for coherent approach across multiple targets/pointings
- technical difficulty of performing required analysis and hence reliance on consortium expertise

Will become legacy datasets of high value to the wider community

White Papers Coming Soon

Under consideration:

- Dark Matter Programme
    - dSph
- Galactic Centre
    - synergy with dark matter prog.
- Galactic Plane Survey
    - catalogue, diffuse emission model, PeVatron candidate list, variable sources
- LMC Survey
- Extragalactic Survey
    - 25% sky catalogue
- Transients
    - synergies to MWL/MM partners
- Cosmic Ray PeV-atrons
- Star Forming Systems
    - from mol. clouds to starbursts
- Active Galactic Nuclei
    - long term monitoring, deep exposures of a few sources
- Galaxy Cluster
    - synergy to cosmic-ray/dark matter prog.
- Non-gamma-ray Science
    - Cosmic ray spectrum, electron spectrum, Intensity Interferometry

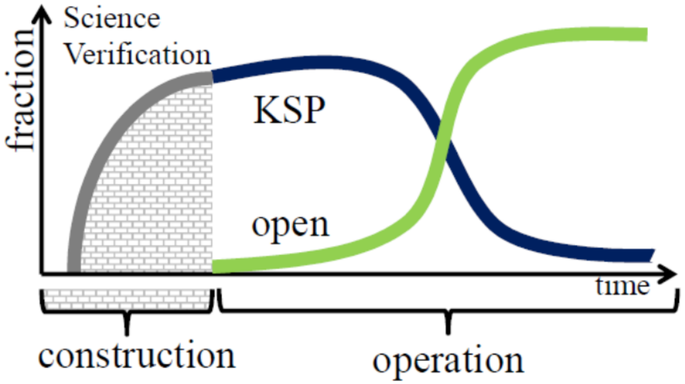

Current assumptions

CTA parties pool the observing time in:

- Open time (for scientists of party countries)
- Consortium time (Key Science Projects)

All data will become fully public after a proprietary period.

The CTA Observatory will provide support to non-expert users

Proposal preparation & submission tools (TAC evaluation)
Calibrated, reconstructed & reduced event data (FITS)
Software to analyse data (Fermi-LAT like)
User documentation
Help Desk, Knowledge, Training

CTA TIMELINE

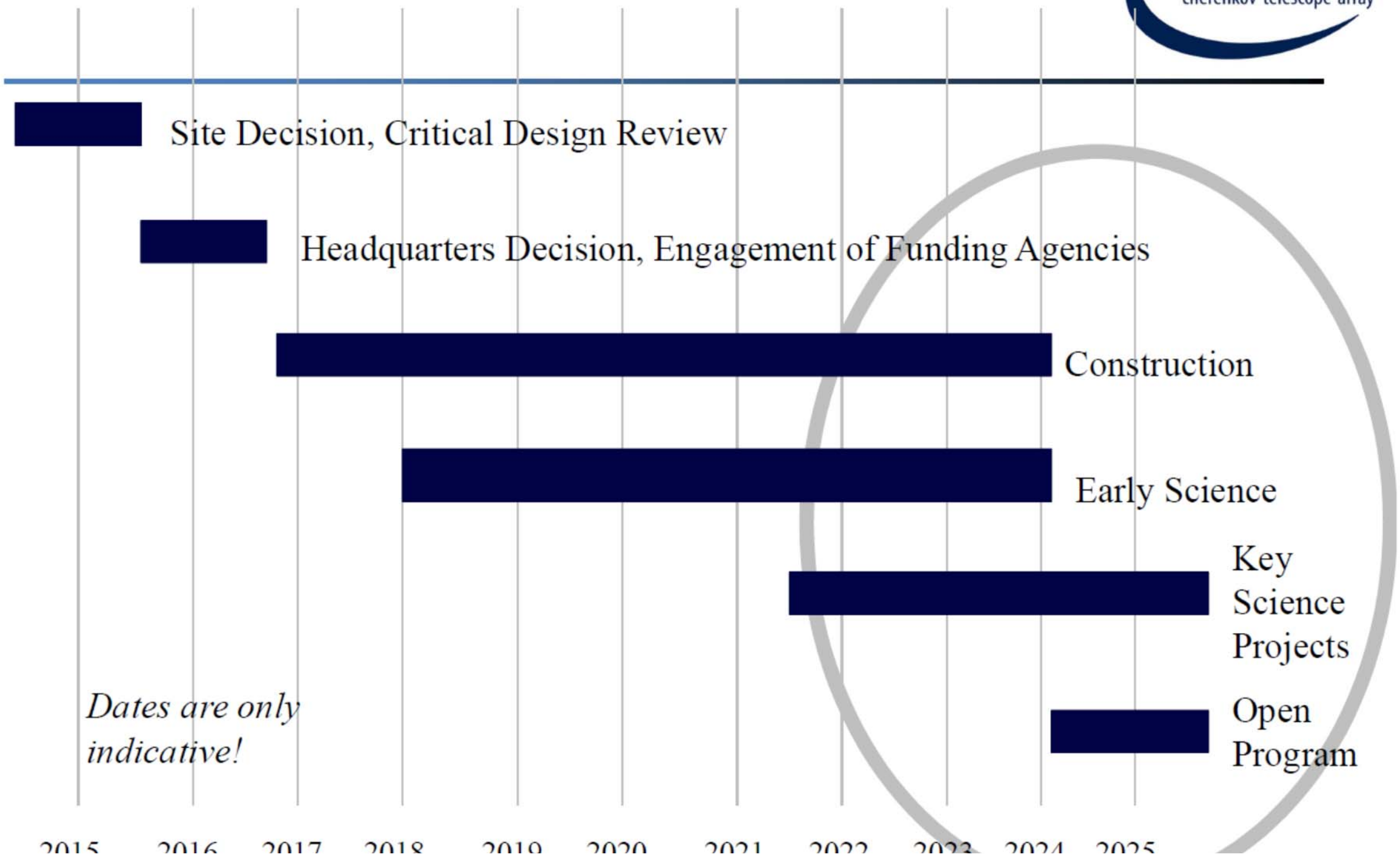

Large Size Telescope Prototype

Ground breaking at La Palma
Oct. 2015

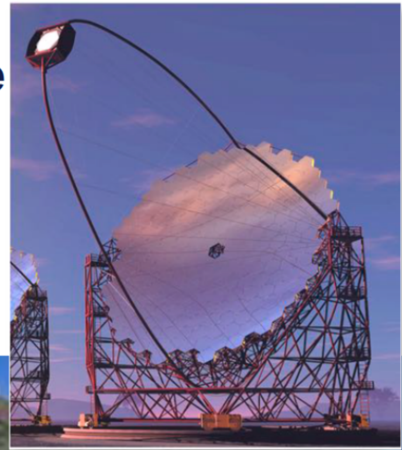

MAGIC Camera

(a) Front side of the M2 camera

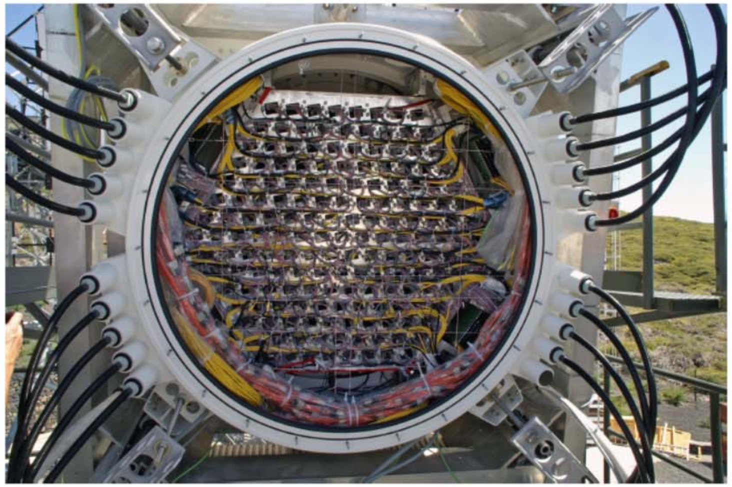

(b) Back side of the M2 camera

CAMERAS

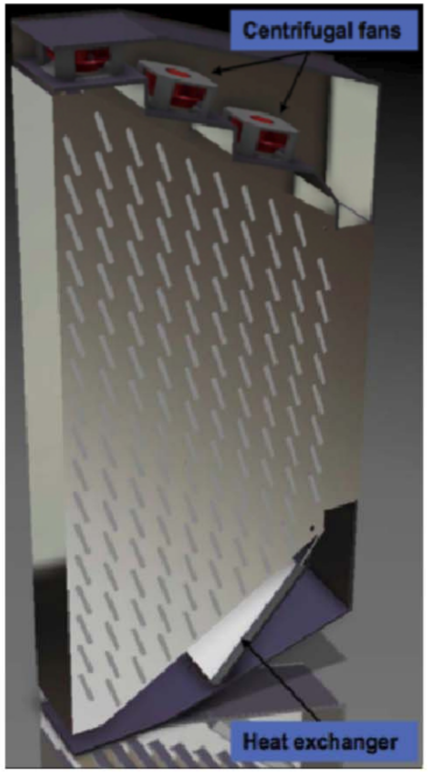

NectarCam cooling studies

FlashCam 144 pixel focal plane

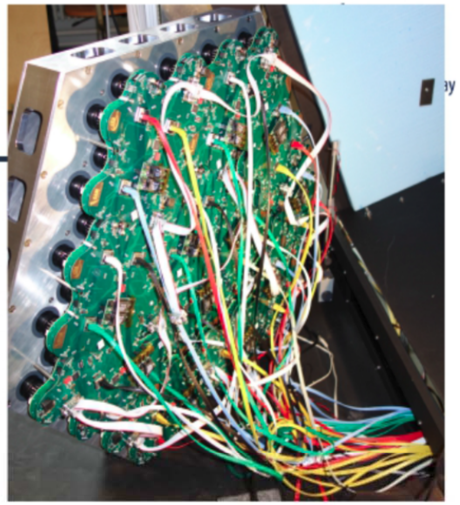

LST camera cluster

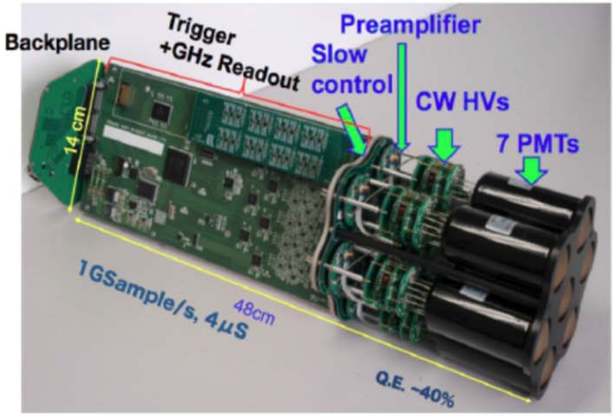

Photodetectors

- Most detectors in particle physics and astrophysics rely on the detection of photons near the visible range, i.e., in the eV energy range. This range covers scintillation and Cherenkov radiation as well as the light detected in many astronomical observations.
- One needs to extract a measurable signal from a small number of incident photons. This can be achieved by generating a primary photoelectron or electron–hole pair by an incident photon (typically by photoelectric effect), amplifying the signal to a detectable level (usually by a sequence of avalanche processes), and collecting the secondary charges to form an electrical signal.
- The important characteristics of a photodetector include:
  - the quantum efficiency QE
  - the overall collection efficiency
  - the gain G
  - the dark noise DN , i.e. the electrical signal when there is no incoming photon;
  - the intrinsic response time of the detector.

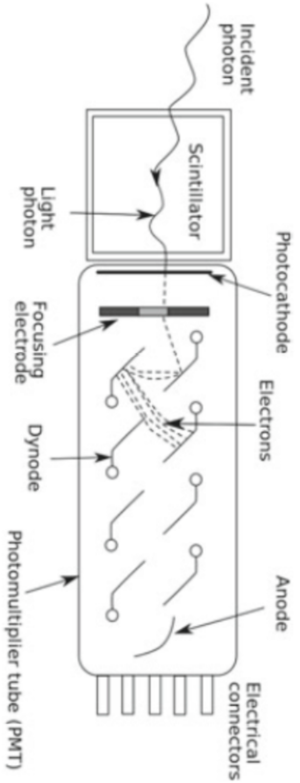

- Prototype: the avalanche photomultiplier tube (PMT)

CTA TELESCOPE DESIGN & PROTOTYPING: SST-1M

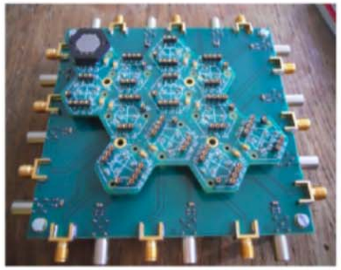

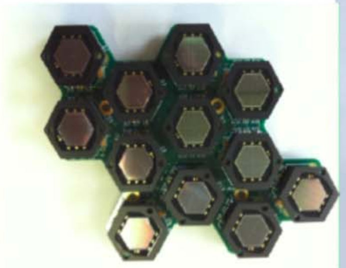

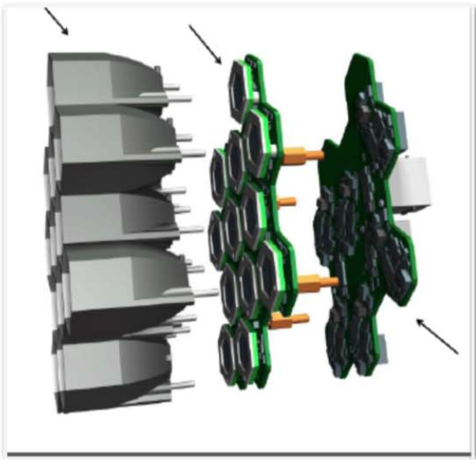

INFN acitivities on SiPM for CTA

CTA

- ~50 INFN scientists working to INFN CTA-RD since September 2012
  - Seevogh meetings every 2nd week, a few physical meetings (Roma, Venezia, Bari,Napoli, …)
- Ordinary financying about 300k€/year
- Since October 2013 Involved in the "Progetto Premiale" TECHE.it
  - Demonstrate the feasibility of an "all-Italian" SiPM Photosensor Unit
  - 1.3 MEUR for INFN: 2/3 for sensors, 1/3 electronics
- Member of GMBH since May 2015
- EoI Submitted in January 2016
  - 3.5M€ for sensors – 8.1sm
  - More funding to be discussed

How to get a SiPM

$$I_D = I_0(e^{\frac{qV_D}{\eta kT}} - 1)$$

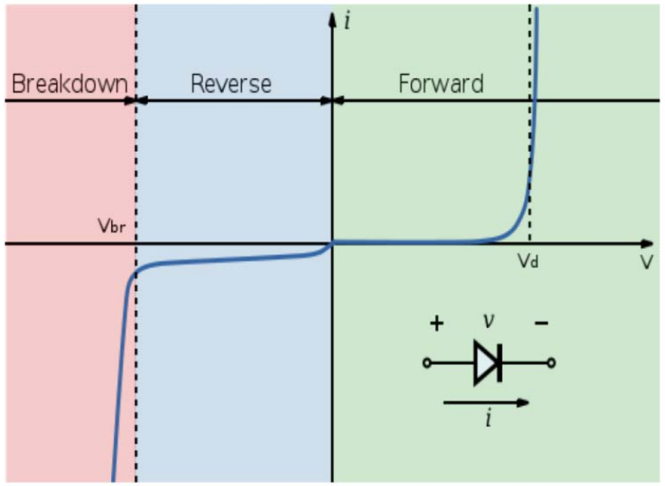

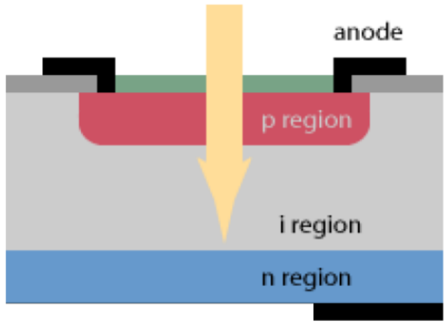

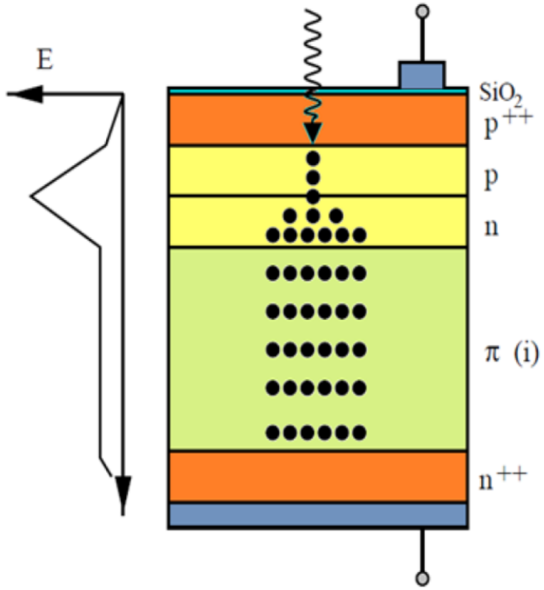

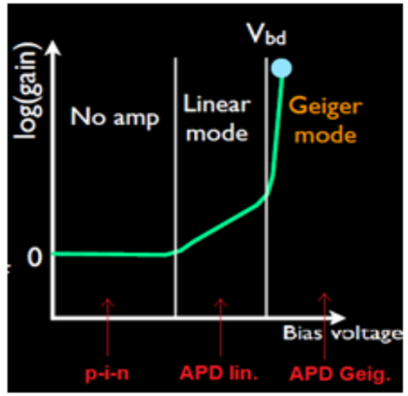

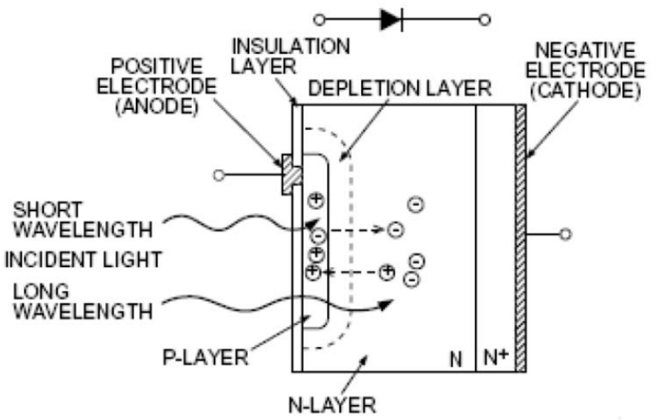
INSULATION LAYER
POSITIVE ELECTRODE (ANODE)
DEPLETION LAYER
NEGATIVE ELECTRODE (CATHODE)
SHORT WAVELENGTH
INCIDENT LIGHT
LONG WAVELENGTH
P-LAYER
N-LAYER
N
N+

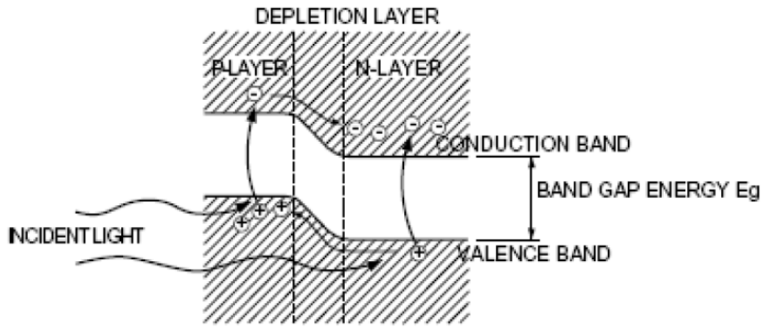
DEPLETION LAYER
P-LAYER
N-LAYER
CONDUCTION BAND
BAND GAP ENERGY Eg
INCIDENT LIGHT
VALENCE BAND

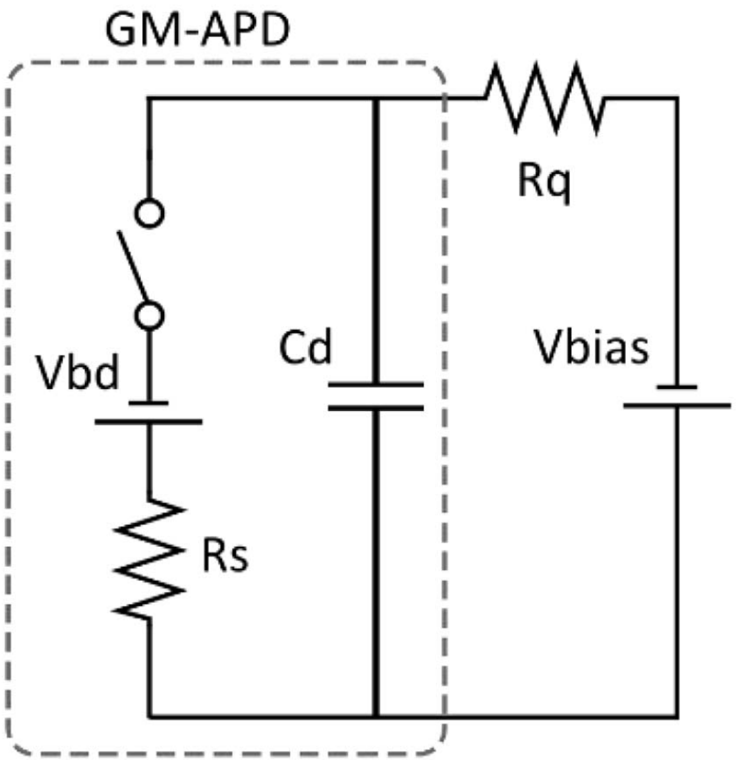
GM-APD
Rq
Vbd
Cd
Vbias
Rs

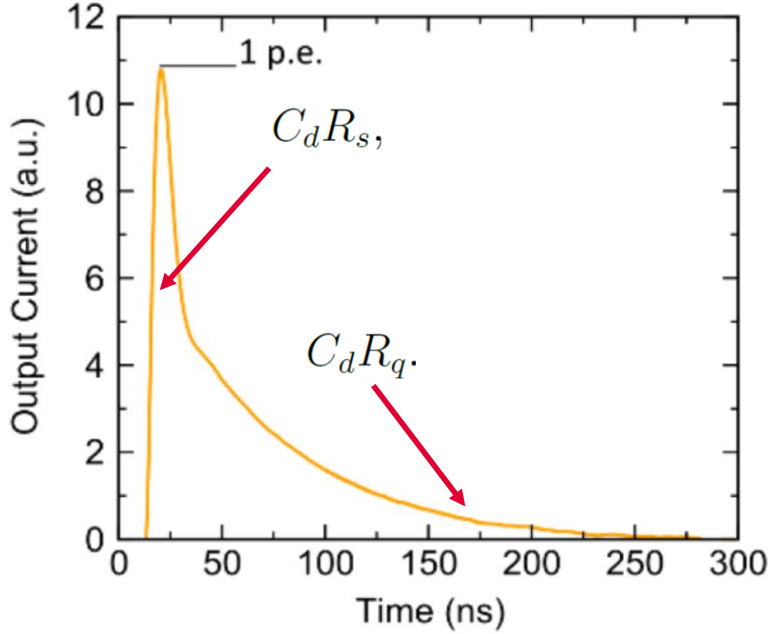
1 p.e.
$C_d R_s$,
$C_d R_q$.
Output Current (a.u.)
Time (ns)

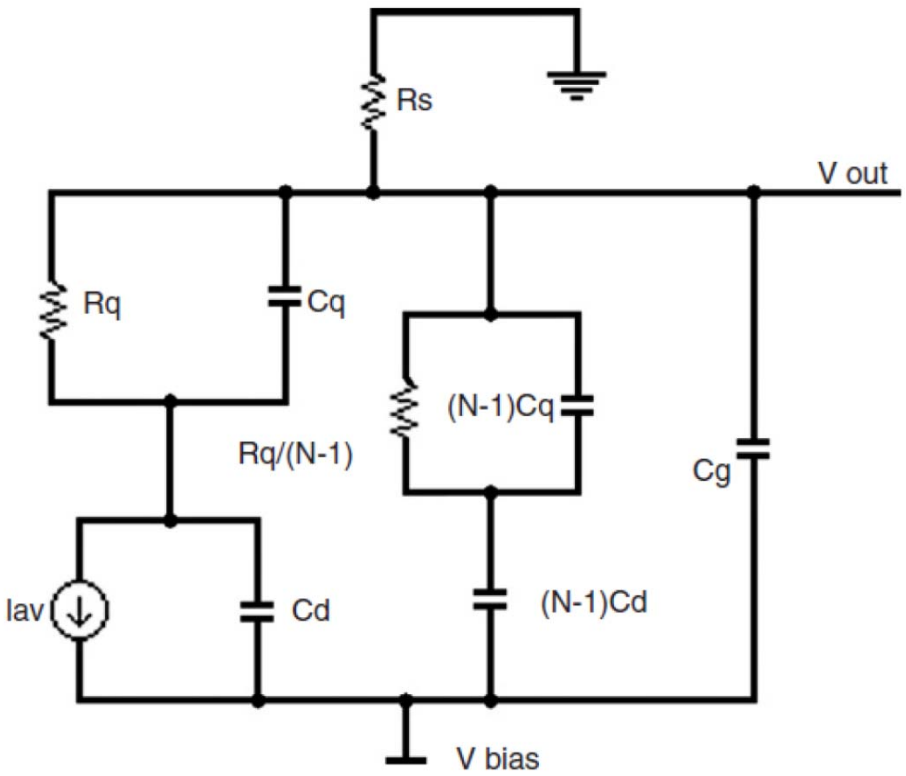
Rs
V out
Rq
Cq
(N-1)Cq
Rq/(N-1)
Cg
Iav
Cd
(N-1)Cd
V bias

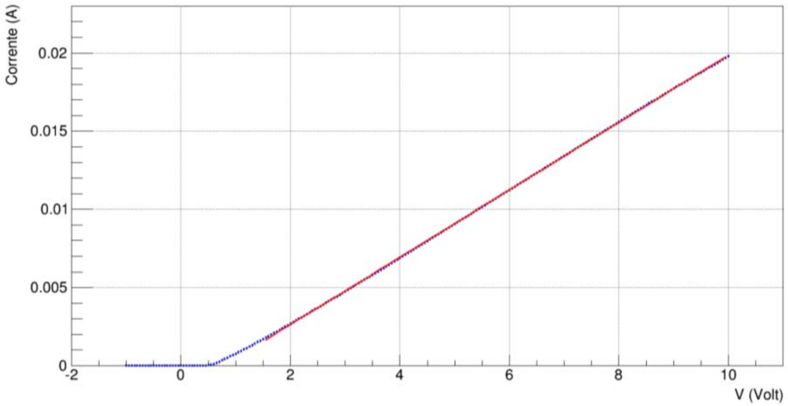

$$Q = (C_d + C_q)\Delta V$$ Gain

CLR Meter -> Gm and Cm @ ω

$$C_{dTOT} = \sqrt{\frac{(1+\omega^2 C^2{}_{TOT} R^2{}_{qTOT})G_m}{\omega^2 R^2{}_{qTOT}}}$$

$$C_{qTOT} = C_{TOT} - CdTOT$$

$$C_g = C_m - C_{dTOT} - \frac{\omega^2 C^2{}_{dTOT} C_{TOT} R^2{}_{qTOT}}{1+\omega^2 C^2{}_{TOT} R^2{}_{qTOT}}$$

$$R_q = 3.87M\Omega$$

$$C_q = 7fF$$

$$C_d = 121fF$$

$$C_g = 95pF$$

The tail cancellation

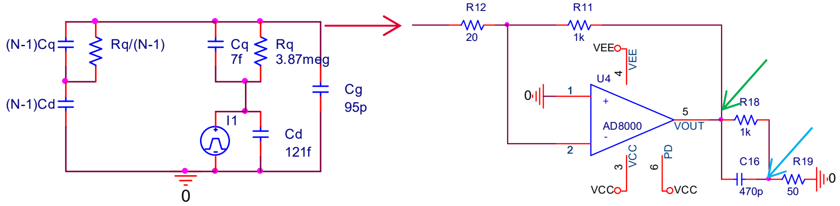

A zero-pole cancellation network has been introduced to reduce the effect of the tail
Trying to not affect the peak

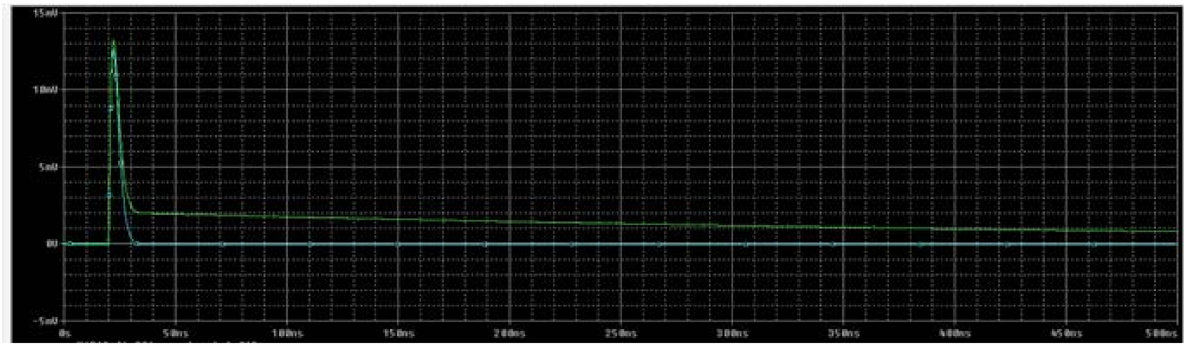

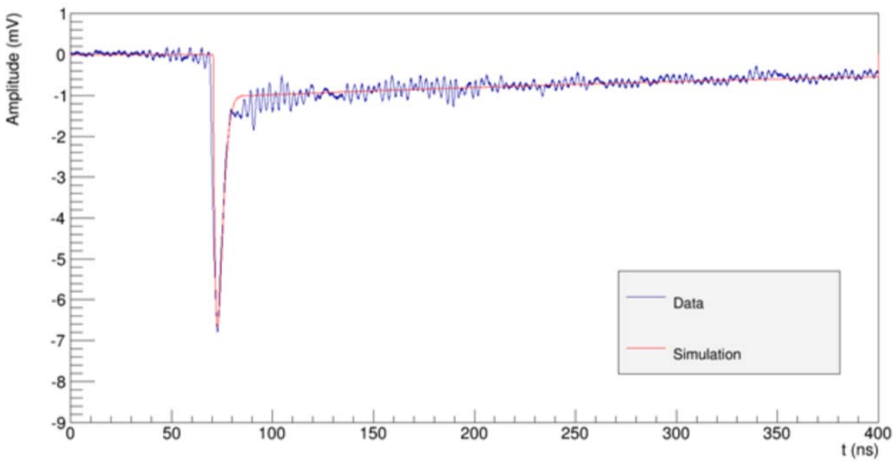
Amplitude (mV)
Data
Simulation
t (ns)

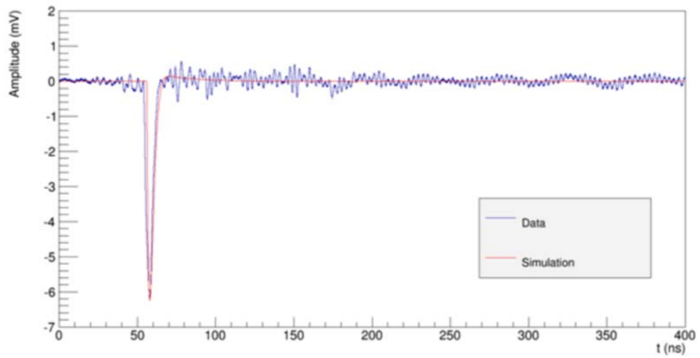
Amplitude (mV)
Data
Simulation
t (ns)

INFN Istituto Nazionale di Fisica Nucleare

2013

- 1 x 1 mm^2 – NUV SiPM 50 um cell
  - 12 pcs, **initial test**
- 3.6 x 3.6 mm^2 – NUV SiPM 50 um cell
  - 50 pcs, **initial test**
- 3.1 x 3.1 mm^2 – NUV SiPM 50 um cell
  - 214 pcs, used for **test, measurement, Matrix assembly of 16**

2014

- 3.1 x 3.1 mm^2, 6 x 6 mm^2 – NUV SiPM 40 um cell
  - used for **test, measurement, Matrix assembly of 16**

2015

- 6 x 6 mm^2 – **CTA-HD SiPM** 30 um cell
  - [production CTA_HD 2015]: 164 SiPM good, **for pSCT**
- 6 x 6 mm^2 – CTA-HD2 SiPM 30 um cell
  - 289 SiPM good, **for pSCT**
  - CTA_HD 2016: 2382 SiPM **mass production for pSCT**

2016

- 6 x 6 mm^2 – CTA-HD3 SiPM 40 um cell
  - 6 wafer – under test

2017

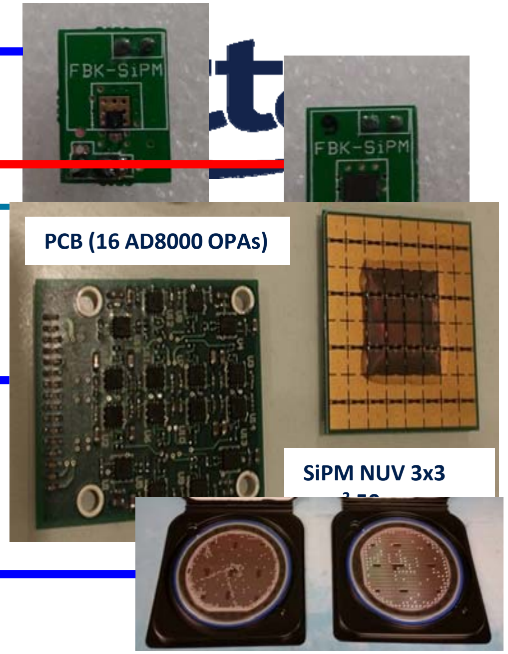

SiPM NUV da 3x3 e 6x6 mm^2 su fette da 6”

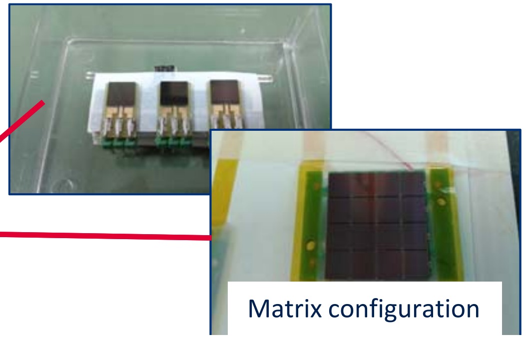

High-Density technology in NUV

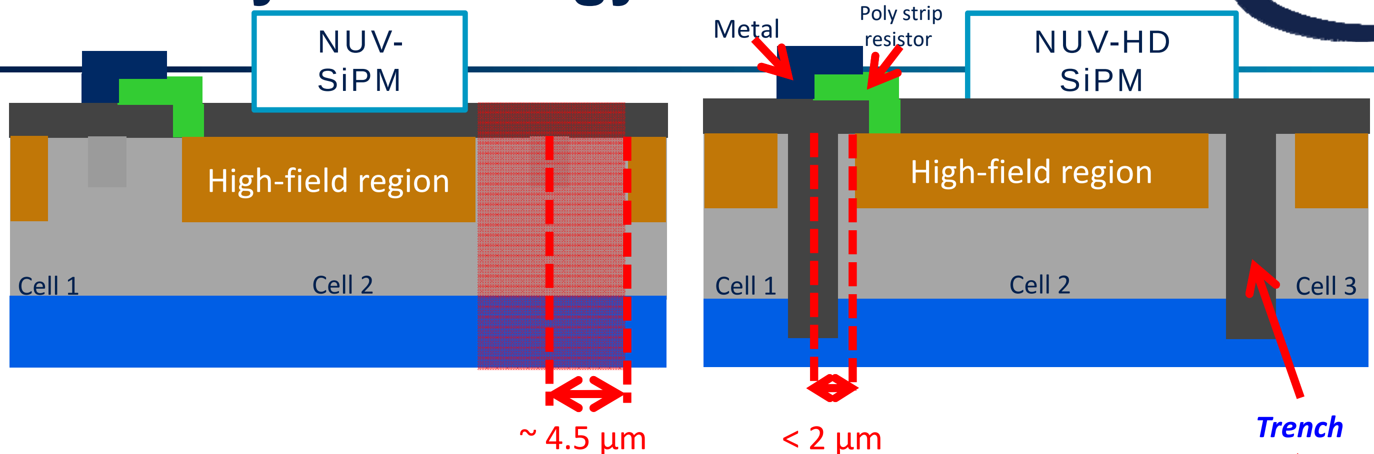

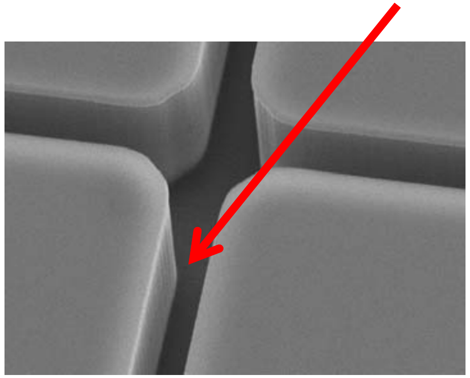

NUV High-Density (HD) technology:

Lower dead border region → Higher Fill Factor

Trenches between cells → Lower Cross-Talk

(C. Piemonte et. al., (2016) IEEE T. Electr. Dev., 10.1109/TED.2016.2516641)

NUV-HD SiPM layout features

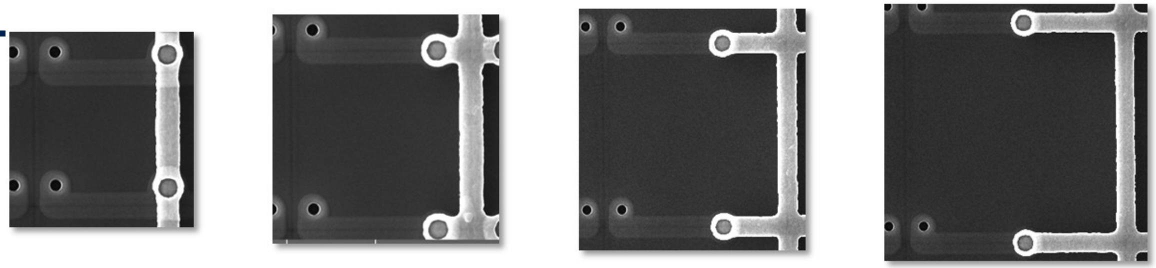

15 µm 20 µm 25 µm 30 µm

High PDE

Cell Pitch	15 µm	20 µm	25 µm	30 µm	35 µm	40 µm
Fill Factor (%)	55	66	73	77	81	83
#cells/mm^2	~ 4444	2500	1600	~ 1111	~ 816	625

High Dynamic Range

Fill Factor in HD technology

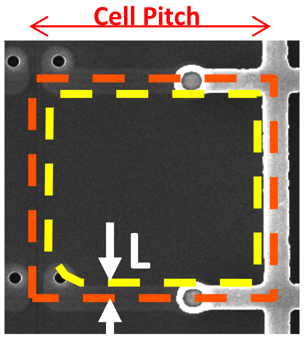

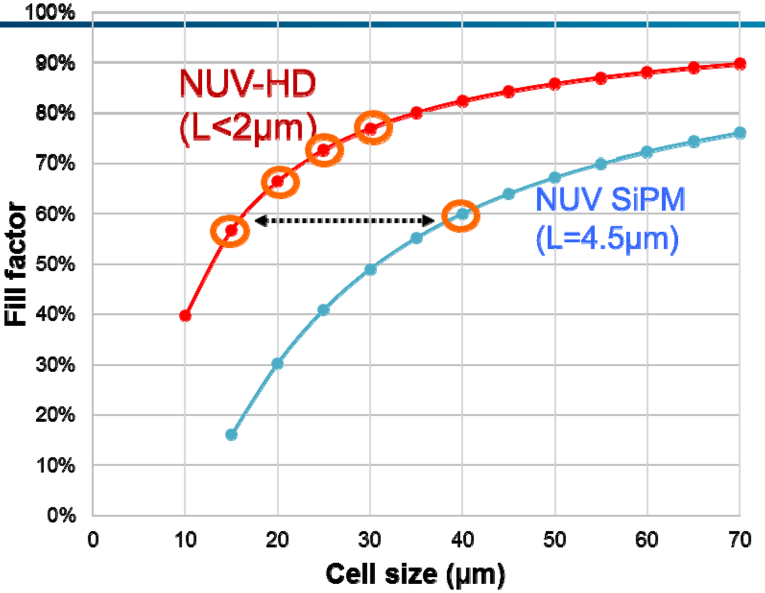

The HD 15 µm pitch is equivalent to the standard 40 µm

FBK SiPM 30 μm chip size, 6mm x 6mm active area

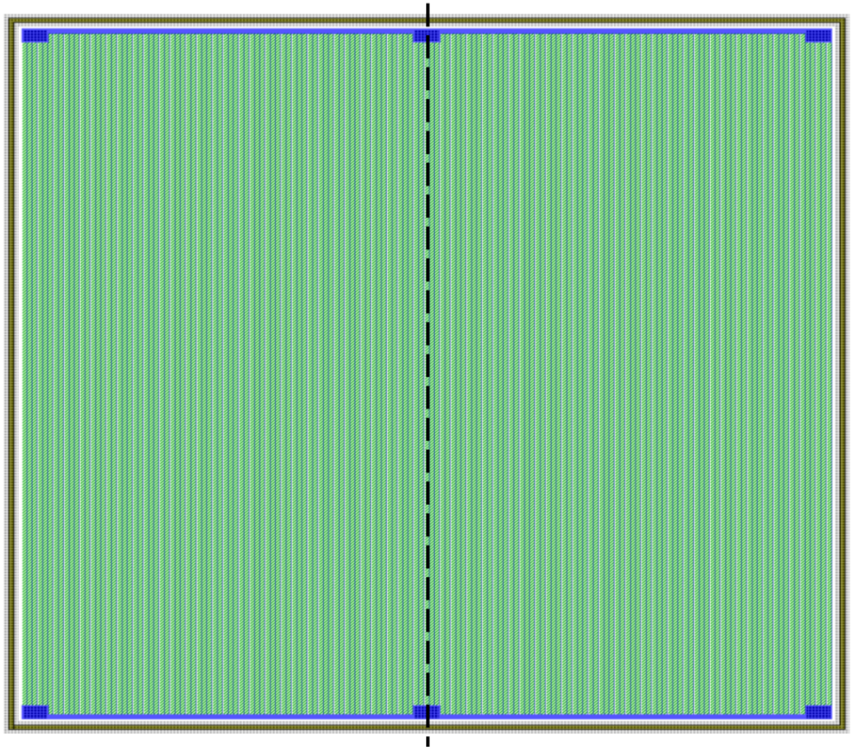

6 bonding pads
(at the 4 corners and at center of two sides, internal to the "active" area)

Nominal chip size (cut-line center):
$6.28 \times 6.8 mm^2$

Effective chip dimension
(after cut):
- Typical: 6.23mm
- Min: 6.21mm
- Max: 6.24mm

Active area:
- X: 6.06mm
- Y: 6.03mm (5.88mm at the bonding pads)

Micro-cell size (pitch):
$30 \times 30 \mu m^2$

Micro-cell geometrical fill factor:
76%

Number of micro-cells:
40394

SiPM effective area: 36.34 mm^2 (taking into account bonding pads dead regions)
SiPM active area: 27.64 mm^2 (taking into account 76% microcell geom. fill factor)

I-V characteristic curve

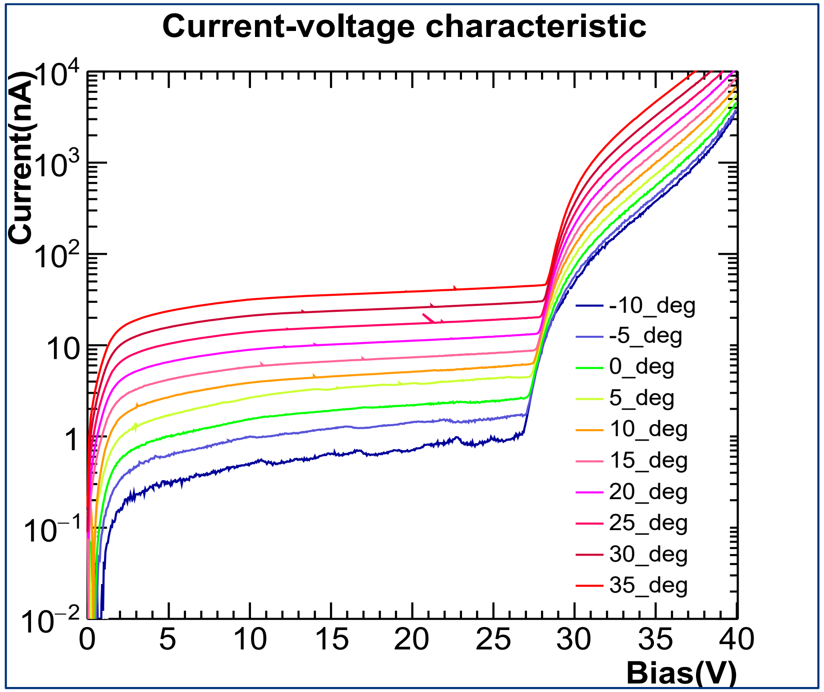

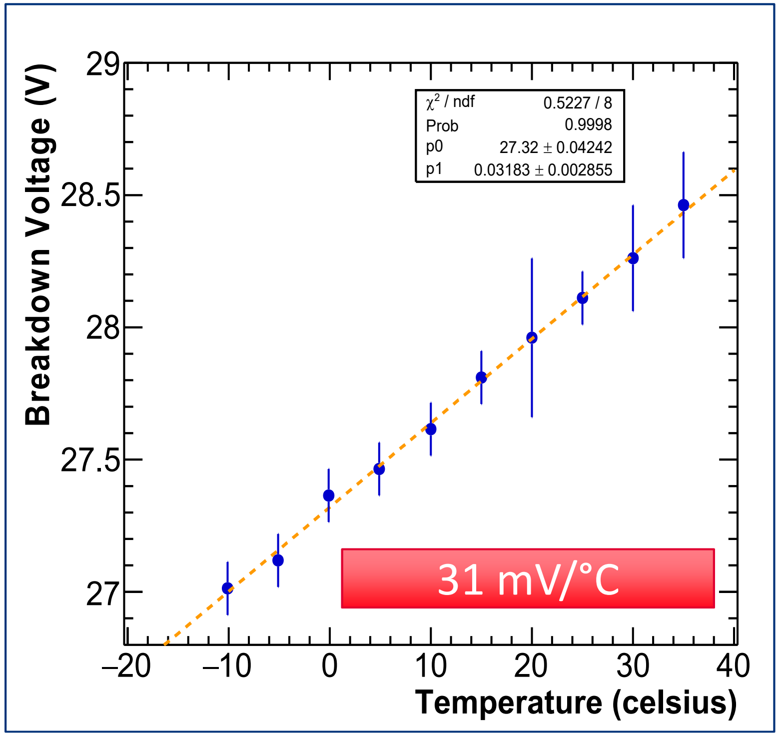

Slight variation of breakdown voltage with temperature

SiPM NUV and NUV – HD

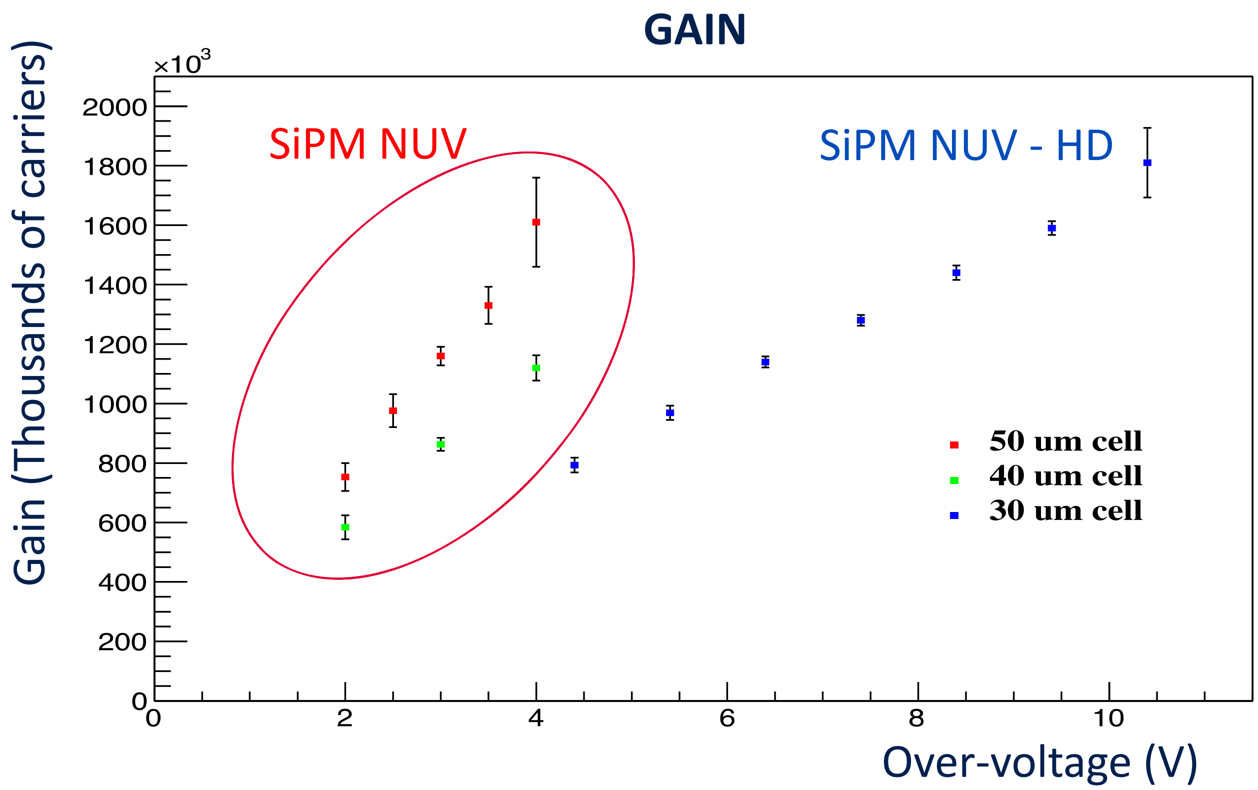

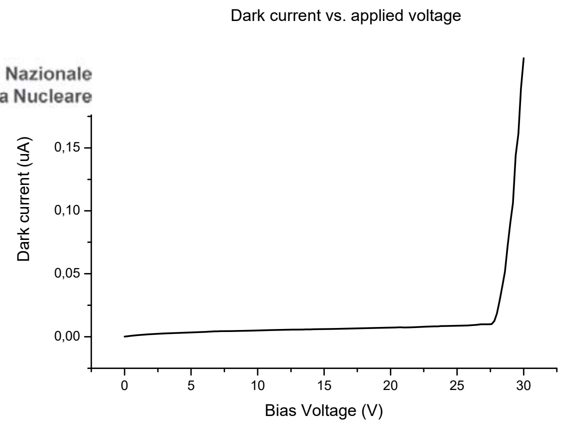
Dark current vs. applied voltage
Dark current (uA)
Bias Voltage (V)

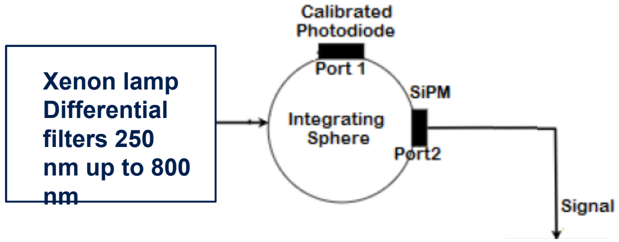
Calibrated Photodiode
Port 1
Xenon lamp Differential filters 250 nm up to 800 nm
Integrating Sphere
SiPM
Port2
Signal

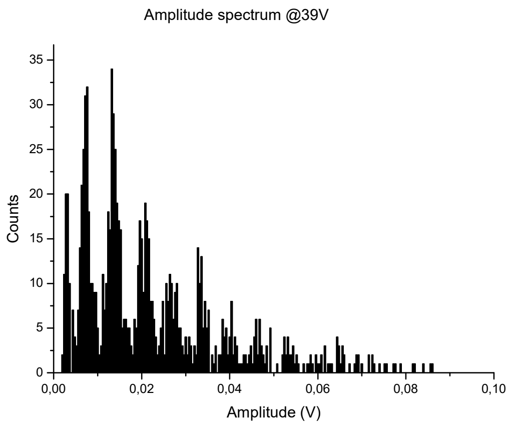
Amplitude spectrum @39V
Counts
Amplitude (V)

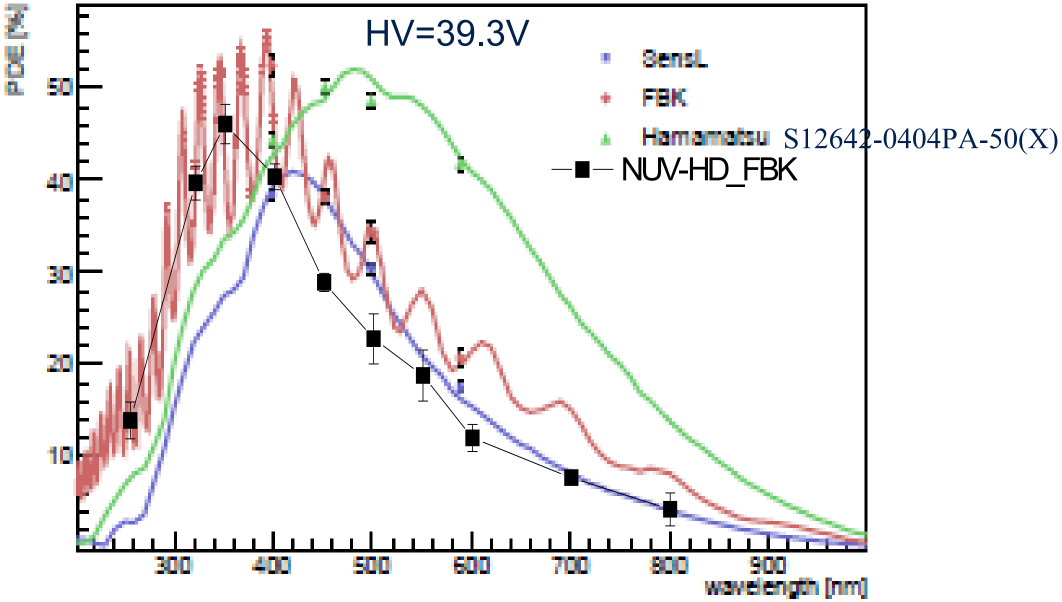
HV=39.3V
PDE [%]
SensL
FBK
Hamamatsu S12642-0404PA-50(X)
NUV-HD_FBK
wavelength [nm]

PDE_INFN_NA

Photon Detection Efficiency

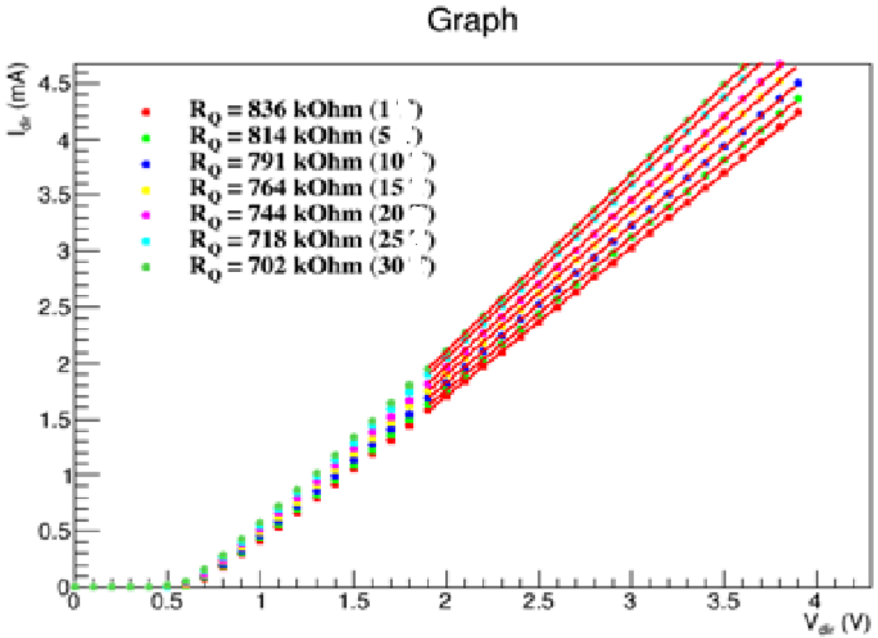

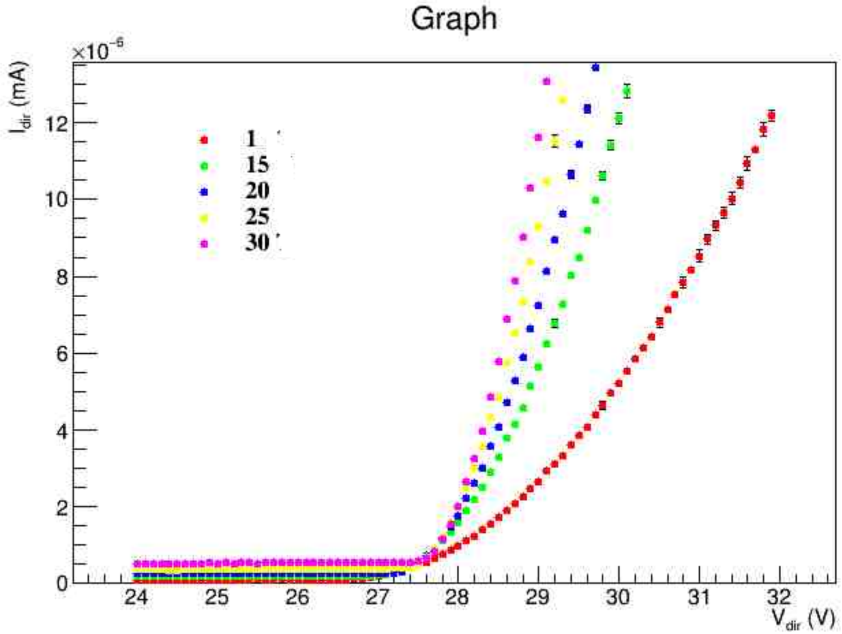

LST: large surface SiPM?

Challenge: single sensor with large area (1 inch diameter)
Amplify-and-sum stage, one output per pixel

Prototype of analog sum scheme will be tested in MAGIC

Prototype cluster using Hamamatsu and developed by MPI mounted on MAGIC Jun 15

9 FBK 6x6 mm^2 sensors
Sensor electronics by INFN Padova
MAGIC cluster control electronics and

Signal: 2 mV per phe; noise: 0.5 mV rms
Linearity: ok to >200 phe

Assembly and test now,; installed in MAGIC October 2015 for comparison with the standard PMT clusters (and with the similar Max Planck SiPM cluster, just installed)

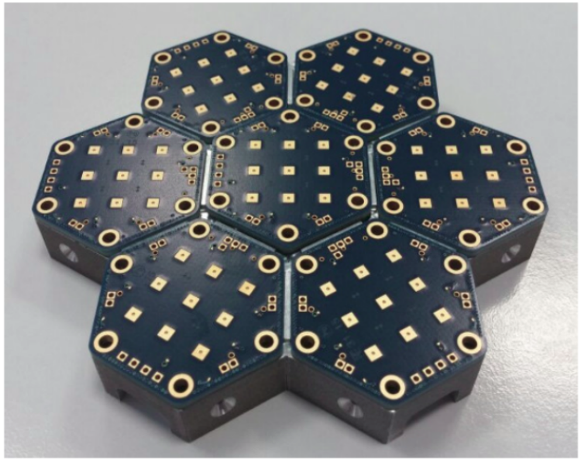

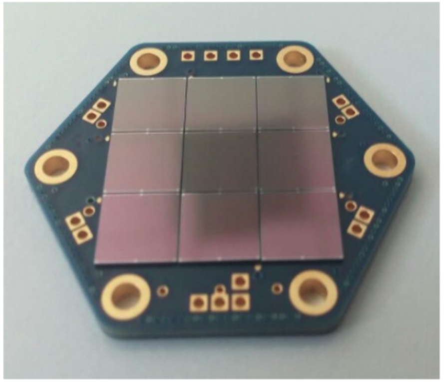

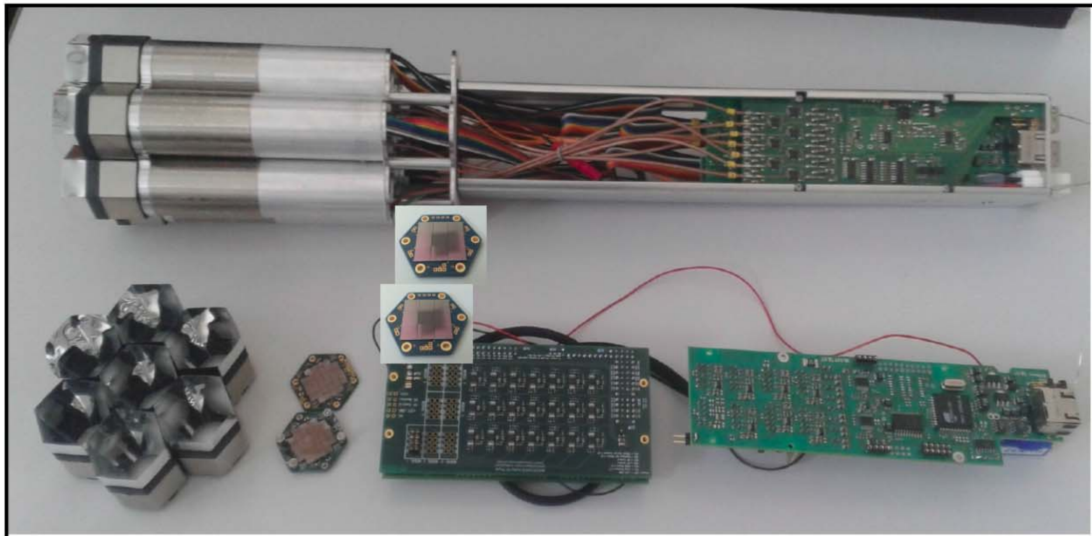

In picture:
Top: standard MAGIC PMT cluster
Bottom: components for SiPM cluster, mechanical structure removed

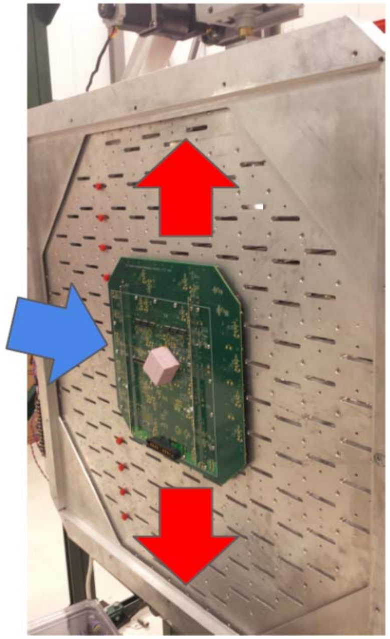

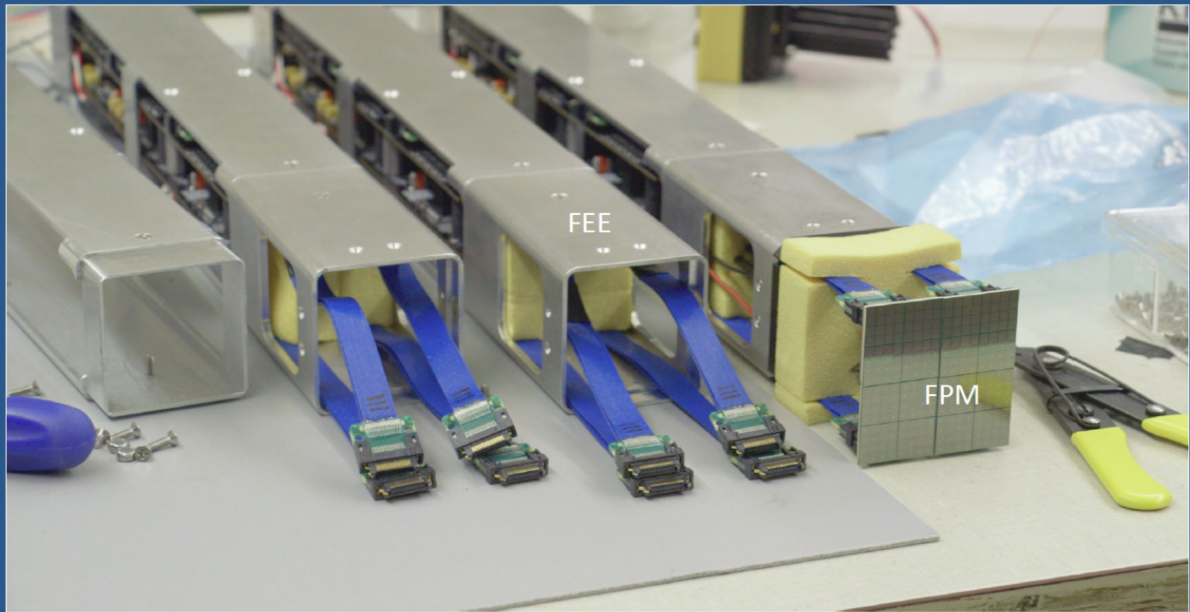

Module = focal plane module (FPM) + front-end electronics (FEE)

MRI pSCT project plans to produce 25 modules, which will populate single backplane board (fully populated pSCT camera consists of 177 modules).

Focal Plane Module

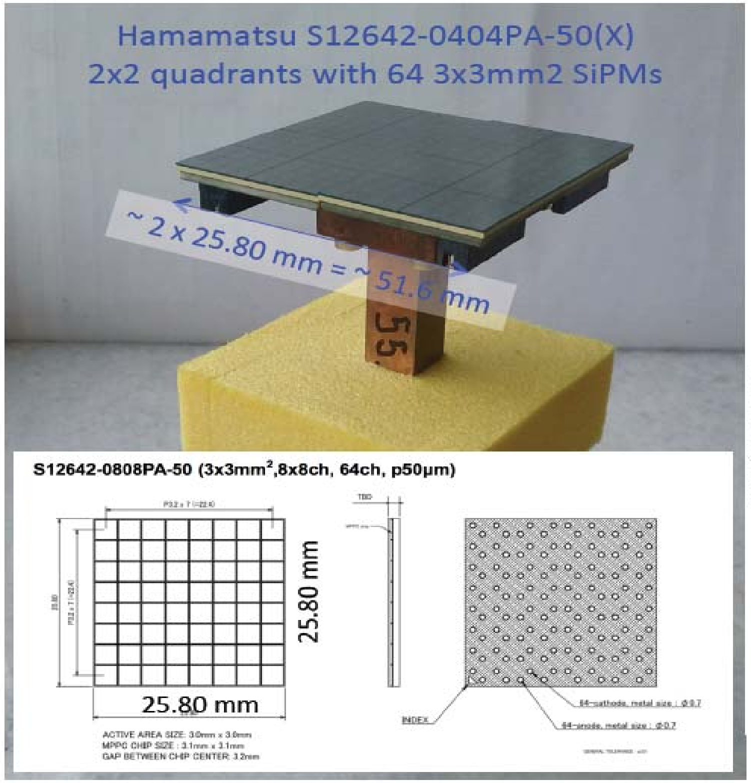

2 x 25.80 mm = 51.6 mm

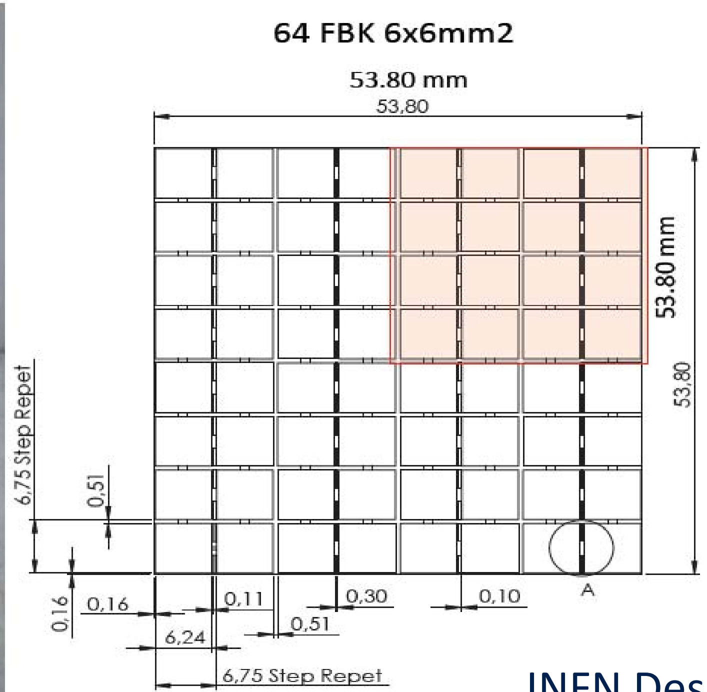

INFN Design

Front end production and R&D

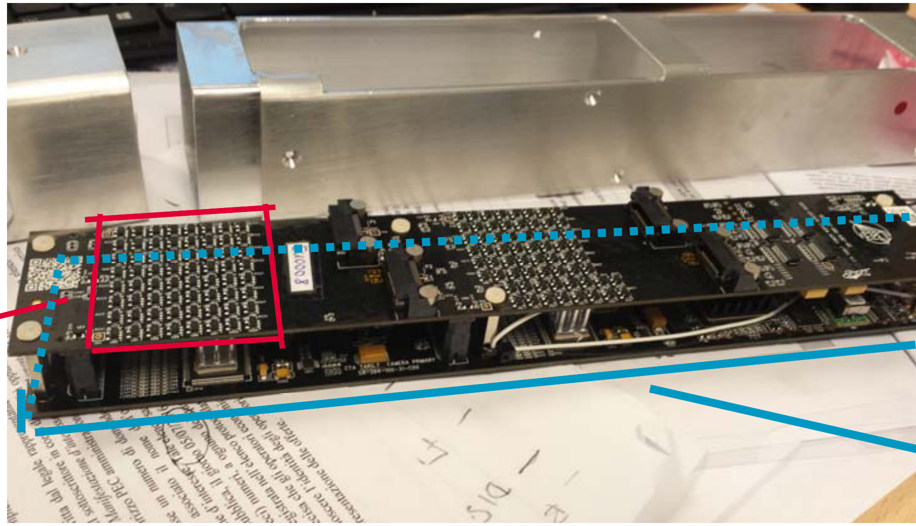

Preamp. Stage
Hybrid tech vs ASIC

Digital Board
T7 vs TC

INFN activity for pSCT

- 25 Photo-detection Modules
  - Each divided in 4 parts -> 100 PCBs -> 16 Pixels each
  - 1600 FBK SiPM NUV-HD 6mmx6mm 30μm cells
- Each sensor will be tested individually
- Each PCB will be tested for acceptance

- New Schedule
  - 9 PCBs & Electronics (T7)
  - 1 complete sector (TC)

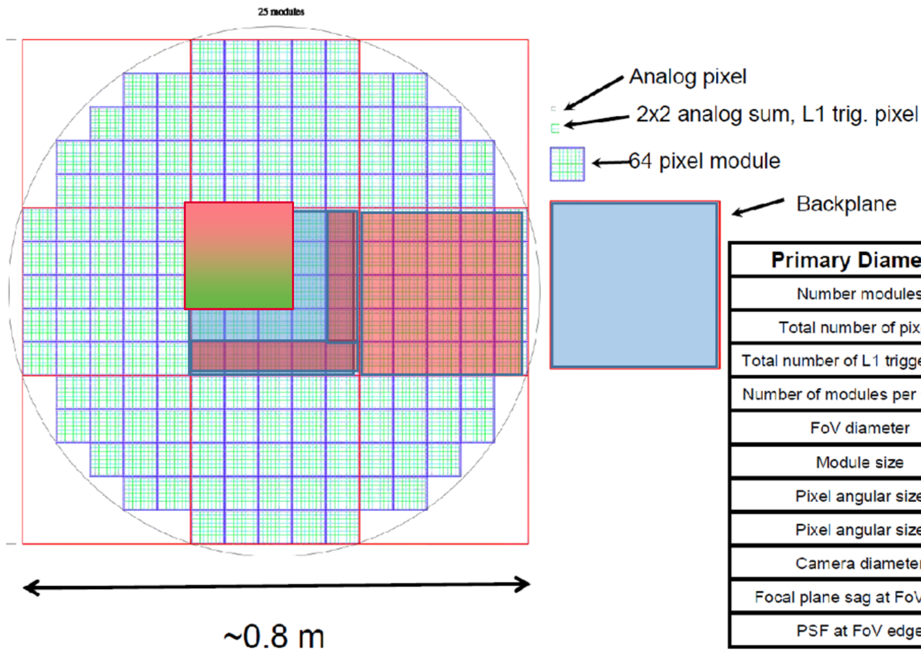

Primary Diameter	9.5 m
Number modules	177
Total number of pixels	11328
Total number of L1 trigger pixels	2832
Number of modules per subfield	25
FoV diameter	8.0°
Module size	52–54 mm
Pixel angular size	0.067°
Pixel angular size	4.0’
Camera diameter	0.78 m
Focal plane sag at FoV edge	-2.2 cm
PSF at FoV edge	3.81’

One quadrant (16 FBK SiPMs)

SOLDER MASK

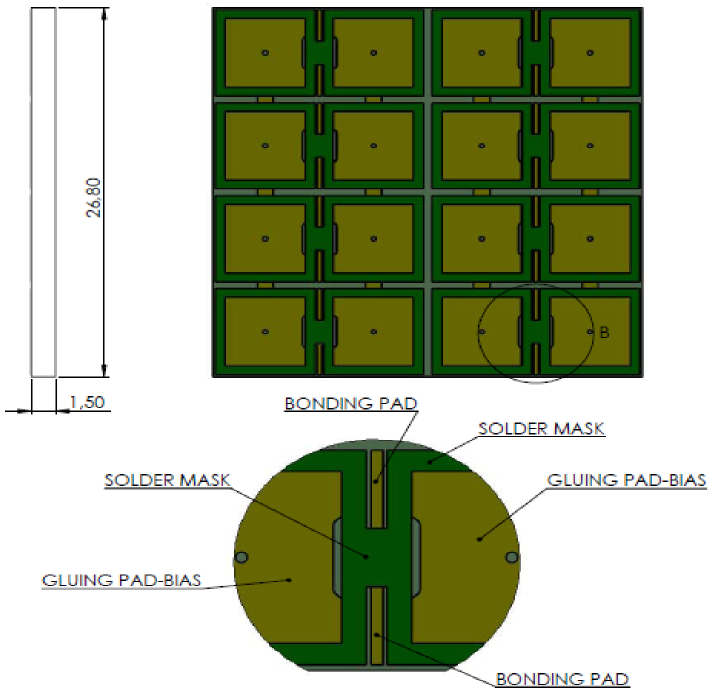

SiPM

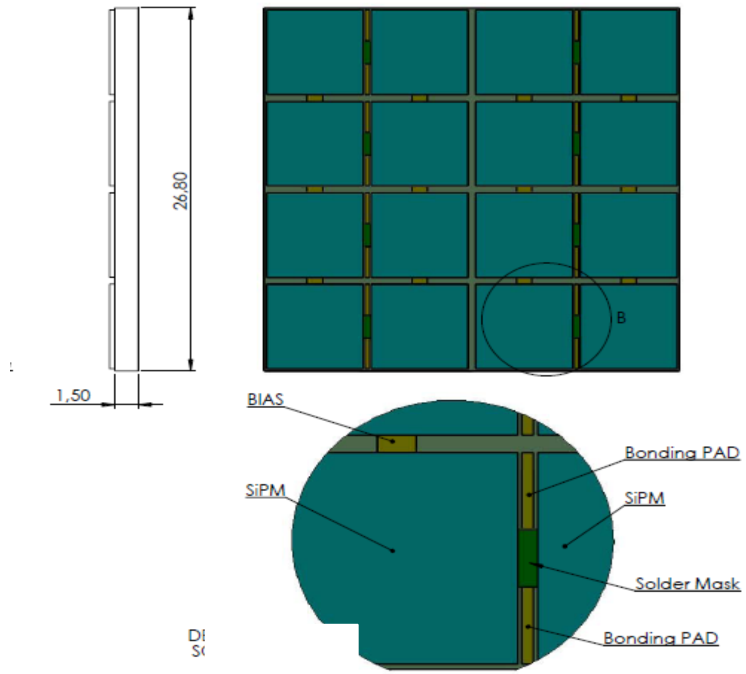

The lay-out

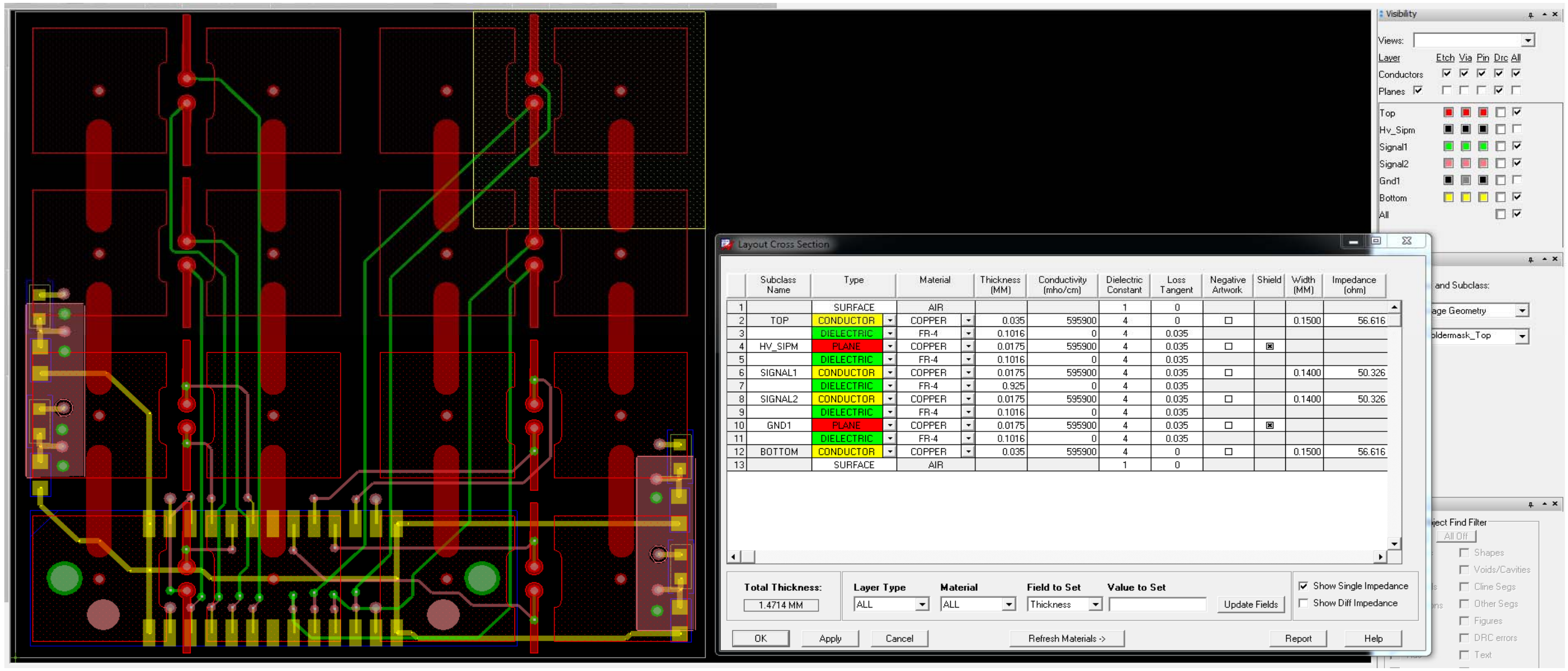
Layout Cross Section
Subclass Name | Type | Material | Thickness (MM) | Conductivity (mho/cm) | Dielectric Constant | Loss Tangent | Negative Artwork | Shield | Width (MM) | Impedance (ohm)
1 SURFACE AIR 1 0
2 TOP CONDUCTOR COPPER 0.035 595900 4 0 0.1500 56.616
3 DIELECTRIC FR-4 0.1016 0 4 0.035
4 HV_SIPM PLANE COPPER 0.0175 595900 4 0.035
5 DIELECTRIC FR-4 0.1016 0 4 0.035
6 SIGNAL1 CONDUCTOR COPPER 0.0175 595900 4 0.035 0.1400 50.326
7 DIELECTRIC FR-4 0.925 0 4 0.035
8 SIGNAL2 CONDUCTOR COPPER 0.0175 595900 4 0.035 0.1400 50.326
9 DIELECTRIC FR-4 0.1016 0 4 0.035
10 GND1 PLANE COPPER 0.0175 595900 4 0.035
11 DIELECTRIC FR-4 0.1016 0 4 0.035
12 BOTTOM CONDUCTOR COPPER 0.035 595900 4 0 0.1500 56.616
13 SURFACE AIR 1 0
Total Thickness:
1.4714 MM
Layer Type
Material
Field to Set
Value to Set
Thickness
Update Fields
Show Single Impedance
Show Diff Impedance
OK
Apply
Cancel
Refresh Materials ->
Report
Help
Visibility
Views:
Layer Etch Via Pin Drc All
Conductors
Planes
Top
Hv_Sipm
Signal1
Signal2
Gnd1
Bottom
All

INFN Istituto Nazionale di Fisica Nucleare

Prodution phase…

cta

- A copper block is used to thermally and mechanically couple the PCB to the camera pods to form a module in a backplane
- It is placed on the PCB back-side with high precision in both X, Y and Z coordinates, before the SiPM placement. This is crucial for the performance of the camera.
- More than 100 copper blocks are available for the assembly
- The blocks have been placed on the dummy PCBs at ARTEL facility with a precision of <100 micron in XY plane, <0.1° degrees in Z coord (16 available)
- The requirements for alignment precision are of ~300 μm in XY plane and < 2° in z (vertical) axis
- Custom mechanical holders are being produced with holes and position pins to achieve a high accuracy for the alignment (~10 μm) in the xy plane and z direction (<0.1°).

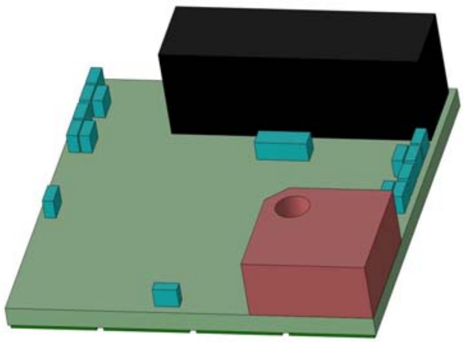

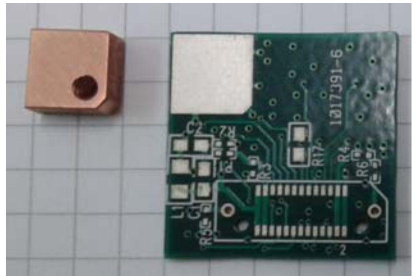

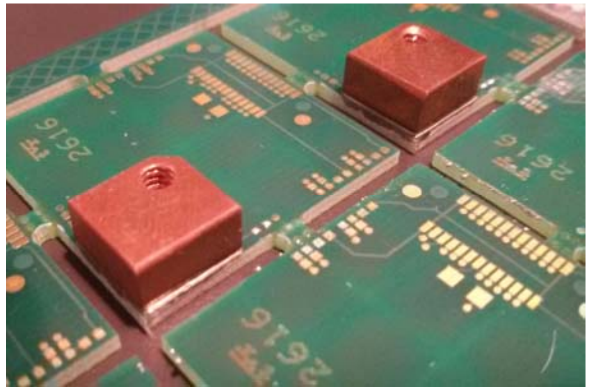

- To speed up the SiPM placement and glueing on the PCBs, a “pick & place” machine is used to first distribute the conductive glue to the PCB top layer metal pads and with a vacuum suction cup to take the sensors out of the custom holder and place them on the PCB with high precision.
- A test to validate the accuracy of the pick & place machine has been run using some NUV-HD SiPM placed over dummy PCBs produced for testing the procedure.

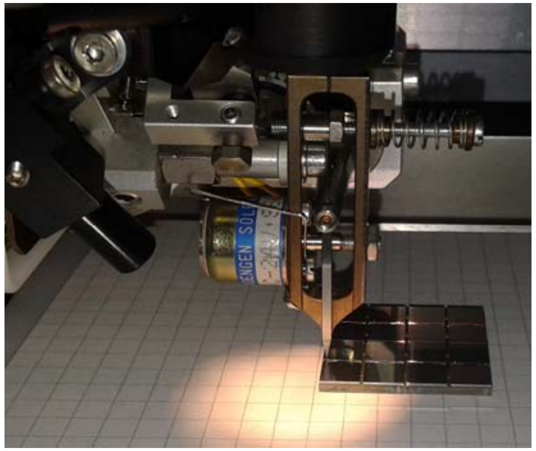

With the jigs, to place and glue SiPm on 104 PCB will require 1 day

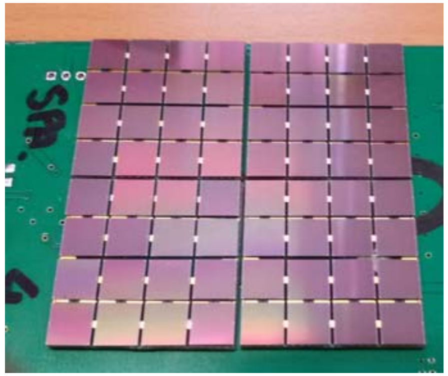

Measured Alignment precision is <30 μm and < 0.5° rotation

The SiPMs

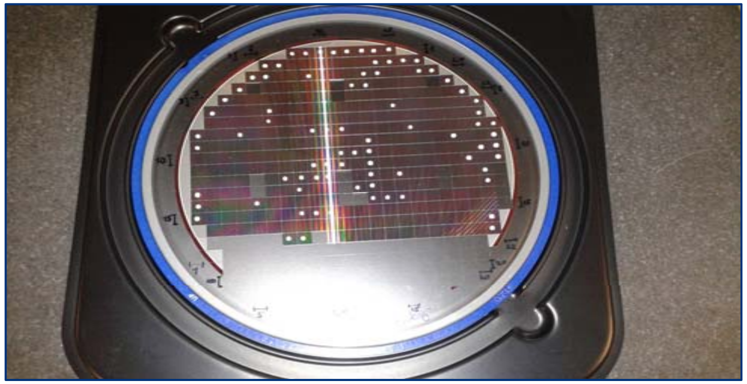

- 6mmx6mm 30um Cells
- Blue tape from FBK
- SiPMs are then arranged in single or matrix configuration

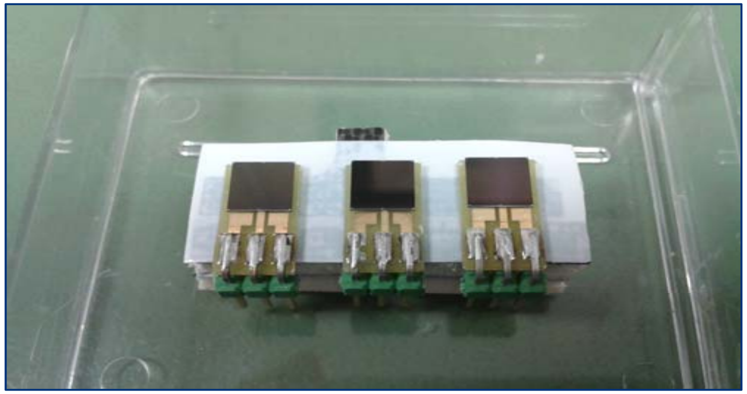

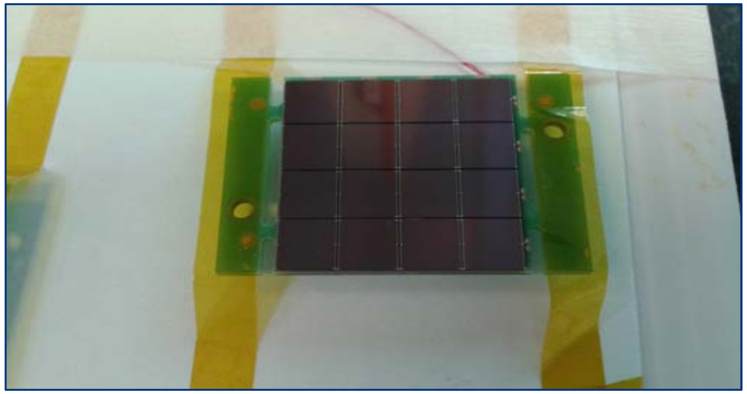

The First FPM

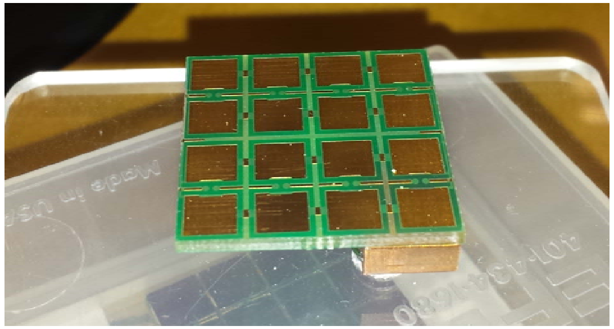

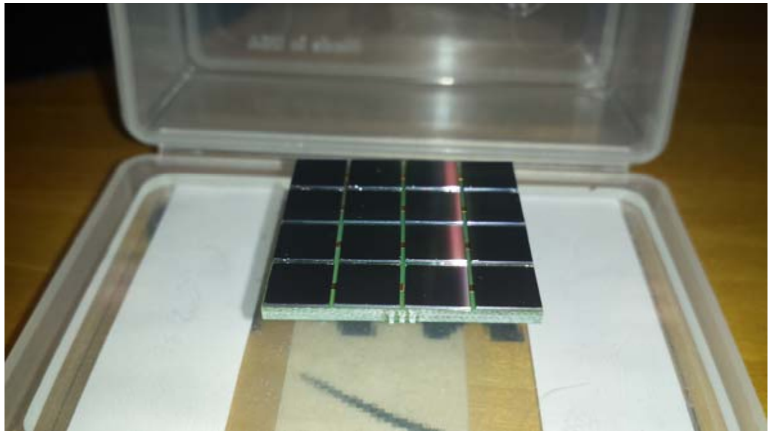

SiPM 6.23x6.23 mm^2
Modules 27x27mm^2
FillFactor = 16 x 6.23x6.23 / (27x27) = 85%
With SiPM we get about 65%

DAQ trigger

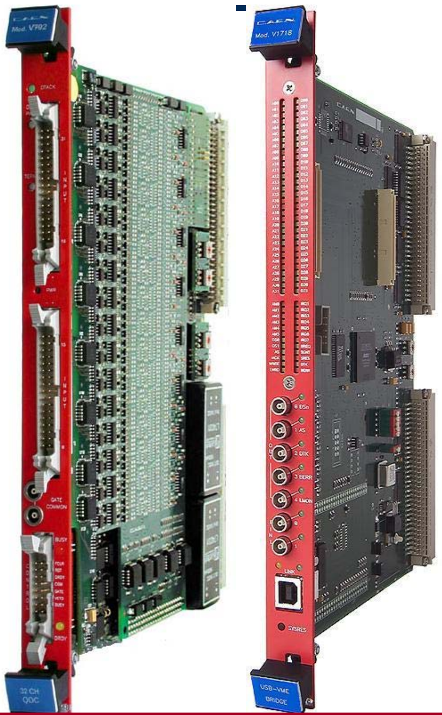

TRIGGER SCHEME

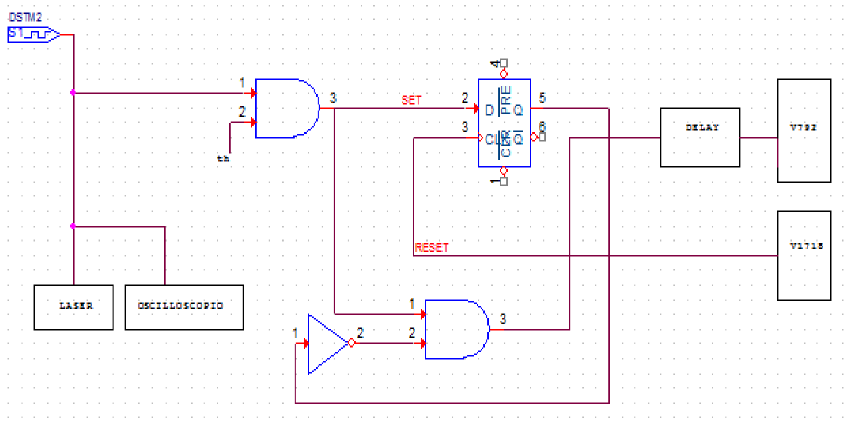

CONTROLLER VME CAEN V1718
QDC CAEN V792 – 32 channels

Extension to 64 channels using two V792 modules should be straigthforward

DAQ: SignaL and Gate

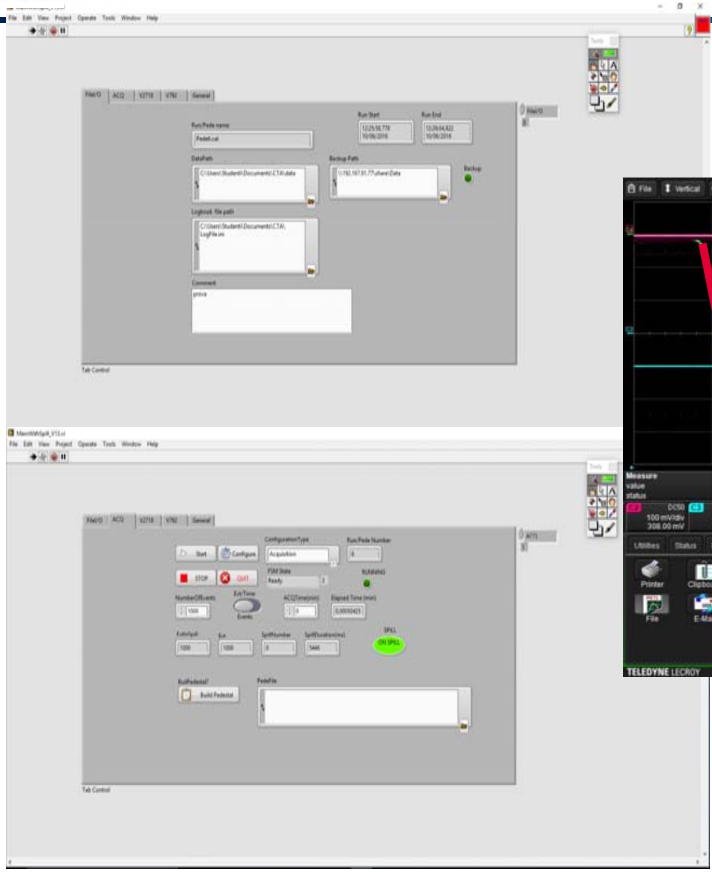

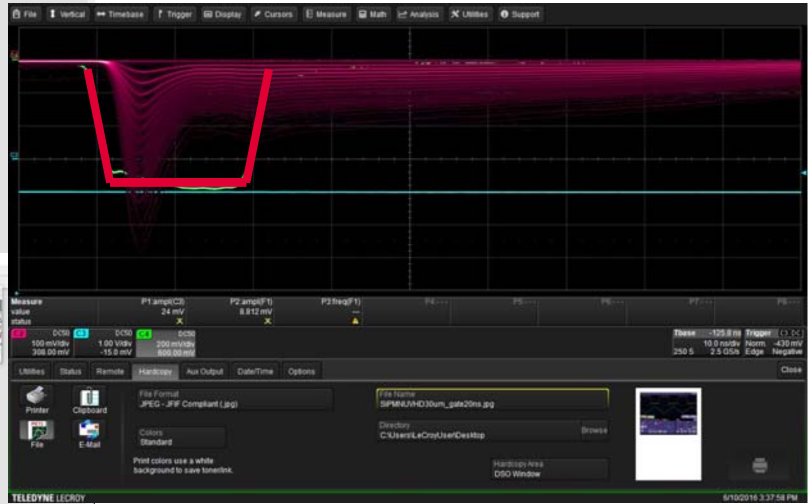

Gate width Study

SiPM: 25um, 1x1mm2, 34V
Waveform amplitude: approx. 35mV/P.E.
Waveform baseline: approx. 17mV

Single channel acquisition (ch31) with different gate windows

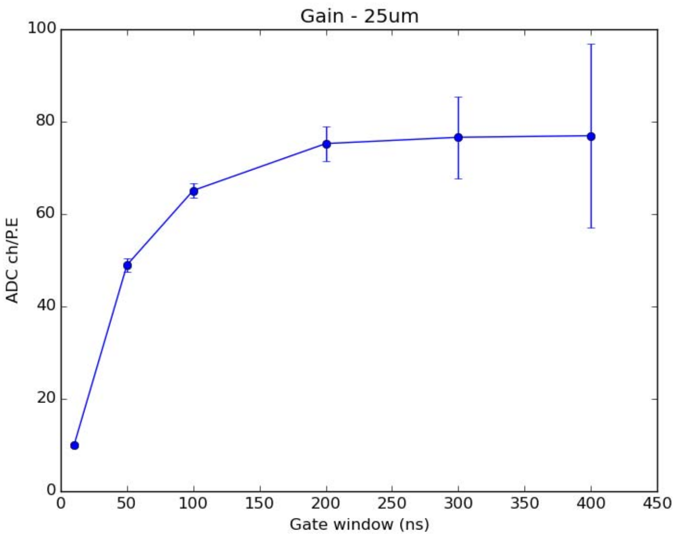

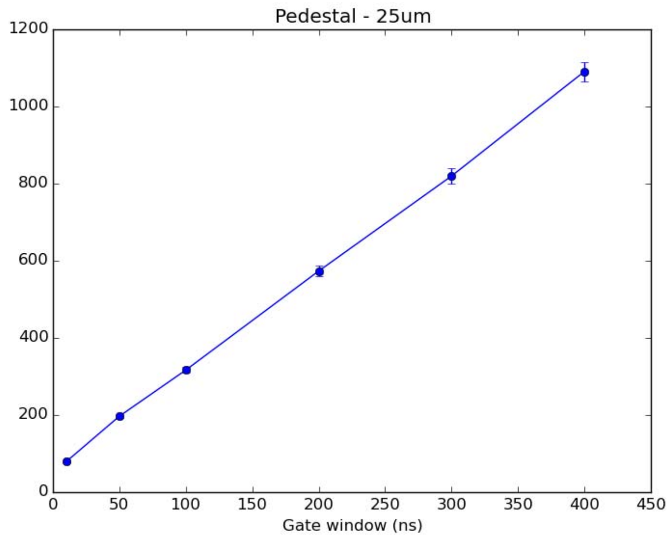

Gate width Study

SiPM: 25um, 1x1mm2, 34V
Waveform amplitude: approx. 35mV/P.E.
Waveform baseline: approx. 17mV

Single channel acquisition (ch31) with different gate windows

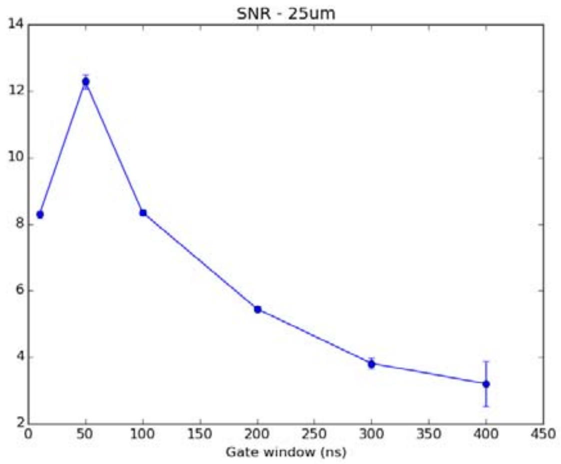

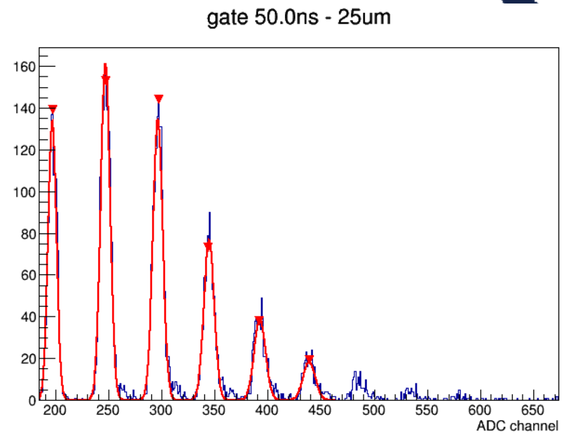

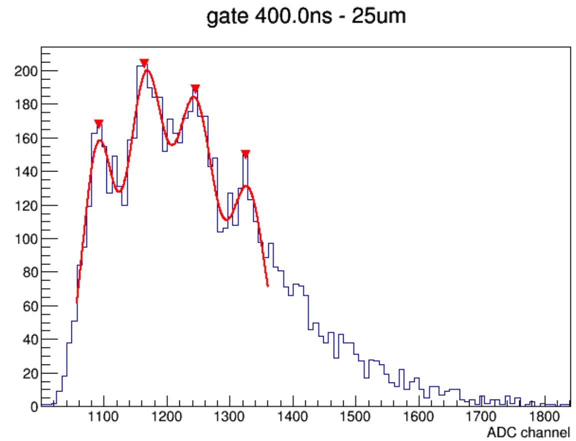

Calibration runs

SiPM: 30um, 1x1mm2, 36V

Waveform amplitude: approx. 53mV/P.E.

Waveform baseline: approx. 17mV

All channels acquired, one channel per run (32runs), with three gate windows (20ns, 50ns, 100ns)

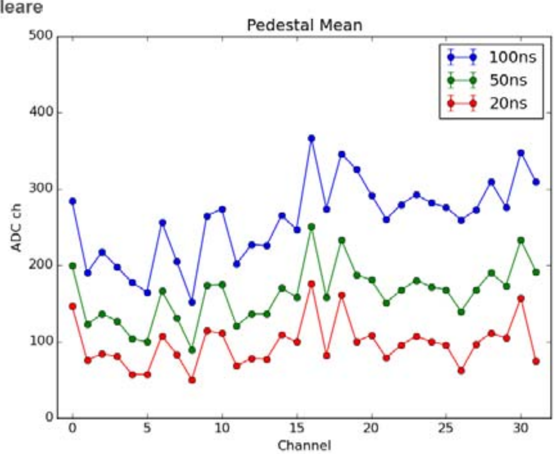

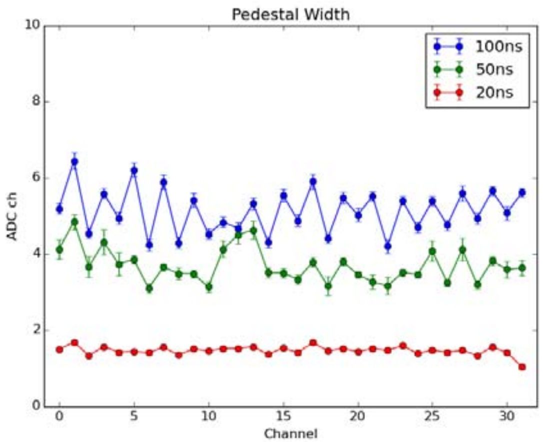

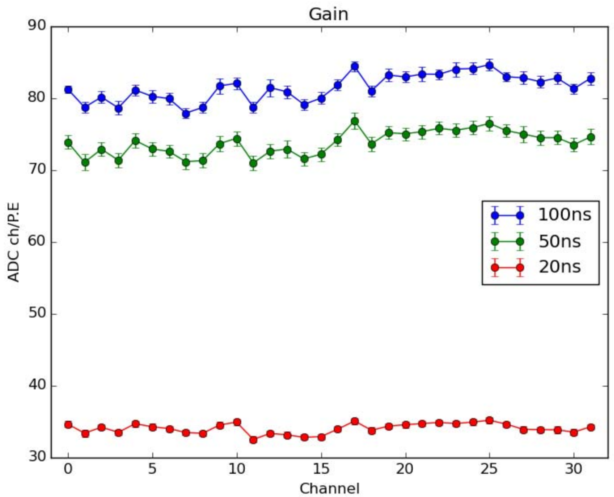

Same signal sent to all channels: all differences in Pedestal and Gain are instrinsic to the V792 module

Estimate of calibration coefficients

Calibration runs

SiPM: 30um, 1x1mm2, 36V
Waveform amplitude: approx. 53mV/P.E.
Waveform baseline: approx. 17mV
All channels acquired, one channel per run (32runs), with three gate windows (20ns, 50ns, 100ns)

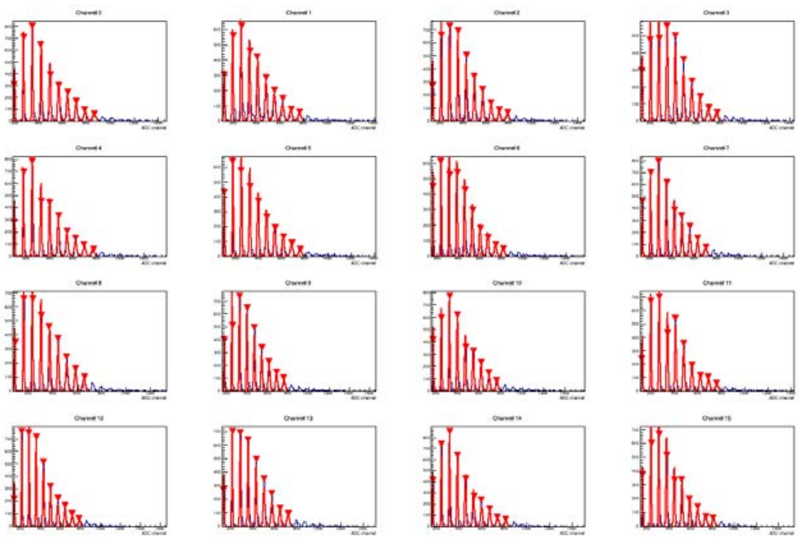

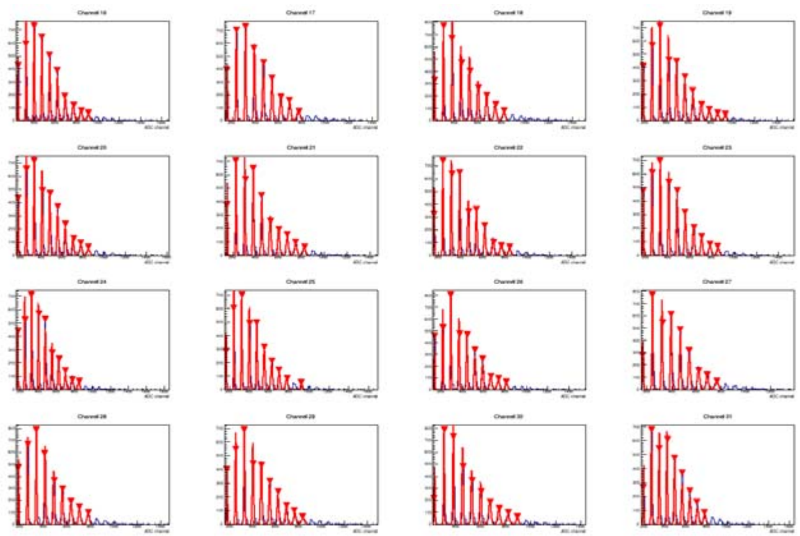

Photon distributions

SiPM: 30um, 1x1mm2, 36V

SiPM signal replicated 32 times using a linear fan-in fan-out (2 modules)

Gate window: 100ns

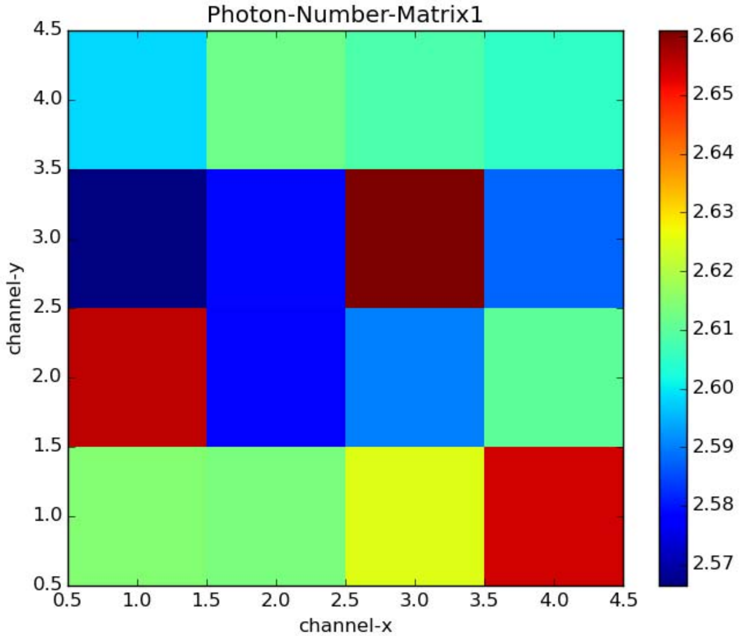

Poisson fit

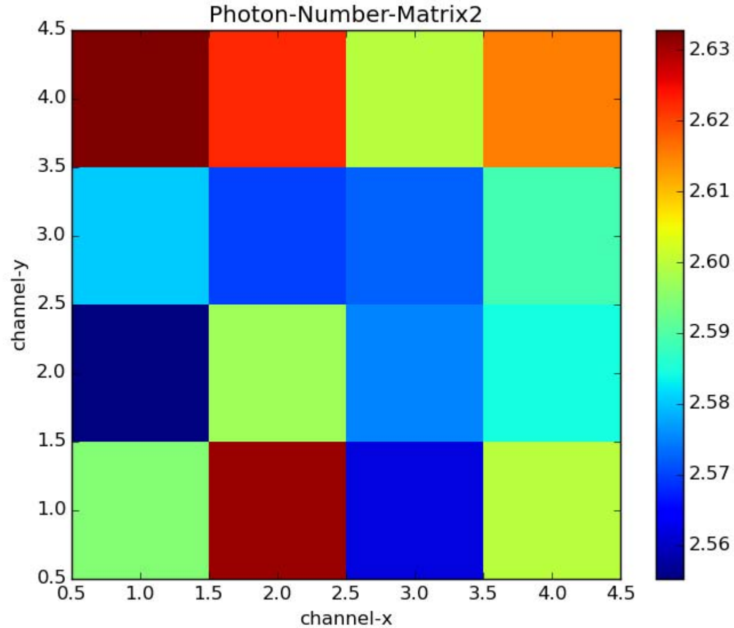

FBK 6 x 6 mm^2 – Advansid preamp

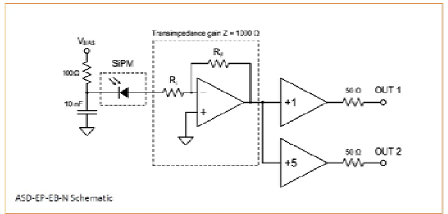

9V$_{OV}$

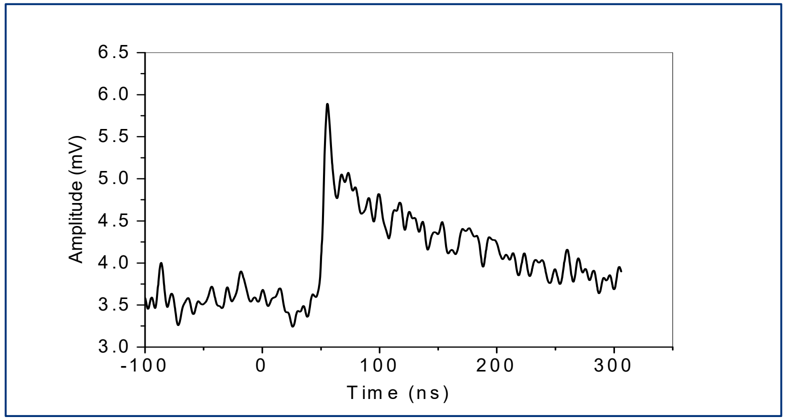

Charge distribution

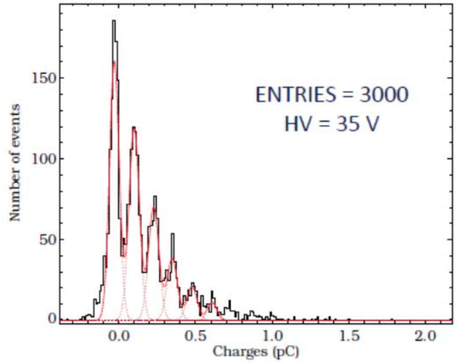

Gain and SNR

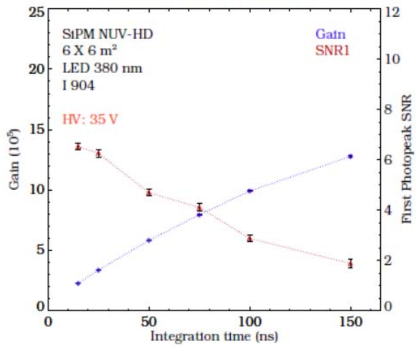

INFN SiPM PreAmplifier

ORCAD Schematic

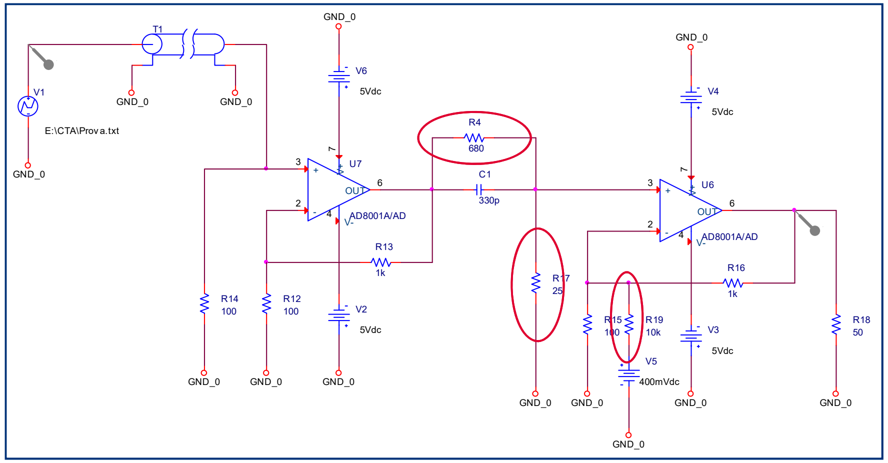

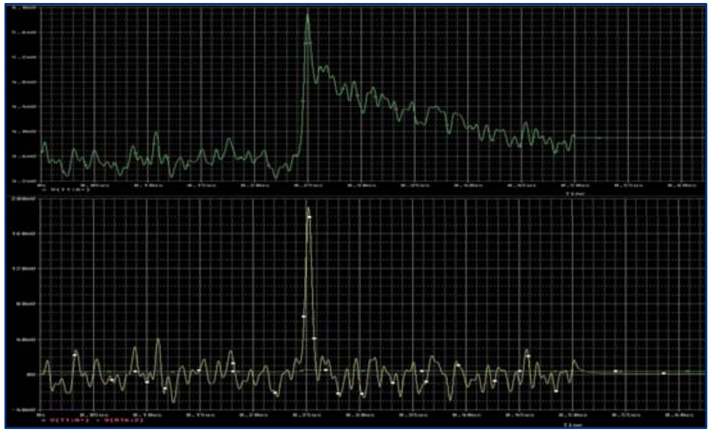

INFN_SiPM_PreAmp

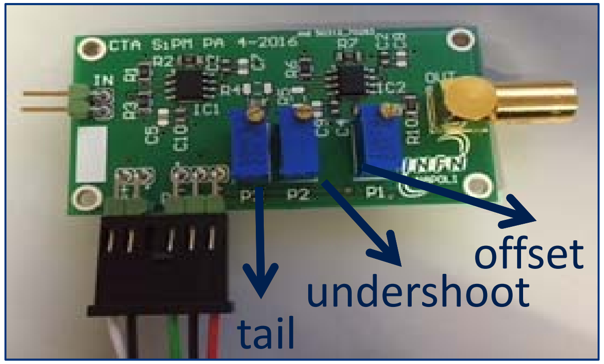

Pole – Zero network

3 Trimmer: P1, P2, P3 to change respectively offset, undershoot and tail

→ different resistance R values

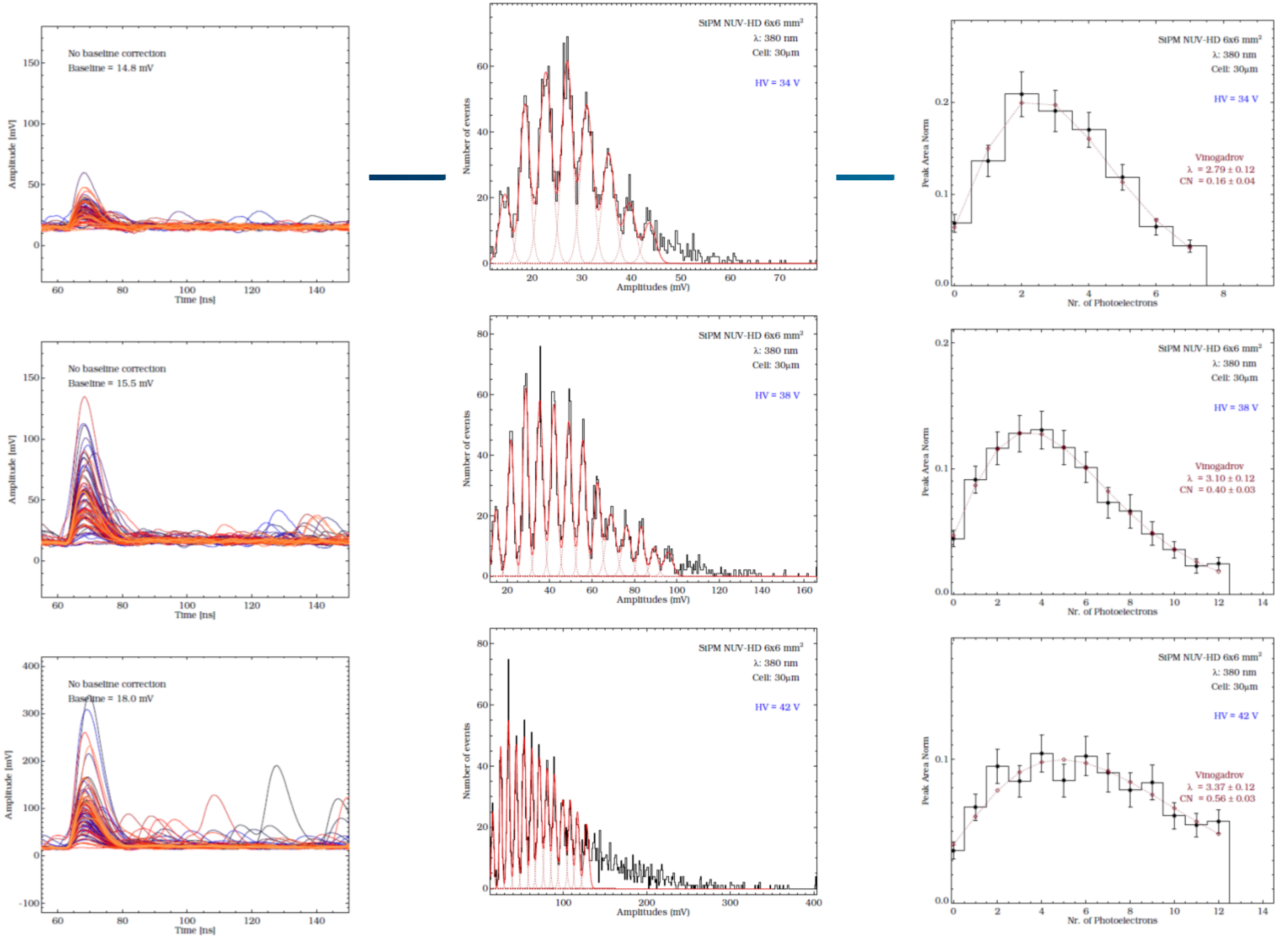
No baseline correction
Baseline = 14.8 mV
Baseline = 15.5 mV
Baseline = 18.0 mV
Amplitude [mV]
Time [ns]
SiPM NUV-HD 6x6 mm²
λ: 380 nm
Cell: 30μm
HV = 34 V
HV = 38 V
HV = 42 V
Number of events
Amplitudes (mV)
Peak Area Norm
Nr. of Photoelectrons
Vinogadrov
λ = 2.79 ± 0.12
CN = 0.16 ± 0.04
λ = 3.10 ± 0.12
CN = 0.40 ± 0.03
λ = 3.37 ± 0.12
CN = 0.56 ± 0.03

Gain and resolution

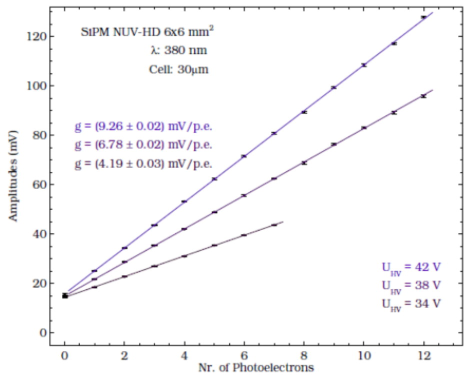

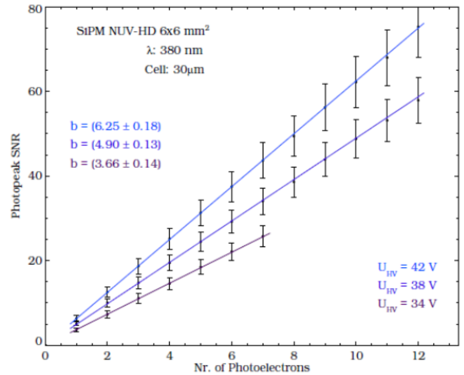

Charge measurements - I

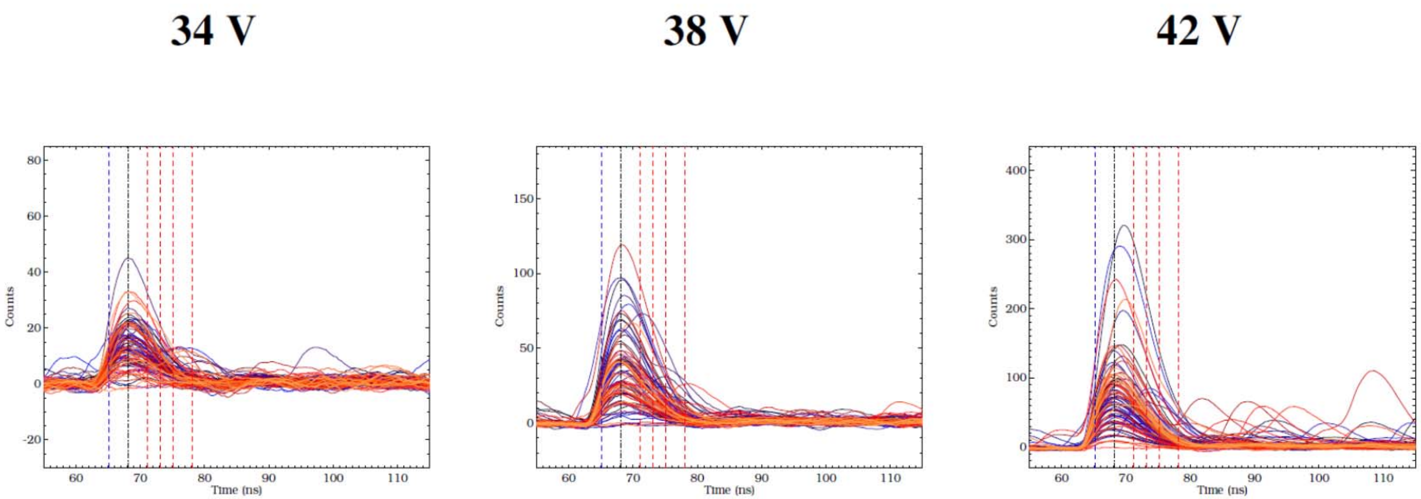

Different bias and different integration time

Charge measurements - II

34V

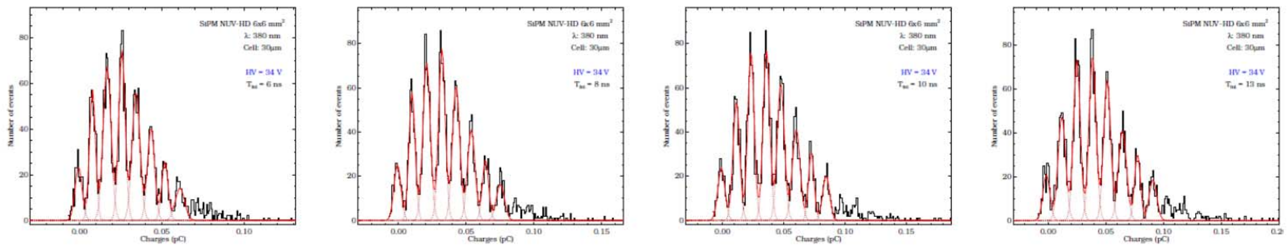

38V

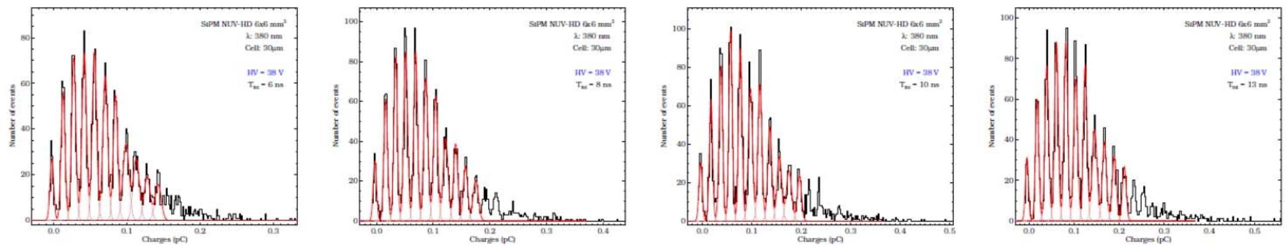

Performances

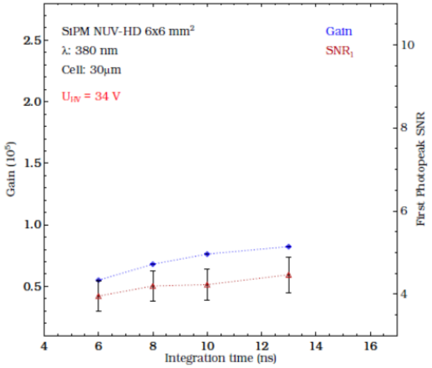

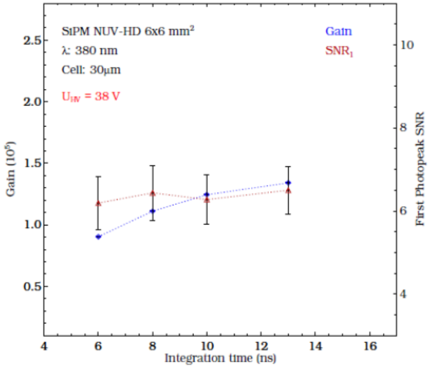

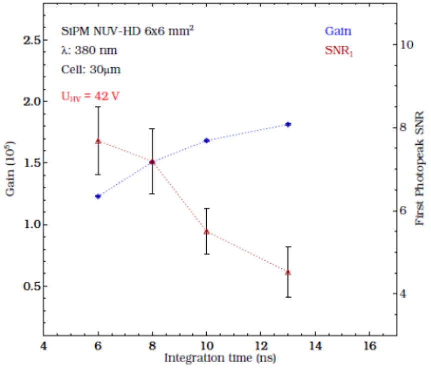

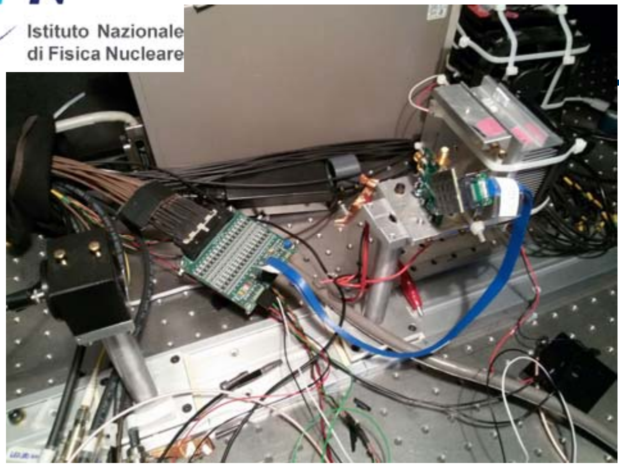

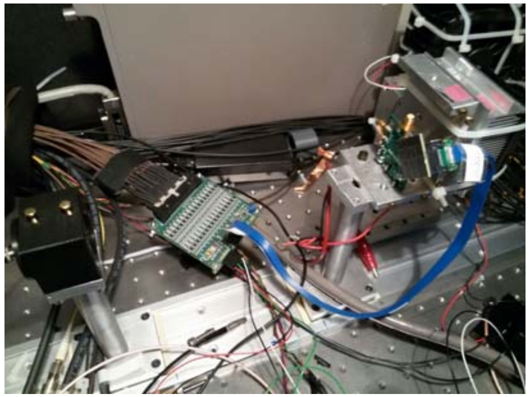

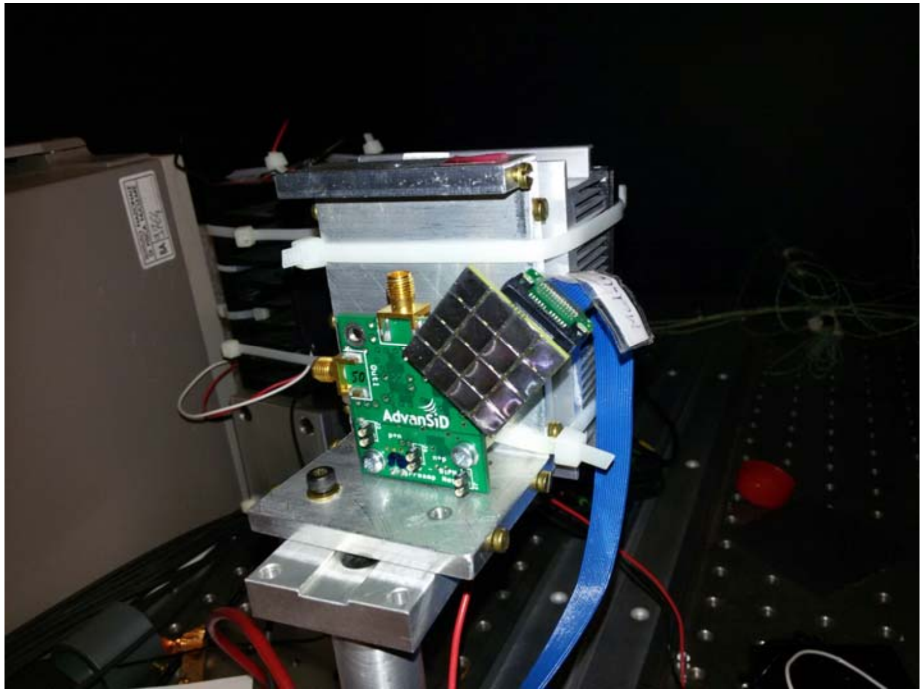
AdvanSiD

Acceptance test results

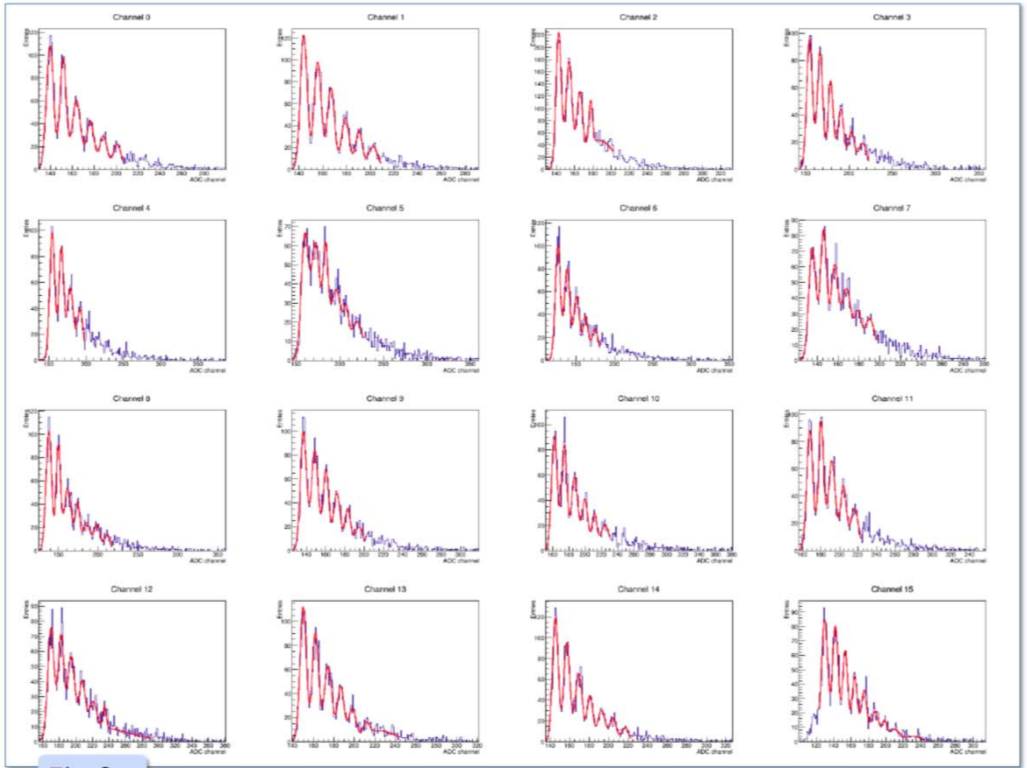

Fig. 8a

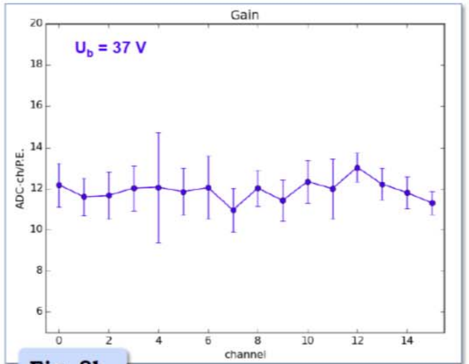

Fig. 8b

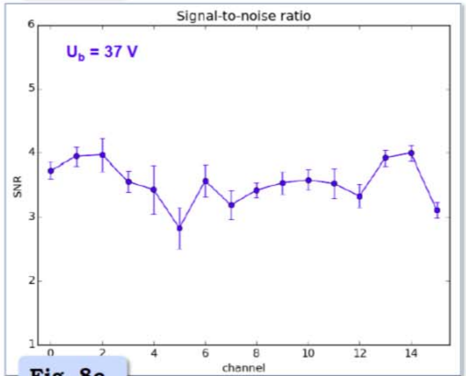

Fig. 8c

pSCT module assembly

16 pixel module
uniform coverage of the camera

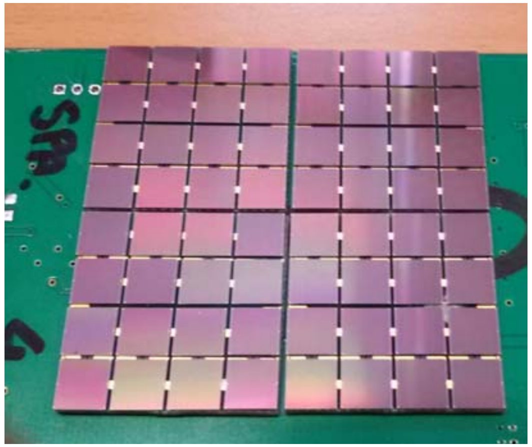

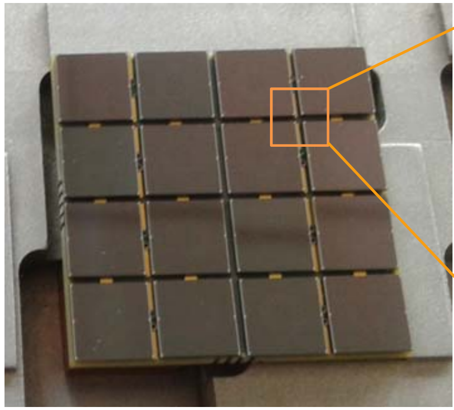

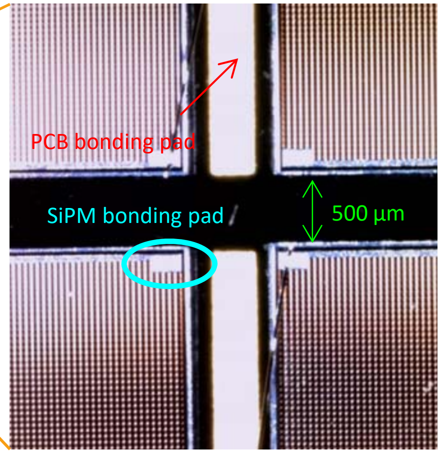

INFN Istituto Nazionale di Fisica Nucleare

pSCT module assembly

nectors ... machine on 100 PCBs.
sted

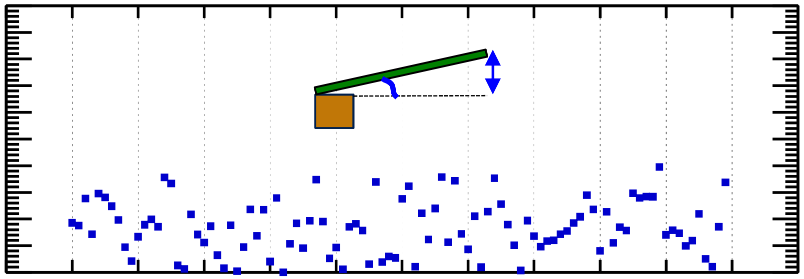

- PCB – Copper cube ZY and ZX angle < 0.4° (corresponding to maximum PCB height difference of 200 µm)
  - Angle Copper cube – PCB border < 1.6° (Y view), 0.4° (X view)

pSCT module assembly

MANUAL sensor assembly

- Optimal alignment, approx 20 mins/matrix

Alignment of sensors in custom frame

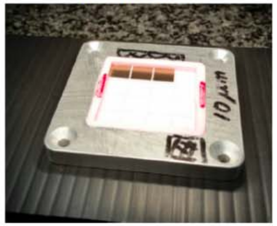

Dispensing of conducting glue

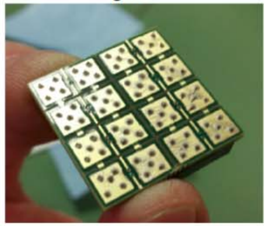

PCB-sensor coupling

Wait for curing and remove PCB from frame

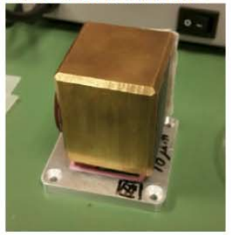

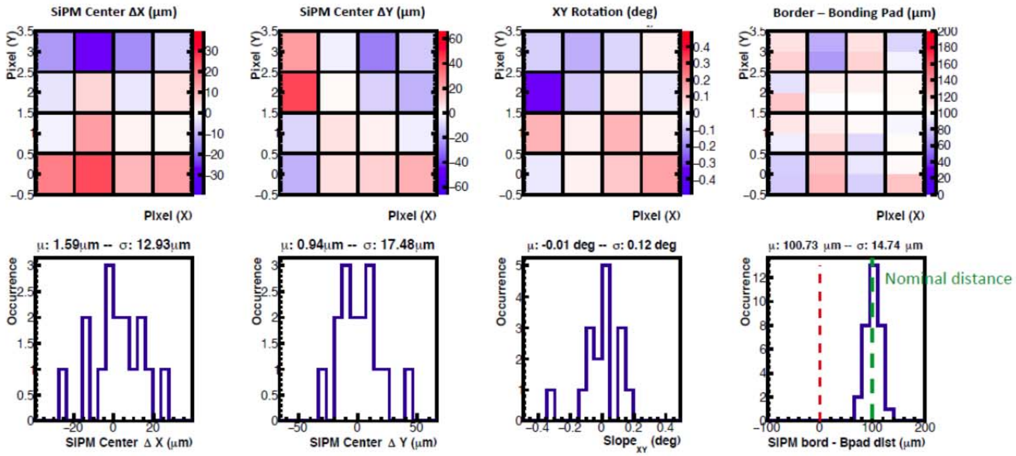

pSCT module assembly

Pick & Place machine sensor assembly

Sensor placement with industrial partner Pick&Place machine

- Very fast, optimized for mass scale productions (approx. 100 modules / half day)
  - Alignment quality not optimal, exploring solution with Die Bonding machine

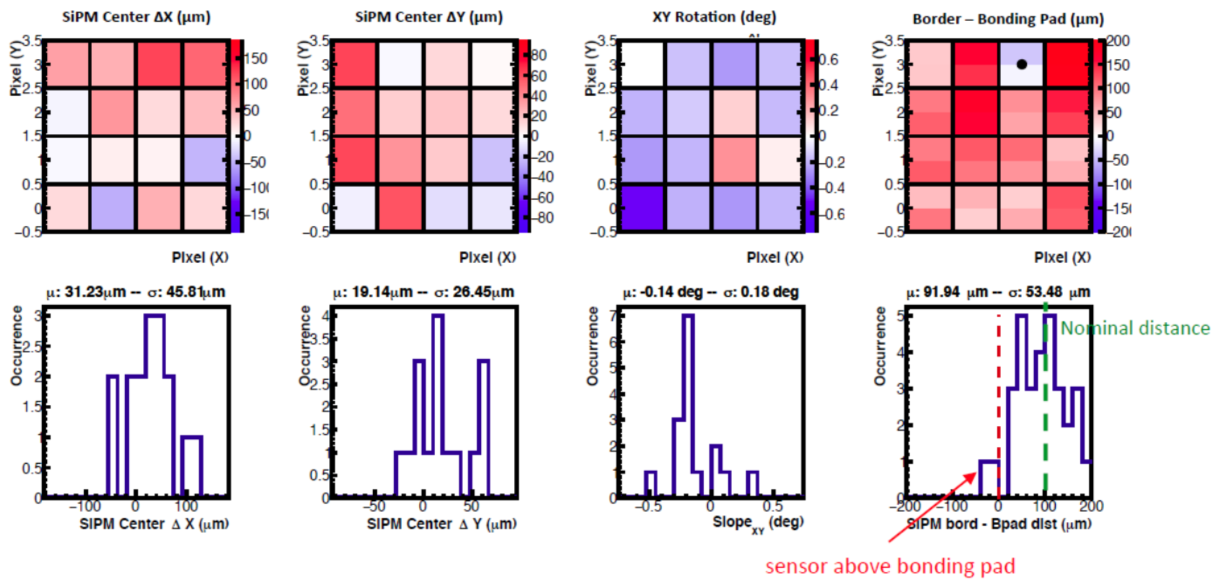

INFN
Istituto Nazionale
di Fisica Nucleare

pSCT module assembly

Placement in bonding&transport jig

Bonding (approx. 15 mins/matrix)

Bonding with 20μm Al/Si wire

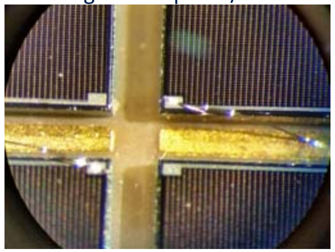

Dispensing of UV-transparent protecting epoxy

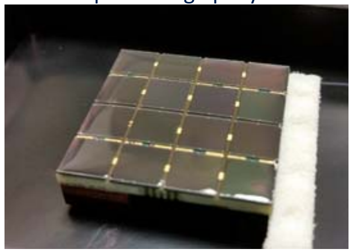

Matrix sensor test before dispensing of protection epoxy. Any defective sensor is replaced

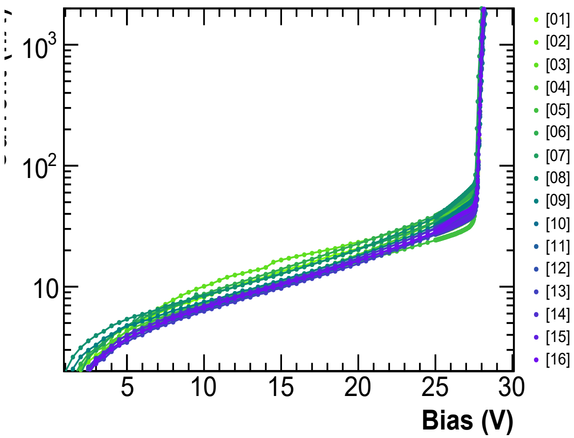

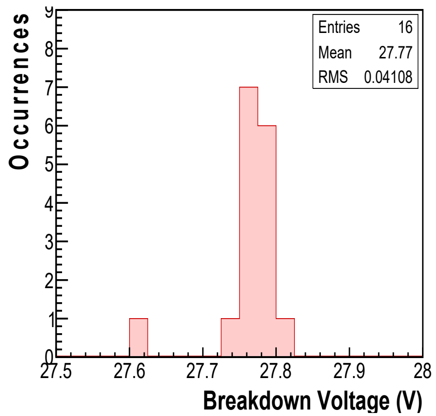

The «NEW» Front end

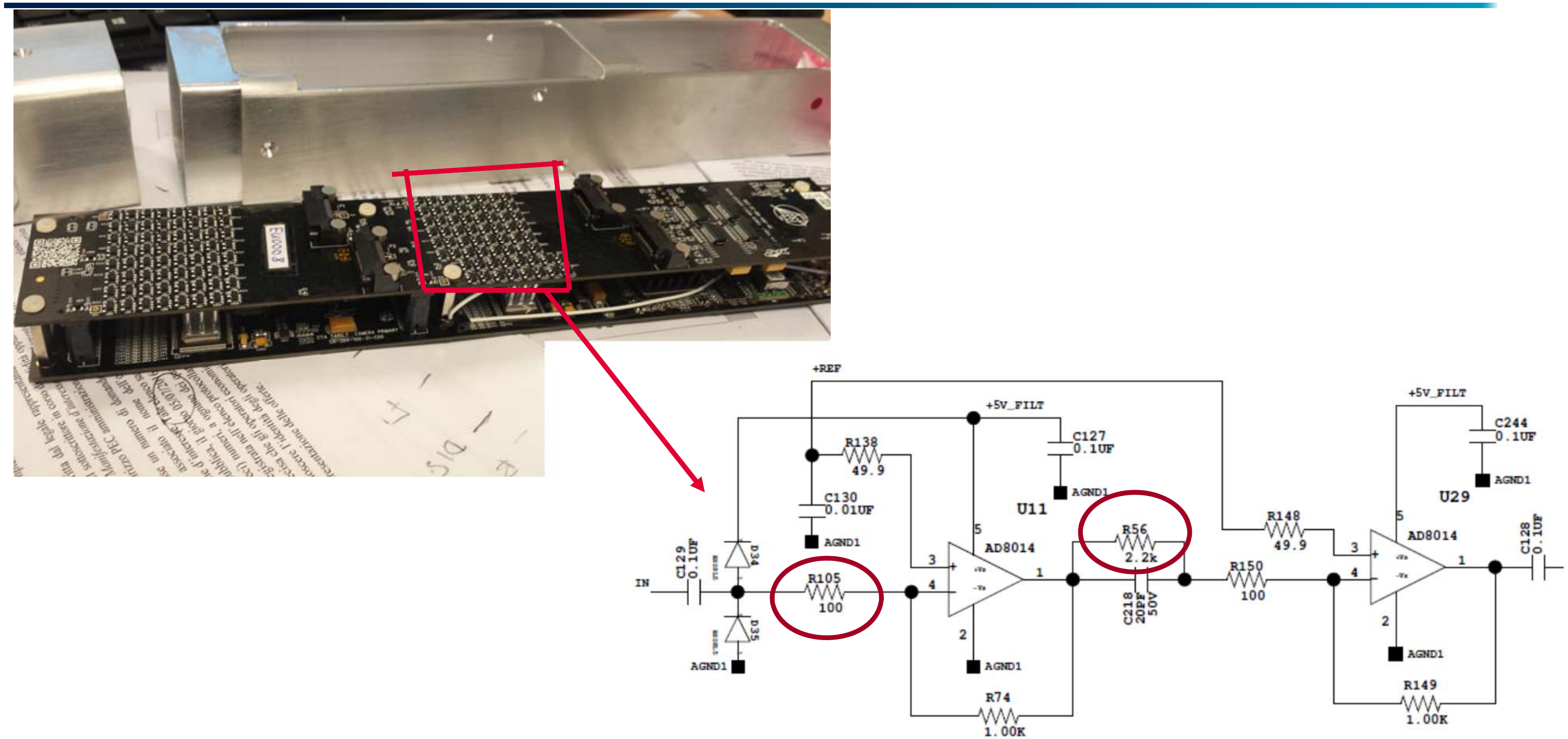

Tests with the T7 module

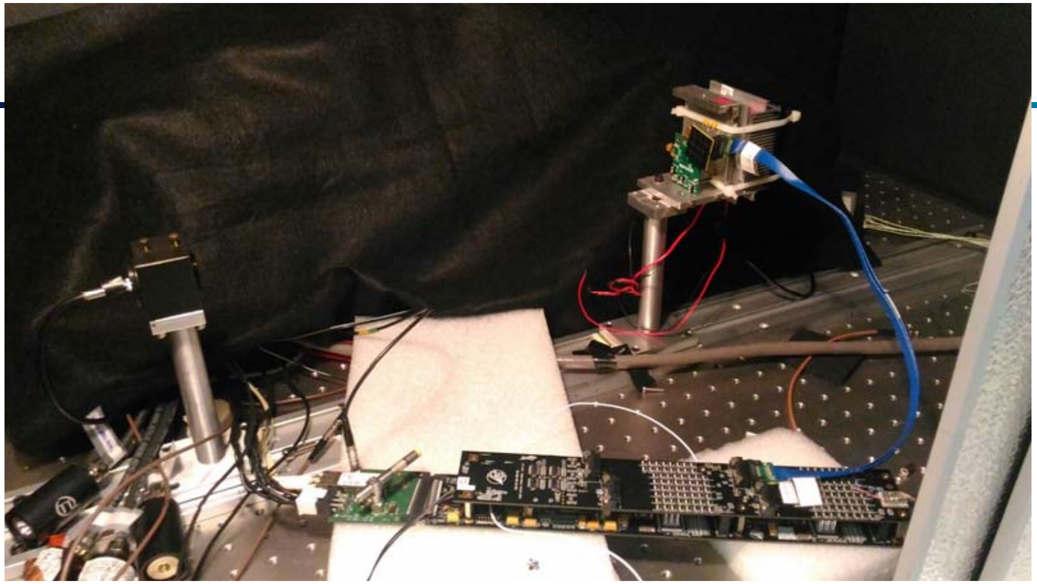

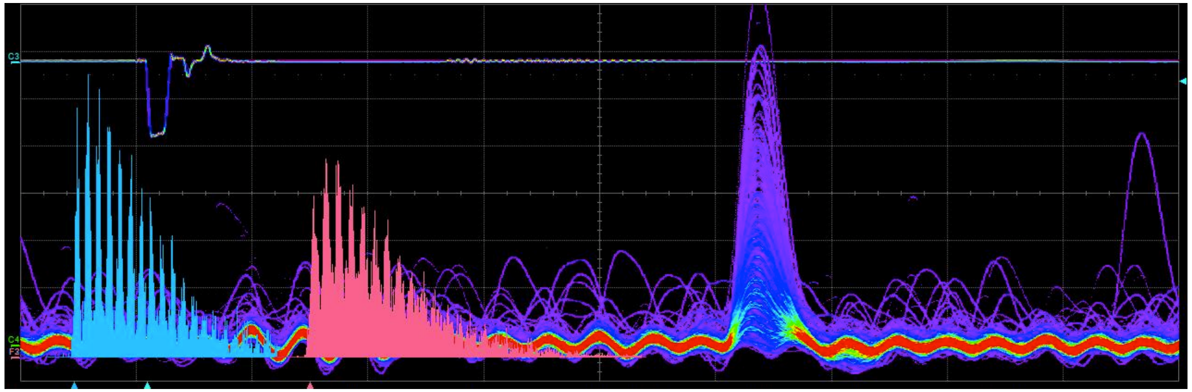

Amplitude analysis @ Oscilloscope

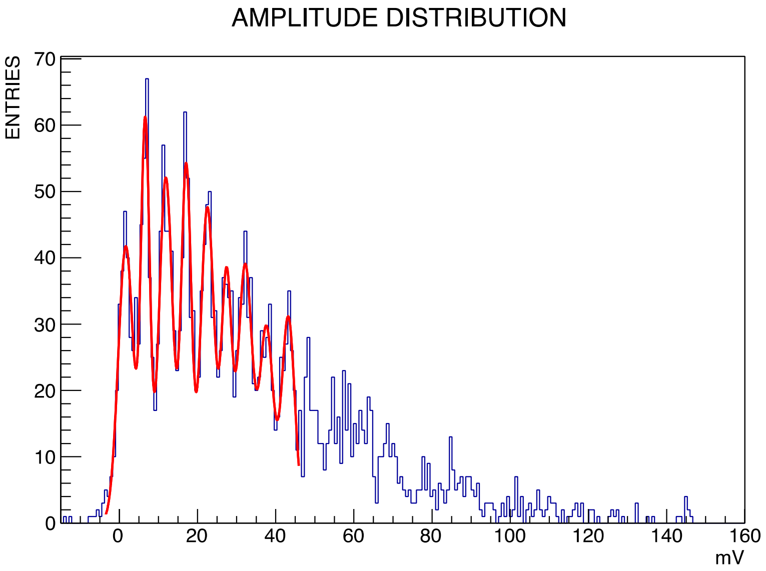

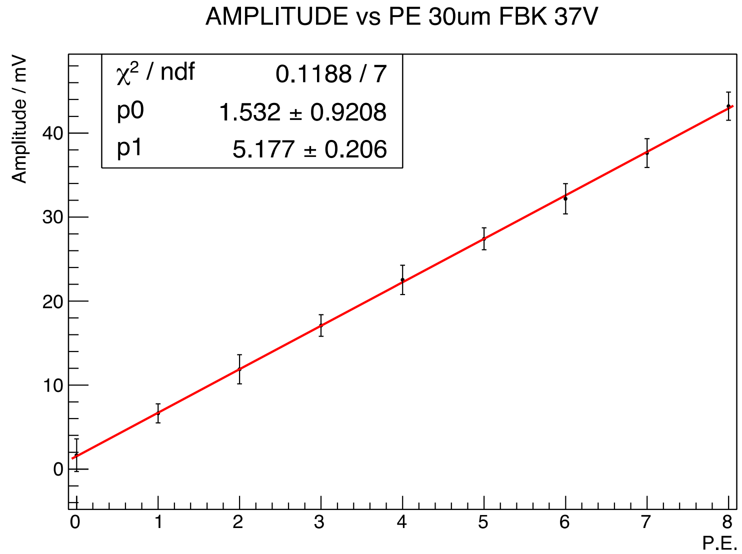

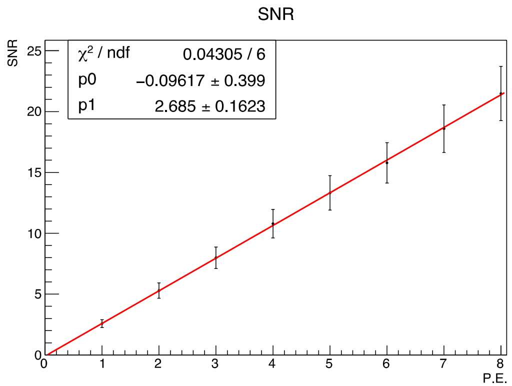

Target7 Data

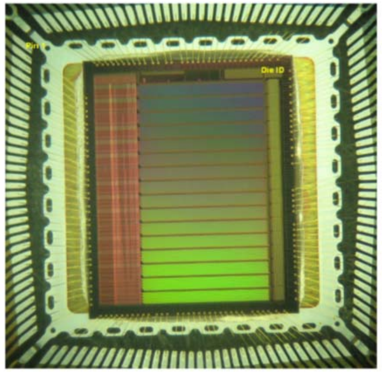

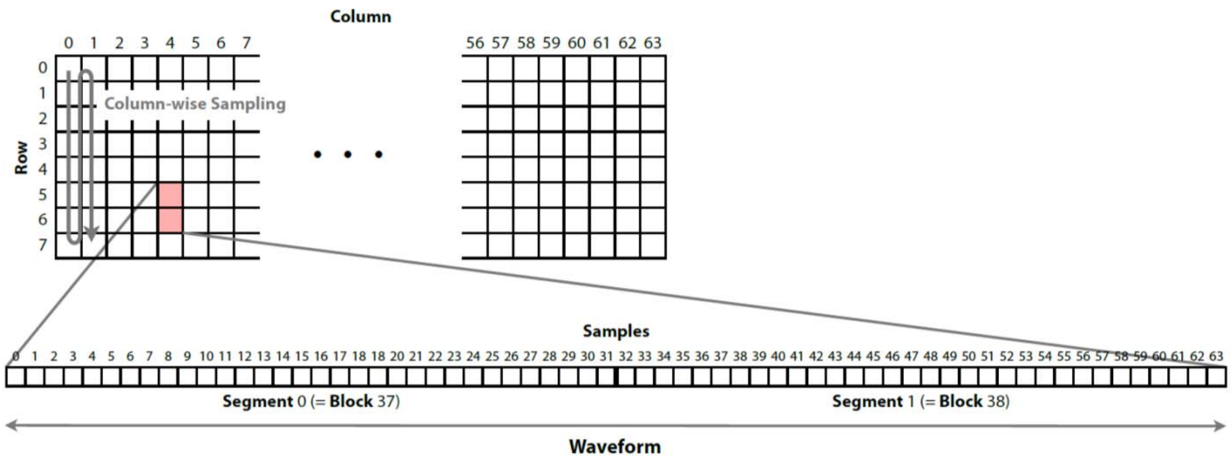

FIGURE 2.4: Storage buffer diagram in TARGET-7.

T7 Pedestal correction

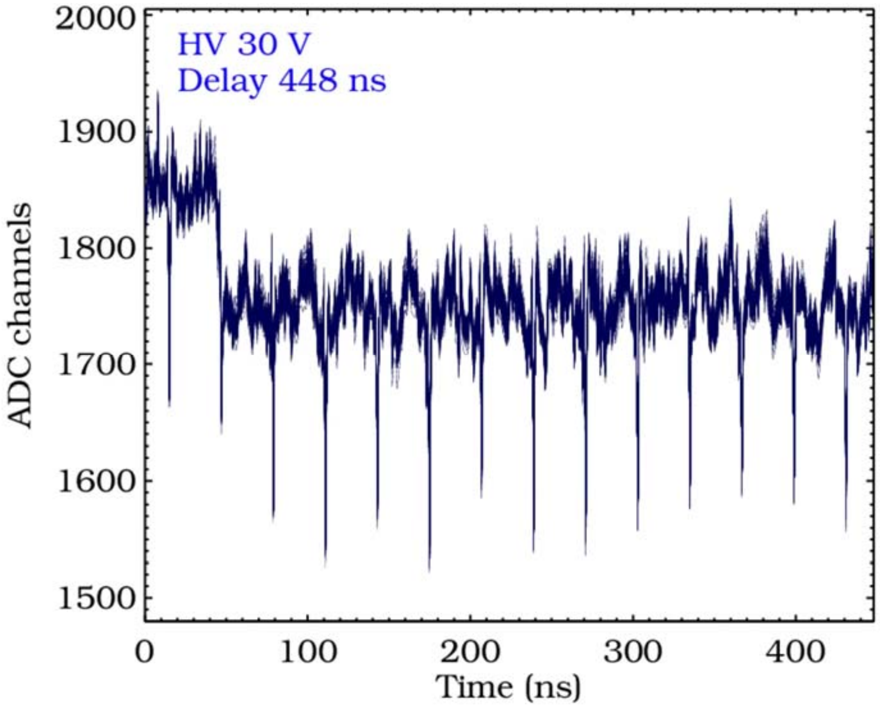

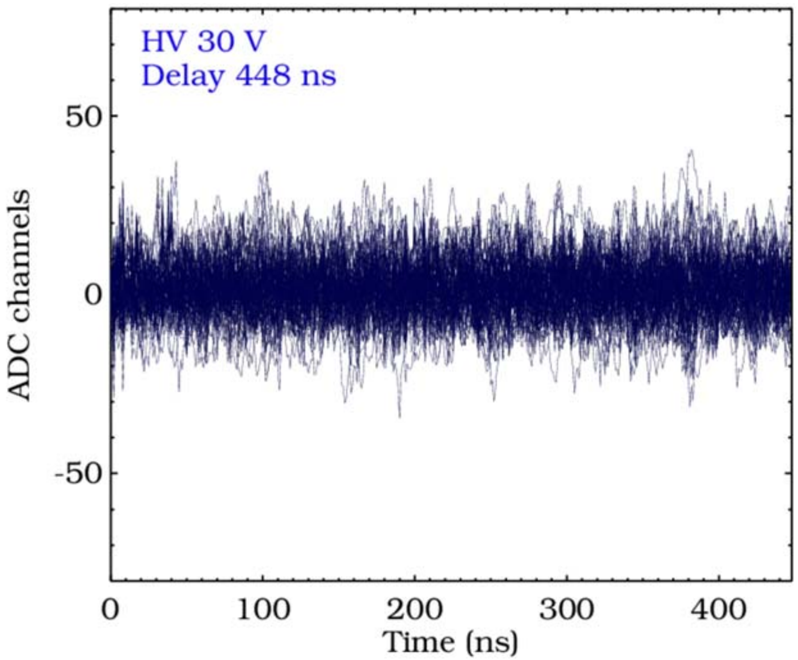

Pedestal Zoom IN

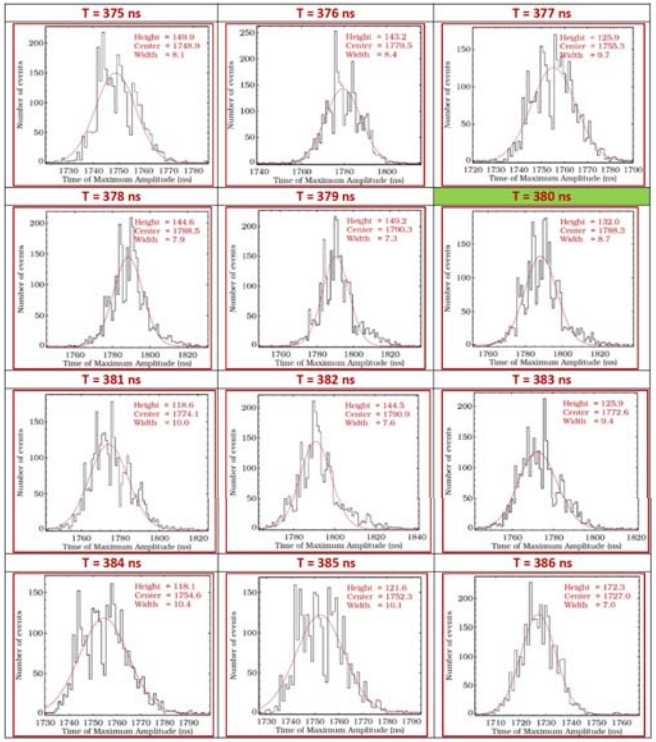

T7 Module results

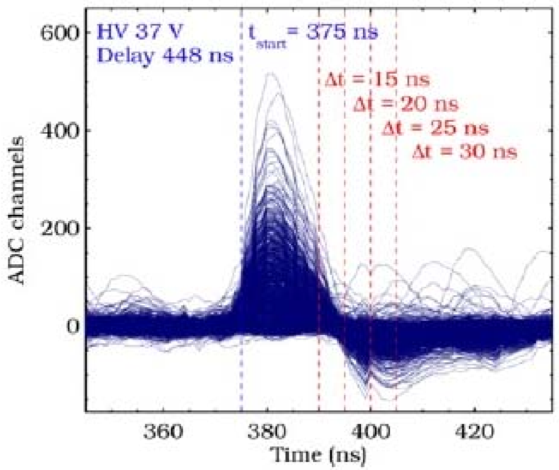

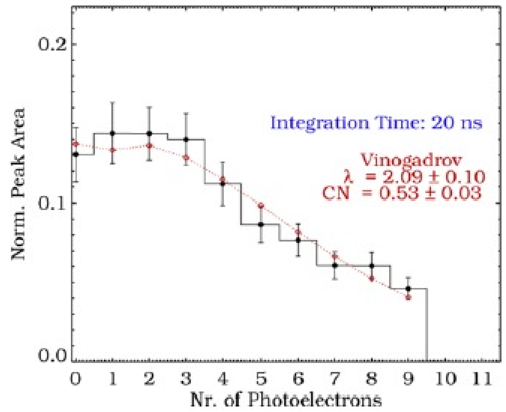

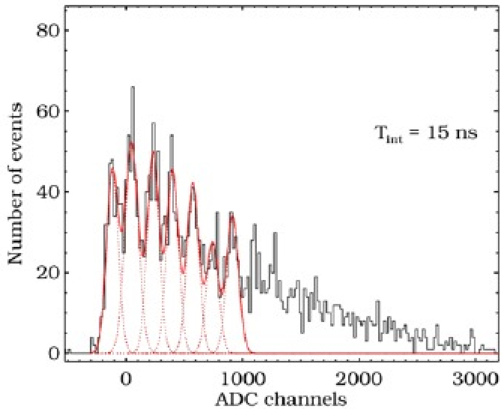

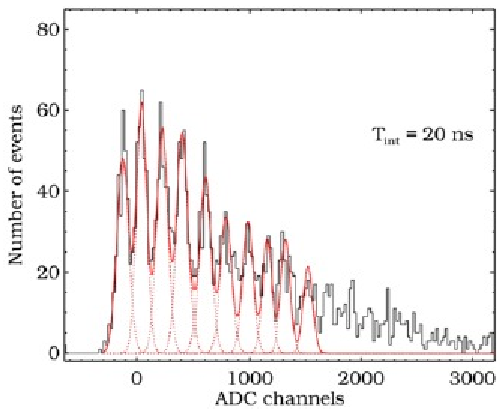

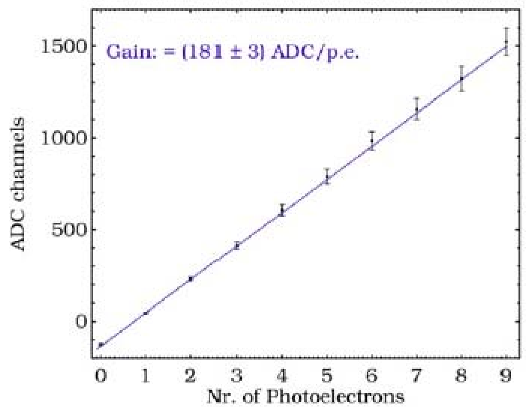

The DCDC test

FBK SiPM sensors require a bias voltage of about 35 V.

We tested a small DC-DC linear regulator TI TPS7A4001 that converts 70 V to about 39 V, in order to use the same HV power supply unit for all modules, Hamamatsu and FBK.

The bias voltage can then be regulated setting the low side HV (0 to 4 V) so the effective range is then 34-39 V.

DC DC High Voltage Linear Regulator TPS7A4001

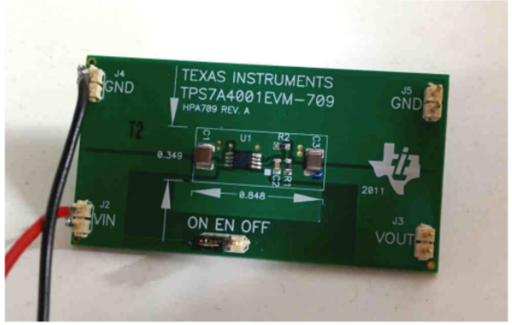

Linear regulator mounted over TARGET7 board

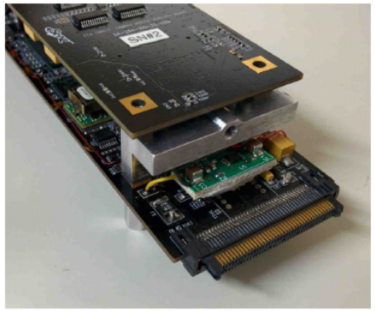

FBK 4x4 pixels quadrant

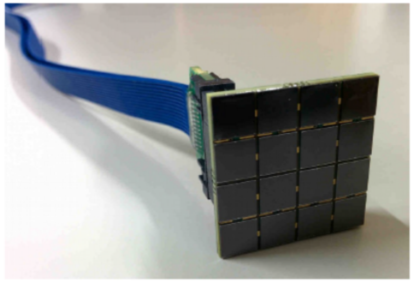

See you in the lab sessions